JETP Letters, Vol. 76, No. 1, 2002, pp. 1–7. Translated from Pis'ma v Zhurnal Éksperimental'noĭ i Teoreticheskoĭ Fiziki, Vol. 76, No. 1, 2002, pp. 3–10.

Example of a Fermion-Nondoubling Amorphous Lattice

S. N. Vergeles

Landau Institute for Theoretical Physics, Russian Academy of Sciences, Chernogolovka, 142432 Russia
e-mail: vergeles@itp.ac.ru
Abdus Salam International Centre for Theoretical Physics, Trieste, Italy

Received April 21, 2002; in final form, June 6, 2002

Abstract—An example of an amorphous lattice featuring no fermion doubling is constructed. The lattice represents a bounded two-dimensional simplicial complex with a disk topology, every internal 0-simplex of which belongs to boundaries of an odd number of 1-simplices. The total number of simplices in the complex tends to infinity. © *2002 MAIK "Nauka/Interperiodica".*

PACS numbers: 04.60.Nc

1. INTRODUCTION

Recently [1], a theory of gravity on a lattice (simplicial complex) was constructed, which included a Dirac field. The Dirac degrees of freedom were determined on 0-simplices, while the degrees of freedom of the gravity field were determined on 1-simplices. Upon naively passing to a continuum limit, the action in this theory converted into the ordinary Gilbert action with a Euclidean signature, including a Dirac field minimally connected to the gravity field.

Since a simplicial complex of the general type belongs to amorphous lattices (to which the Brillouin zone concept is inapplicable), the construction of the proposed discrete gravity theory encountered the old problem of the doubling of the fermion states [2–6]. Nielsen and Ninomiya [5] showed that the problem is solved in favor of fermion doubling in the case of a periodic lattice featuring a momentum representation and the Brillouin zone. However, some researchers put forward a hypothesis that the phenomenon of fermion doubling (also known as Wilson's doubling) takes place on the amorphous lattices as well.

The aim of this letter is to offer an example of a two-dimensional (2D) amorphous lattice on which Wilson's doubling does not take place. Since such lattices appear in connection with the discrete gravity theory, it is natural to start the presentation with a definition of the fermion part of action in this theory.

2. OUTLINE OF THE DISCRETE GRAVITY THEORY

A detailed description of the discrete gravity theory variant used in this study was presented elsewhere [1]. Here, we only introduce the necessary notation for the 2D case under consideration. The definitions and some properties of simplicial complexes were described previously [1], while a systematic presentation of the theory can be found in monographs [7].

Let $\mathfrak{K}$ be a 2D simplicial complex. Below, the following pairs of concepts are treated as synonyms: 0-simplex and vertex; 1-simplex and edge; 3-simplex and triangle. Let us assume that the geometric realization of complex $\mathfrak{K}$ is a 2D surface with a disk topology and a boundary $\partial\mathfrak{K}$, representing a 1D simplicial complex with a circle topology, and denote by α_q ($q = 0, 1, 2$) the number of q-simplices in complex $\mathfrak{K}$. For certainty, let us consider the 2D Dirac matrices γ^a ($a = 1, 2$) in the form of $\gamma^1 = \sigma^1$ and $\gamma^2 = \sigma^2$, where σ^α ($\alpha = 1, 2, 3$) are the Pauli matrices. The Dirac spinors ψ_i and $\bar{\psi}_i$, determined at each vertex a_i of the complex $\mathfrak{K}$, are represented by 2D column and row matrices, respectively. Indices $i, j, k, \ldots$ run through the complex vertices. Let us bring each oriented edge $a_i a_j$ into correspondence with an element $\Omega_{ij} = \Omega_{ji}^{-1}$ of group Spin(2) (Abelian group in the 2D case). Elements of the holonomy group Ω_{ij} produce a parallel transfer of spinor ψ_j from vertex a_j to vertex a_i. Let V denote a linear space with the basis set γ^a. Then, each oriented edge $a_i a_j$ corresponds to the element $e_{ij}^a\gamma^a \equiv \hat{e}_{ij} \in V$, where

$$\hat{e}_{ij} = -\Omega_{ij}\hat{e}_{ji}\Omega_{ji}. \quad (1)$$

Index A will run through the triangles of complex $\mathfrak{K}$. Complex indices of types (Ai), (Aij), … indicate that vertices a_i and a_j belong to triangle A.

Consider a complex $\mathfrak{K}$ with a disk topology. Such complexes admit orientation. Let us set the orientation of $\mathfrak{K}$ by determining the orientation of each triangle in this complex. If two triangles are sharing an edge, the two orientations of this edge set by orientations of the corresponding triangles are opposite. Let a_{Ai}, a_{Aj}, and a_{Ak} denote the vertices of a triangle with index A. Then,

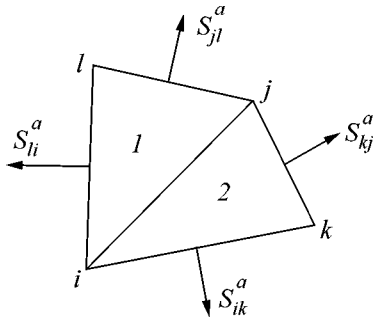

Fig. 1.

by definition, $\varepsilon_{Aijk} = \pm 1$ depending on whether the order of vertices $a_i a_j a_k$ corresponds to the positive or negative orientation of this triangle.

Now we can write the fermion part of the action as

$$I_\psi = \frac{1}{6}\sum_A \sum_{i,j,k} \varepsilon_{Aijk}\varepsilon_{ab}\Theta^a_{Aij}e^b_{Aik},$$
$$\Theta^a_{Aij} = \frac{i}{2}(\bar\psi_{Ai}\gamma^a\Omega_{Aij}\psi_{Aj} - \bar\psi_{Aj}\Omega_{Aji}\gamma^a\psi_{Ai}). \quad (2)$$

Here, the dynamic variables are represented by the quantities Ω_{ij}, e_{ij} (describing the gravitational degrees of freedom) and the fields ψ_i, $\bar\psi_i$ (representing material fields).

Action (2) is of interest for studying the fermion (Wilson's) doubling, since this fermion part possesses the following properties:

(i) action (2) is local;

(ii) in the naive continuum limit, action (2) passes into a gravity action in the Palatini form plus the action of Dirac fields minimally connected to the gravity field;

(iii) the fermion part of action (2) is both phase-invariant and γ^5-invariant, that is, invariant with respect to the following transformations: (a) $\psi \longrightarrow \exp(i\alpha)\psi$, $\bar\psi \longrightarrow \bar\psi\exp(-i\alpha)$; (b) $\psi \longrightarrow \exp(i\beta\gamma^5)\psi$, $\bar\psi \longrightarrow \bar\psi\exp(i\beta\gamma^5)$. Here, α and β are the real continuous global parameters and $\gamma^5 = i\gamma^1\gamma^2$.

Since the fermion measure on a lattice is also invariant with respect to the latter transformations (even in a local variant), the theory under consideration is characterized by the conservation of both the vector current and the axial vector current (more precisely, of the total axial vector current comprising, in the case of fermion doubling, a sum of several terms).

As is well known [2–4, 6], any fermion action possessing the properties (i)–(iii) on a hypercubic lattice exhibits the phenomenon of Wilson's doubling. In addition, this doubling is also known [5] to take place on periodic lattices for which the fermion action has the form

$$I = \sum_{\mathbf{x},\mathbf{y}} \bar\psi_{\mathbf{x}}\hat H(\mathbf{x}-\mathbf{y})\psi_{\mathbf{y}} \quad (3)$$

($\mathbf{x}$, $\mathbf{y}$ denote the radius-vectors of the lattice sites) and possesses the properties (i)–(iii). However, the question as to whether fermion action possessing these properties leads to fermion doubling on an arbitrary lattice remained unanswered. Below, we present examples of lattices (simplicial complexes) on which the action of type (2) does not lead to Wilson's doubling. It should be emphasized that action (2) does not reduce to form (3) for complexes of the general type.

The problem of the discrete gravity theory is to calculate a finite-dimension integral over dynamic variables with the exp$I$ weight. In order to solve the problem of Wilson's doubling, we assume that the Universe has expanded so that fluctuations of the gravity field can be ignored and fluctuations of the fermion field can be taken into account by determining the eigenmodes of the discrete Dirac operator in (2), which are retained in the continuum limit.

In order to solve this problem, the situation has to be idealized in this direction. To this end, below we assume that

$$\Omega_{ij} = 1, \quad (e^a_{ij} + e^a_{jk} + \ldots + e^a_{li}) = 0, \quad (4)$$

where the sum in parentheses is taken over any closed path composed of 1-simplices. Equations (4) imply that both the curvature and the torsion are zero. Thus, the geometric realization of complex $\mathfrak{K}$ occurs in a 2D Euclidean plane, and e^a_{ij} are the components of a vector in a certain orthogonal basis set in this plane, the beginning and end of this vector occurring at the vertices a_i and a_j, respectively. Note that conditions (4) imply that $\Theta^a_{ij} = -\Theta^a_{ji}$. In what follows, two vertices bounding the same edge will be called adjacent.

Let us write an equation describing the eigenmodes of a discrete Dirac operator. Consider two fixed adjacent vertices, a_i and a_j, and separate the contribution of action (2) proportional to Θ^a_{ij}. Figure 1 shows a part of the complex containing 1-simplex $a_i a_j$, where indices i, j, k, l refer to vertices and index A, indicating triangles, takes the values 1 and 2. Note that everywhere $s^a_{ij} = \varepsilon_{ab}e^b_{ij}$, which implies that vector s^a_{ij} is obtained by rotating e^a_{ij} clockwise through the angle $\pi/2$. The contribution to the action in question is

$$\Delta I_{\psi ij} = \frac{1}{3}\Theta^a_{ij}S^a_{ij}, \quad S^a_{ij} = s^a_{kj} + s^a_{jl}.$$

Here, vector S_{ij}^a can be called the umbrella of vertex a_i from the side of adjacent vertex a_j. The umbrella S_{ij}^a is uniquely determined by the adjacent vertices a_i and a_j, and relations (4) show that $S_{ij}^a = -S_{ji}^a$. Now, let us separate a subcomplex $\mathfrak{A}_i$, including all 2-simplices containing vertex a_i, from the initial complex. This subcomplex will be called the vicinity of vertex a_i. The vertices belonging to the boundary $\partial\mathfrak{A}_i$ will be enumerated so that vertex a_{j+1} follows a_j when the boundary $\partial\mathfrak{A}_i$ is traversed in the counterclockwise direction; index j is defined as mod$n$, where n is the number of vertices in $\partial\mathfrak{A}_i$. The fact that index j runs through the vertices in $\partial\mathfrak{A}_i$ is indicated by writing $j(i)$. Now, we can readily separate a contribution proportional to the spinor $\bar{\psi}_i$ from action (2):

$$\Delta I_{\bar{\psi}_i} = \frac{1}{3}\sum_{j(i)} \Theta_{ij}^a S_{ij}^a. \tag{5}$$

Using Eqs. (2), (4), and (5), we obtain an equation determining eigenmodes of the discrete Dirac operator for the internal vertices a_i:

$$\frac{\delta\Delta I_{\bar{\psi}_i}}{\partial\bar{\psi}_i} = \frac{i}{6}\sum_{j(i)} \hat{S}_{ij}\psi_j = \epsilon\left(\frac{1}{3}S_i\right)\psi_i, \tag{6}$$

where S_i is the area of the vicinity $\mathfrak{A}_i$. The second equation (4) leads to the identity

$$\sum_{j(i)} \hat{S}_{ij} \equiv 0. \tag{7}$$

Indeed, every vector $s^a_{j(i),\,j(i)+1}$ enters into two and only two umbrellas in the latter sum. Identity (7) implies that Eq. (6) possesses a difference character, whereby the left-hand part of this equation depends only on differences of the type $\psi_{j(i)} - \psi_{k(i)}$.

A system of equations for the eigenmodes acquires a neat form in the complex notation. Let x_j^a be the Cartesian coordinates of vertex a_j and $z_j = x_j^1 + ix_j^2$, the corresponding complex coordinate. Denoting the top and bottom components of the Dirac spinor ψ as φ and χ, respectively, we can rewrite Eq. (6) as

$$-\frac{1}{2}\sum_{j(i)} (\bar{z}_{j+1} - \bar{z}_{j-1})\chi_j = \epsilon S_i \varphi_i, \tag{6a}$$

$$\frac{1}{2}\sum_{j(i)} (z_{j+1} - z_{j-1})\varphi_j = \epsilon S_i \chi_i. \tag{6b}$$

For the zero mode ($\epsilon = 0$), we obtain

$$\sum_{j(i)} (z_{j+1} - z_{j-1})\varphi_j = 0 \longleftrightarrow \sum_{j(i)} z_j(\varphi_{j+1} - \varphi_{j-1}) = 0. \tag{8}$$

Below, the difference variables are denoted by $\psi_{i,j} \equiv \psi_i - \psi_j$.

3. LATTICE CONSTRUCTION

We are interested in all zero modes of the discrete Dirac operator obeying zero boundary conditions for the difference variables $\varphi_{k,k'}$. The obvious solution $\varphi_i = \text{const}$ will be called the trivial zero mode.

In order to clear up the situation with zero modes, let us consider a particular example. Assume that $\partial\mathfrak{A}_i$ possesses an even number of vertices (such vertices a_i will be called even). Then the set of indices $j(i)$ can be divided into two equal groups. The indices in one group will be marked by a prime and those in the other group, by a double prime. When the boundary $\partial\mathfrak{A}_i$ is continuously traversed, the vertices with primed and doubly primed indices alternate. In application to this case, Eq. (8) can be written as

$$\left[\sum_{j'(i)} z_{j'}(\varphi_{j'+1} - \varphi_{j'-1})\right] + \left[\sum_{j''(i)} z_{j''}(\varphi_{j''+1} - \varphi_{j''-1})\right] = 0. \tag{9}$$

Now, let us assume that all internal vertices of the complex possess an even number of adjacent vertices, and, in addition, let the set of internal vertices be divided into a finite number of subsets—in this case, three: $\{a_{i'}\}$, $\{a_{i''}\}$, and $\{a_{i'''}\}$—such that the system of Eqs. (8) for the zero modes contains only differences of the type $(\psi_{j'_1} - \psi_{j'_2})$, $(\psi_{j''_1} - \psi_{j''_2})$, and $(\psi_{j'''_1} - \psi_{j'''_2})$. It is important to note that the vertices occupy general positions. The fields $\psi_{j'}$, $\psi_{j''}$, and $\psi_{j'''}$ will be called the branches of zero and near-zero soft modes. In this system, the phenomenon of Wilson's doubling takes place for certain (the boundary effect for $\alpha_0 \longrightarrow \infty$ can be ignored). Such an example is depicted in Fig. 2, where the vertices representing three subsets are indicated by symbols 0 and ($\pm$). A nontrivial zero mode can be taken, for example, in the form of $\varphi^0 = c \neq 0$, $\varphi^\pm = [\exp(\pm 2\pi i/3)]c$. Here, φ^0 and $\varphi^\pm$ are values of the field φ at the vertices denoted by indexes 0 and ($\pm$), respectively. This nontrivial mode is orthogonal to the trivial one (in terms of the measure $\sum_i \bar{\psi}_i\psi_i$, which is natural for a regular lattice) and, hence, is independent. This example presents a nontrivial zero mode with three branches.[1]

[1] In connection with this problem, we should like to point out review [8], where a difference Laplace operator factorizable in terms of the first-order operators is studied on a regular triangular lattice. Comparing the values of variables in adjacent vertices, these operators are qualitatively different from those in Eq. (8).

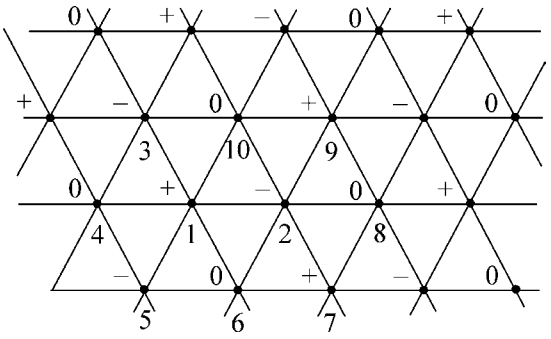

Fig. 2.

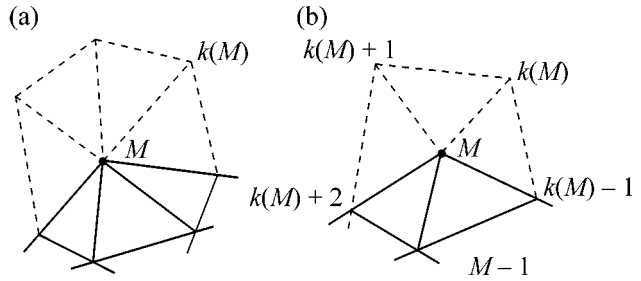

Fig. 3.

Let us consider the question of whether there is a lattice on which no nontrivial zero modes can exist. In order to answer this question, it is necessary to study some properties of the solution to system (8), which requires certain special constructions.

For Wilson's doubling to take place, there must be different solutions of system (8). Corresponding to a zero set of variables $\psi_{k,k-2}$ on the boundary $\partial\Re$. In other words, for zero values of variables $\psi_{k,k-2}$ on $\partial\Re$, system (8) must have nonzero solutions for some variables $\varphi_{i,j}$. As demonstrated below, all difference internal variables $\psi_{k,k'}$ turn to zero, according to system (8), for the so-called odd complexes at zero values of variables $\psi_{k,k-2}$ on the boundary $\partial\Re$.

The fact that the internal variables $\psi_{j(i),j(i)-2}$ are zero by no means always implies that Wilson's doubling is absent. Indeed, for the lattice depicted in Fig. 2, $\psi_{j'_1} = \psi_{j'_2} = \ldots$, $\psi_{j''_1} = \psi_{j''_2} = \ldots$, $\psi_{j'''_1} = \psi_{j'''_2} = \ldots$, but $\psi_{j'} \neq \psi_{j''} \neq \psi_{j'''}$.

Now, let us consider a simplicial complex in which the boundary of each vicinity $\partial\mathfrak{a}_i$ contains an odd number of vertices. The properties of such complexes, called odd complexes, are, in a certain sense, opposite to those of the complex depicted in Fig. 2.

Consider an inductive procedure of constructing odd complexes. In the first stage, we may take any complex composed of an odd number of triangles sharing a vertex which is the only internal vertex. Let us assume that a complex with $M-1$ internal vertices is constructed. Then, we take any vertex a_M at the boundary and render this vertex internal by adding new elements to the complex.

Solid lines in Fig. 3 show an old part of the complex with $M-1$ internal vertices, while dashed lines represent the new part added. In Fig. 3a (3b), the boundary vertex a_M belonged initially to boundaries of an even (odd) number of 1-simplexes. Upon additional construction, the lattice in Fig. 3a (3b) acquires an odd (even) number of new vertices and the corresponding number of 1-simplices. If the external boundary angle at a_M in Fig. 3b is sharp, the modification may consist in adding a single 1-simplex with the boundary vertices $a_{k(M)-1}$ and $a_{k(M)+2}$; as a result, the number of boundary vertices decreases by one.

Below, the consideration will be restricted to complexes constructed using this inductive scheme. Note that the property of oddness is not a necessary condition.

A difference variable $\varphi_{k,i}$ will be referred to as the regular internal variable, provided that $a_k \in \partial\Re$, $a_i \notin \partial\Re$. A set of regular internal variables $\{\varphi_{k_i,i}\}_M$, $i = 1, \ldots, M$ (M is the number of internal vertices) represents an independent regular set of internal variables, provided that all internal vertices a_i are pairwise distinct. In what follows, the term "regular" is omitted. The other $L-1$ independent variables (L being the number of vertices on $\partial\Re$]) will represent the independent difference variables $\{\varphi_{k_\alpha,k'_\alpha}\}$, a_{k_α}, $a_{k'_\alpha} \in \partial\Re$.

Consider a system of M equations (8) for a complex with M internal and L boundary vertices in $(M+L-1)$ independent variables $\{\varphi_{k_i,i}\}_M$ and $\{\varphi_{k_\alpha,k'_\alpha}\}$:

$$\sum_{j=1}^{M} X_{i,j}\varphi_{k_j,j} + \sum_{\alpha=1}^{L-1} Y_{i,\alpha}\varphi_{k_\alpha,k'_\alpha} = 0, \quad i = 1, \ldots, M, \tag{10}$$

where the coefficients $X_{i,j}$ and $Y_{i,\alpha}$ are linear combinations of the variables z_i.

Statement 1. *The $M \times M$ matrix $\|X_{i,j}\|$ with even M is nondegenerate.*

Proof. Consider a complex with $M = 2$. For example, this can be a subcomplex of a complex depicted in Fig. 4, composed of the triangles with numbers from 1 to 8. The internal variables are the differences $\{\varphi_{10,1}, \varphi_{7,2}\}$, while the boundary variables are represented by the differences $\{\varphi_{8,3}, \varphi_{9,7}, \varphi_{10,8}, \varphi_{11,9}, \varphi_{8,7}\}$. Then, the

system of two equations (10) for two vertices a_1 and a_2 yields the matrix ($z_{i,j} = z_i - z_j$)

$$\|X_{i,j}\| = \begin{pmatrix} 0 & -z_{9,3} \\ z_{9,3} & 0 \end{pmatrix},$$

with $\det X_{i,j} = z_{9,3}^2 \neq 0$.

Now consider a complex with $M = 4$, representing a subcomplex of the complex in Fig. 4, composed of the triangles with numbers from 1 to 13. The internal and boundary difference variables are as follows: $\{\varphi_{10,1}, \varphi_{7,2}, \varphi_{8,3}, \varphi_{7,4}\}$ and $\{\varphi_{8,6}, \varphi_{9,7}, \varphi_{10,8}, \varphi_{11,9}, \varphi_{10,5}, \varphi_{11,6}\}$, respectively. In this case, the system of four equations (10) for four vertices a_1–a_4 yields the matrix

$$\|X_{ij}\| = \begin{pmatrix} 0 & -z_{9,3} & z_{7,2} & 0 \\ z_{9,3} & 0 & -z_{11,1} & 0 \\ -z_{7,2} & z_{11,1} & 0 & -z_{11,7} \\ 0 & 0 & z_{11,7} & 0 \end{pmatrix},$$

with $\det X_{i,j} = z_{9,3}^2 z_{11,7}^2 \neq 0$. Assuming that the statement is proved for an even number $M - 2$, let us check its validity for a complex with M internal variables.

Consider the case of reconstruction of the complex depicted in Fig. 4, whereby vertices a_5 and a_6 are sequentially rendered internal by adding triangles with numbers 14–16 and then 17 and 18. We may assume that vertices a_5 and a_6 are identified with a_{M-1} and a_M. Let the numbers of equations in the new system (10) correspond to the numbers of internal vertices. The old boundary variables of type $\varphi_{k_1, M-1}$ and $\varphi_{k_2, M}$, which have became internal in the modified complex, can be expressed through the new internal variables $\varphi_{k(M-1), M-1}$ and $\varphi_{k(M), M}$ and the new boundary variables. Thus, on the passage from a complex with $M-2$ internal vertices to the complex with M internal vertices in the new system of equations (10), only the $(M-2)$th equation contains nonzero coefficients $X_{M-2, M-1}$ and $X_{M-2, M}$. It is important to note that the other coefficients $X_{i,j}$ ($i, j = 1, \ldots, (M-2)$) remain unchanged. On the other hand, in the $(M-1)$th and Mth equations (see Fig. 4),

$$X_{M-1, j} = 0, \quad X_{M, j} = 0, \quad j = 1, 2, \ldots, (M-3).$$

Let us consider a linear combination of the two last rows in matrix $X_{i,j}$:

$$Y_j = c_{M-1} X_{M-1, j} + c_M X_{M, j}, \quad c_{M-1}^2 + c_M^2 > 0.$$

Since vertices a_{M-1} and a_M are adjacent, it can be readily checked that $(Y_{M-1}^2 + Y_M^2) > 0$. Assume that

$$Y_j = \sum_{i=1}^{M-2} c_i X_{i,j}, \quad 1 \leq j \leq M, \qquad (11)$$

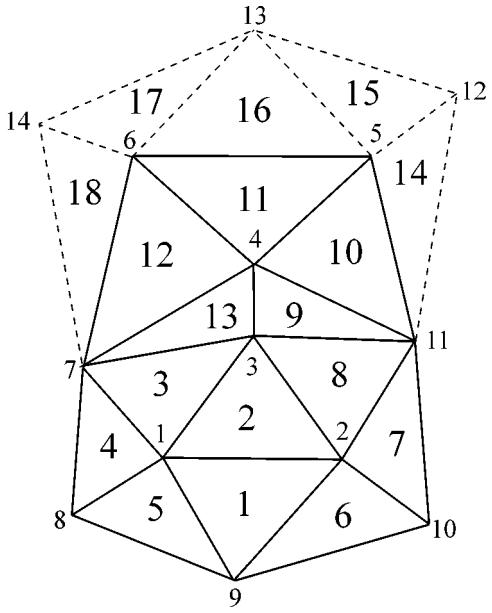

Fig. 4.

where c_i are certain coefficients. There are two possibilities:

(i) $Y_j = 0$, $1 \leq j \leq (M-2)$. Then, by virtue of the inductive assumption and conservation of the matrix $X_{i,j}$, $1 \leq i, j \leq (M-2)$ on the transition $(M-2) \longrightarrow M$, the equality (11) for $1 \leq j \leq (M-2)$ requires that $c_1 = \ldots = c_{M-2} = 0$. However, in that case condition (11) is not satisfied for $j = (M-1)$ and M.

(ii) $Y_{M-2} \neq 0$. In this case, as can be seen from Fig. 4, $c_{M-3} \neq 0$ and, hence, $c_{M-4} \neq 0$. This indicates a contradictory character of (11). Indeed, $Y_j = 0$ for $j = 1, \ldots, M-4$, while the corresponding terms in the right-hand part of (11) can be equal to zero only provided that $c_1 = \ldots = c_{M-4} = 0$.

Thus, equality (11) cannot be satisfied and, hence, the above statement is valid in the case depicted in Fig. 4.

In all other cases, the statement is proved similarly. In the course of inductive consideration, it is only important that the vertices a_{M-1} and a_M be adjacent.

In the case of complexes with an odd number of internal vertices, the statement is incorrect in terms of the variables employed. However, upon insignificant modification of these variables, an analogous statement can be formulated and proved. This will be done in a more extended publication.

At this stage, we should formulate a clearer criterion of the presence of Wilson's doubling. Let us assume that the number M of independent internal variables in system (10) and the corresponding number of independent boundary variables can be selected so that the total number of independent variables is smaller than $M + L - 1$. Then, the vanishing of boundary variables in system (10) does not imply that all the differ-

ence variables $\varphi_{i,j}$ for the internal vertices a_i and a_j vanish. In this case, Wilson's doubling take place. This criterion is applicable to a part of the complex as well. For example, for the part of the complex restricted to 2 internal and 8 boundary vertices in Fig. 2 (enumerated 1 to 10), the system of two Eqs. (10) contains only 7 independent difference variables: 2 internal ($\varphi_{1,7}$ and $\varphi_{2,3}$) and 5 boundary ($\varphi_{5,3}$, $\varphi_{9,7}$, $\varphi_{4,6}$, $\varphi_{10,6}$, $\varphi_{8,6}$). The total number of independent difference variables in this subcomplex is 9. Owing to system (10), the vanishing of the aforementioned 5 boundary variables implies the vanishing of internal variables $\varphi_{1,7}$ and $\varphi_{2,3}$, but not of $\varphi_{1,2}$, which, according to our criterion, is evidence of Wilson's doubling. For an arbitrarily large subcomplex of the complex depicted in Fig. 2, the result is the same.

It can be readily seen that, in an odd lattice, the system of Eqs. (10) necessarily contains all $M + L - 1$ independent difference variables. This follows from the identity

$$\varphi_{j(i)+1,\,j(i)} \equiv \sum_{0 \le k \le (n-1)/2} \varphi_{j(i)+2k+2,\,j(i)+2k}, \qquad (12)$$

where n is the (odd) number vertices on the boundary $\partial\mathfrak{A}_i$. Equation (12) shows that any difference variables can be expressed through the difference variables entering into system of Eqs. (8). Therefore, the vanishing of all boundary variables in system (10) implies the vanishing of all variables $\varphi_{i,j}$.

This result can be alternatively formulated as follows. Let us consider a system of Eqs. (8) for finite subcomplexes of an odd complex with M internal vertices. Let vertex a_i and at least one of the vertices $a_{j(i)}$ and $a_{j(i)-2}$ be internal. For the odd complex, there exist M independent variables of type $\varphi_{j(i),j(i)-2}$, entering into system (8), through which all the difference variables of type $\varphi_{i,j}$ can be expressed, with the minor determinant of these variables being nonzero. Indeed, in an odd complex, the transition from an independent system of regular internal variables to an independent system of variables of type $\varphi_{j(i),j(i)-2}$ reduces to a linear nondegenerate transformation of variables.[2] Therefore, as $M \longrightarrow \infty$, the minors of all independent sets of variables $\{\varphi_{j(i),j(i)-2}\}$, through which all the difference variables of type $\varphi_{i,j}$ are expressed in the finite part of the complex, are nonzero. Thus, we arrive at an important result:

Statement 2. *Wilson's doubling does not take place on odd complexes.*

4. ANOTHER APPROACH

Let us consider an interesting qualitative reasoning in favor of the absence of Wilson's doubling on the amorphous lattice considered above.

[2] Such a transformation of variables is impossible for the complex depicted in Fig. 2.

Assume that the field ψ_i varies very slowly on the passage to neighboring sites, so that the field ψ_i can be considered as a sufficiently smooth function of coordinates z. Then,

$$\psi_j = \psi_i + (z_j - z_i)\partial_z\psi_i + (\bar{z}_j - \bar{z}_i)\partial_{\bar{z}}\psi_i + \ldots,$$

where (..) stands for the contribution of higher derivatives of the field ψ. Taking into account the relations

$$\sum_{j(i)} (z_{j+1} - z_{j-1})z_j = 0,$$
$$\sum_{j(i)} (z_{j+1} - z_{j-1})\bar{z}_j = 4iS_i, \qquad (13)$$

Eqs. (6) or (6a) and (6b) for the eigenmode can be written as

$$i\gamma^a\partial_a\psi + \alpha^a_{bc}(z,\bar{z})\gamma^a\partial_b\partial_c\psi + \ldots = \epsilon\psi, \qquad (14)$$

where (…) stands for the contribution of the third and higher derivatives of the field ψ. The quantities $\alpha^a_{bc}(z,\bar{z})$ are random functions depending on the arrangement of lattice sites. It should be emphasized that Eq. (14) is valid for the long-wave soft modes "growing" above the trivial zero mode.

An analogous equation for the soft modes "growing" above the nontrivial zero modes (if such exist) appears as

$$i\sum_{\xi = ',\,'',\,\ldots} \alpha^{a(\xi)}_b(z,\bar{z})\gamma^a\partial_b\psi^{(\xi)}(a_i) + \ldots = \epsilon\psi(a_i), \qquad (15)$$

where (…) stands for the contribution of the second and higher derivatives of the field ψ, and the quantities $a^{a,(',\,'',\,\ldots)}_b(z,\bar{z})$ are random functions depending on the arrangement of lattice sites, for which $\sum_{\xi = ',\,'',\,\ldots} \alpha^{a(\xi)}_b(z,\bar{z}) = \delta^a_b$. Thus, the random factor in Eq. (15) is always on the order of unity. The form of this equation is related to the fact that separate sums with respect to the primed, double-primed, etc., vertices obey the conditions (cf. Eq. (13)) $\sum_{j'(i)} (z_{j'+1} - z_{j'-1})z_{j'} \neq 0$ and to the fact that the sums $\sum_{j'(i)} (z_{j'+1} - z_{j'-1})\bar{z}_{j'}$ are not proportional to the area S_i.

Based on the theory of wave propagation in disordered media, we may conclude (see, e.g. [9]) that the solutions to Eq. (15) are qualitatively different from plane waves. On the contrary, the contribution of higher derivatives to the solution of Eq. (14) in the long-wave limit decreases. We may ascertain that long-wave soft modes are "growing" above the trivial zero modes. No such conclusion can be derived for the nontrivial zero modes if $\partial_a\psi^{(')} \neq \partial_a\psi^{('')} \neq \ldots$. In this case, according to Eqs. (14) and (15), the properties of soft modes "grow-

ing" above the trivial and nontrivial zero modes are qualitatively different, which excludes Wilson's doubling.

Thus, the physically acceptable soft modes "growing" above nontrivial zero modes can exist only provided that $\partial_a\psi^{(\prime)} = \partial_a\psi^{(\prime\prime)} = \ldots$ and that each of the branches $\psi^{(\prime)}$, $\psi^{(\prime\prime)}$, … satisfies equations of type (14). Since $(\psi^{(\prime)} - \psi^{(\prime\prime)}) = \text{const} \neq 0$, a solution satisfying Eq. (6) leads to the limitation of the entire $2(M + L)$-dimensional space of variables $\{z_i\}$ to a $2(M + L - N + s - 1)$-dimensional subspace, where N is the number of internal odd vertices of the complex and s is the number of branches of the nontrivial zero mode. Indeed, the corresponding branches of the nontrivial zero mode obey the conditions $\varphi' = c'$, $\varphi'' = c''$, etc. Then each internal odd vertex a_i ($i = 1, \ldots, N$) yields an equation of the type

$$c'\sum_{j'(i)} z_{j'+1,\,j'-1} + c''\sum_{j''(i)} z_{j''+1,\,j''-1} = 0. \qquad (16)$$

Excluding a finite (equal to s) number of constants c', c'', … from system (16), we obtain additionally $N - s + 1$ equations connecting variables $z_{i,f}$, which accounts for the limitation of the entire space of variables $\{z_i\}$.[3] In the initial statistical sum, this subspace is of measure zero and, hence, nontrivial zero modes are insignificant. Thus, we arrive again at the same conclusion that Wilson's doubling is impossible on odd amorphous lattices.

5. CONCLUSION

Now, we can formulate the conclusion that, in the model under consideration, all bilinear forms with respect to the fermion field in the long-wave limit contain a single component. More precisely, this means the possibility of introducing a single Weyl field, with the the single Weyl field (rather than the Dirac field) remaining in the continuous limit. This can be achieved with the aid of the well-known projection operators. For example, in separating the φ component of the Dirac field in action (2), we should make substitutions $\bar\psi \longrightarrow \bar\psi\,[1/2(1 + \gamma^5)]$, $\psi \longrightarrow [1/2(1 - \gamma^5)]\psi$.

The author is grateful to A. Ioselevich, S. Savchenko, G. Volovik, and R. Zaitsev for fruitful discussions and to E. Kuznetsov and P. Grinevich for useful critical remarks.

This study was supported by the Russian Foundation for Basic Research, Leading Scientific Schools Program, project no. 00-1596579.

REFERENCES

1. S. N. Vergeles, Zh. Éksp. Teor. Fiz. **120**, 1069 (2001) [JETP **93**, 926 (2001)].
2. K. G. Wilson, *Erice Lecture Notes* (1975).
3. J. Kogut and L. Susskind, Phys. Rev. D **11**, 395 (1975).
4. L. Susskind, Phys. Rev. D **16**, 3031 (1977).
5. H. B. Nielsen and M. Ninomiya, Nucl. Phys. B **185**, 20 (1981); Nucl. Phys. B **193**, 173 (1981).
6. M. Luscher, hep-th/0102028.
7. L. S. Pontryagin, *Foundations of Combinatorial Topology* (Nauka, Moscow, 1976); P. J. Hilton and S. Wylie, *Homology Theory, an Introduction to Algebraic Topology* (Cambridge Univ. Press, Cambridge, 1960; Mir, Moscow, 1966).
8. S. P. Novikov and I. A. Dynnikov, Usp. Mat. Nauk **52**, 175 (1997).
9. I. M. Lifshits, S. A. Gredeskul, and L. A. Pastur, *Introduction to the Theory of Disordered Systems* (Nauka, Moscow, 1982; Wiley, New York, 1988); B. I. Shklovskiĭ and A. L. Efros, *Electronic Properties of Doped Semiconductors* (Nauka, Moscow, 1979; Springer-Verlag, New York, 1984).

Translated by P. Pozdeev

[3] Note that if the vertex a_i were even, the set of vertices with the indices $j(i)$ could be separated into two subsets with the indices $j'(i)$ and $j''(i)$ such that $\sum_{j'(i)} z_{j'+1,\,j'-1} \equiv 0$ and $\sum_{j''(i)} z_{j''+1,\,j''-1} \equiv 0$. In this case, Eq. (16) would be identically satisfied, leading to no relations between the variables z_j.

JETP Letters, Vol. 76, No. 1, 2002, pp. 11–16. From Pis'ma v Zhurnal Éksperimental'noĭ i Teoreticheskoĭ Fiziki, Vol. 76, No. 1, 2002, pp. 14–19.

Magnetic Field Rectifiers Using Semicircular Josephson Junctions[1]

P. D. Shaju and V. C. Kuriakose

Department of Physics, Cochin University of Science and Technology, Cochin, 682022 India

e-mail: pds@cusat.ac.in; vck@cusat.ac.in

Received April 15, 2002

Abstract—A novel method for rectifying alternating magnetic fields is demonstrated using fluxons in semicircular Josephson junctions. An external magnetic field applied parallel to the dielectric barrier of the semicircular junction has opposite polarities at the ends of the junction and supports penetration of opposite polarity fluxons into the junction in the presence of a constant dc bias. When the direction of the field is reversed, flux penetration is not possible and a flux-free state exists in the junction. Thus, effective rectification of an alternating magnetic field can be achieved in semicircular Josephson junctions. This unique phenomenon is specific to this geometry and can be employed in rf SQUID magnetometers. *© 2002 MAIK "Nauka/Interperiodica".*

PACS numbers: 85.25.Cp; 74.50.+r

Two superconductors separated by a thin oxide layer are called a Josephson junction (JJ), which allows the superconducting Cooper pairs to tunnel through the barrier [1]. Long JJs offer the possibility of studying solitons that account for the magnetic-flux quanta (fluxons) moving along the tunnel barrier [2]. A fluxon is basically a quantum of magnetic field which can be used for the transmission of information or can be an object based on which certain Josephson devices such as flux-flow oscillators [3], voltage rectifiers [4], logic gates [5], etc. can be implemented. Fluxons can be trapped in the junction either during the normal–superconducting transition or by applying an external magnetic field to the junction. In the superconducting state, only fluxons or antifluxons can exist in the junction [6], and they are driven by the Lorentz force associated with a dc current. Different geometries are proposed for JJ to study the fluxon dynamics, and, among them, annular geometries offer the advantage of reflectionless motion of fluxons and are extensively studied both theoretically and experimentally [7]. In the absence of an external magnetic field, trapped fluxons cannot escape from a linear junction, and they make successive reflections at the edges of the junction [8]. Progressive fluxon motion in JJ is associated with a dc voltage which can be detected across the junction.

Josephson junctions are the best transducers that can convert magnetic energy into electrical energy. They are widely used in SQUID magnetometers [9], SIS mixers [10], and in voltage standard applications [11]. Recently, fluxon-based voltage rectifiers [4, 12] have attracted much attention due to the fact that they can find important applications in Josephson digital devices [13]. Various geometries and external conditions are investigated towards this end [14]. The influence of an artificially created ratchet potential on fluxon dynamics in nonuniform JJ has been studied, and voltage rectification properties of these JJs are demonstrated in recent papers [15]. The net unidirectional motion exhibited by a particle in a ratchet potential is the key factor which is employed in rectifying bias currents. However, the working of all these voltage rectifiers critically depend on the ratchet potential and we cannot expect stable performance from these devices, because ratchet potentials are highly sensitive to external perturbations. Amplitude ranges of rectification are limited in these devices, and the rectified output in these devices does not have a linear relationship with the input. In all these works, rectification properties are studied using alternating bias currents, and effective ways of rectifying alternating magnetic fields are not discussed.

In this letter, we demonstrate a novel method to construct fluxon-based diodes for rectifying harmonically oscillating magnetic fields. Investigations on a dc biased semicircular JJ placed in an alternating magnetic field applied parallel to the plane of the dielectric barrier shows that the junction supports flux flow only in alternate half cycles of the field. The fluxes linked to the edges of the junction have opposite polarities and support the penetration of fluxons and antifluxons simultaneously from the opposite ends of the junction under a constant dc bias. When the direction of the field is reversed, flux penetration is not possible and a flux-free state exists in the junction. Thus, with this geometry, effective rectification of oscillating fields can be achieved. This is a unique phenomenon associated with semicircular junctions. In this letter, we first formulate the model equations corresponding to the proposed

[1] This article was submitted by the authors in English.

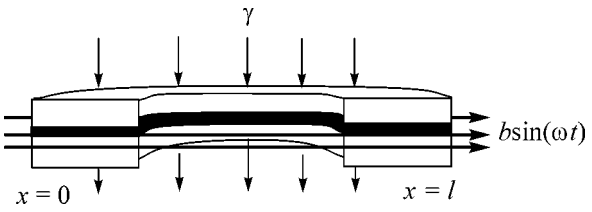

Fig. 1. A sketch of the semicircular JJ with the applied field $b\sin(\omega t)$ parallel to the plane of the dielectric barrier of uniform thickness (not drawn to scale).

junction with an applied alternating magnetic field and study the behavior of the junction in static fields and then in time-varying fields to demonstrate rectification properties.

Theoretical model. A JJ with a semicircular geometry is considered with an external harmonically varying magnetic field applied parallel to the dielectric barrier of uniform thickness (see Fig. 1). The external field is applied in such a way that it is directed radially at the left end ($x = 0$) of the junction. The field interacts with the interior as well as through the boundaries of the junction, and the flux linked to the junction can be expressed as $d\varphi(x) = \varepsilon(\bar{H}(t) \cdot \bar{n}) = \varepsilon H\sin(\omega t)\cos(kx)dx$ [16], where H is the strength of the applied magnetic field, $\bar{n}$ is the unit vector normal to the junction plane, ε is the coupling factor which links the external field to the junction, $k = \pi/l$ is the geometrical constant defining the magnetic field inside the semicircular junction, the spatial coordinate x is normalized to λ_J (Josephson penetration depth), and l ($\gg\lambda_J$) is the normalized length of the junction. The time t is normalized to the inverse plasma frequency, $\omega_0 = \tilde{c}/\lambda_J$, $\tilde{c}$ is the maximum velocity of the electromagnetic waves in the junction, and ω is the normalized frequency of the oscillating field. Therefore, the field-induced current in the junction is $d\varphi(x)/dx = \varepsilon H\sin(\omega t)\cos(kx)$. This current term gives a net zero value over the length of the junction and, therefore, circulates in closed form across the junction. Thus, the effect of an external field in the junction is to induce spatially varying currents. Thus, a semicircular JJ under a time-varying magnetic field with a dc bias is modeled with the general perturbed sine-Gordon (SG) partial differential equation [16, 17]

$$\varphi_{tt} - \varphi_{xx} + \sin\varphi = -\alpha\varphi_t + b\sin(\omega t)\sin(kx) - \gamma, \quad (1)$$

where $\varphi(x, t)$ is the superconducting phase difference between the electrodes of the junction, α is the dissipation parameter due to the quasiparticle current, $b = \varepsilon Hk$, and γ is the normalized amplitude of the dc bias. The boundary conditions of the junction can be obtained from the induced current term $d\varphi(x)/dx = \varepsilon H\sin(\omega t)\cos(kx)$ as

$$\varphi_x(0, t) = \frac{b}{k}\sin(\omega t); \quad \varphi_x(l, t) = -\frac{b}{k}\sin(\omega t). \quad (2)$$

These boundary conditions are consistent with the fact that the effective field linked to the junction has opposite polarities at the ends. For sufficiently higher positive values of γ in Eq. (1), fluxons can enter the junction from $x = 0$, and antifluxons can enter the junction from $x = l$ (right end) and can move in opposite directions. The propagation of the fluxons in one direction and antifluxons in the opposite direction produce a nonzero voltage across the junction. As the boundary conditions are not reflective, after a transitory motion, fluxons and antifluxons exit from the junction. When the direction of the field is reversed, fluxon (or antifluxon) penetration becomes impossible, and a flux-free state exists in the junction.

Equation (1) with boundary conditions [Eq. (2)] represents a semicircular JJ in an alternating magnetic field. In the absence of perturbations ($\alpha = b = \gamma = 0$), Eq. (1) becomes the SG equation, which is a conservative nonlinear dispersive wave equation that supports special solutions called solitons. A SG soliton is a localized wave with particle-like properties and analytically described by the formula [17]

$$\varphi(x, t) = 4\tan^{-1}\left[\exp\left\{\frac{\sigma(x - x_0)}{\sqrt{1 - u^2}}\right\}\right], \quad (3)$$

where $x_0 = ut + x_0'$ is the location of the soliton, with u being the velocity of the soliton, and x_0' as the initial location center; $\sigma = \pm 1$ is the polarity of the soliton. A long JJ could support the resonant propagation of fluxons trapped in the junction, the fluxon being a 2π jump in the phase difference φ across the insulating barrier separating the two superconductors. There are two possible orientations for the flux. A flux quantum with $\sigma = +1$ is called fluxon and that with $\sigma = -1$ is called antifluxon. A moving fluxon is accompanied by a voltage pulse φ_t, which can be detected across the junction.

To get some information on the fluxon dynamics, we first determine the potential induced by the external field inside the junction and then find the energy change associated with a moving fluxon in the junction. The Lagrangian density of Eq. (1) with $\alpha = \gamma = 0$ is

$$\mathbf{L} = \left\{\frac{\varphi_t^2}{2} - \frac{1}{2}\left(\varphi_x - \frac{b}{k}\sin(\omega t)\cos(kx)\right)^2 - (1 - \cos\varphi)\right\}. \quad (4)$$

Therefore, the corresponding potential energy density is (second term of the above equation)

$$\mathbf{U}_{x,t} = \frac{1}{2}\left\{\varphi_x^2 - \frac{2b}{k}\sin(\omega t)\cos(kx)\varphi_x + \left(\frac{b}{k}\sin(\omega t)\cos(kx)\right)^2\right\}. \quad (5)$$

The first term is independent of the applied field, and the third term is independent of the flux motion in the junction. Therefore, the change in the potential due to the combined effect of applied field and flux motion in the junction can be determined from the second term as

$$U(x, t) = -\frac{b}{k}\int_{-\infty}^{+\infty}\varphi_x \sin(\omega t)\cos(kx)dx. \quad (6)$$

Substituting Eq. (3) in (6) and integrating, we get

$$U(x_0, t) = -2bl\,\mathrm{sech}\left(\frac{\pi^2}{2l}\sqrt{1-u^2}\right)\sin(\omega t)\cos(kx_0). \quad (7)$$

For long junctions and relativistic velocities, $u \sim 1$, Eq. (7) becomes

$$U(x_0, t) = -C\sin(\omega t)\cos(kx_0), \quad (8)$$

where $C = 2bl$ is a constant. Equation (8) shows that the potential is oscillating at the frequency of the applied field. This oscillating potential controls the flux flow inside the junction and helps in the rectification of the field.

The energy of the unperturbed SG system is

$$H^{SG} = \int_0^l \left[\frac{1}{2}(\varphi_t^2 + \varphi_x^2) + 1 - \cos\varphi\right]dx. \quad (9)$$

Perturbational parameters modulate the soliton velocity and may cause energy dissipation. The rate of dissipation is calculated by computing

$$\frac{d}{dt}(H^P) = [\varphi_x\varphi_t]_0^l + \int_0^l [-\alpha\varphi_t^2 + (b\sin(\omega t)\sin(kx) - \gamma)\varphi_t]dx, \quad (10)$$

where the first term on the right-hand side accounts for the boundary conditions. From Eq. (3), we get $\varphi_t = -u\varphi_x$, and from Eq. (2) we get $\varphi_x^2(0, t) = \varphi_x^2(l, t)$ (symmetric boundary conditions). Substituting these expressions, we find that the first term in the right-hand side of the above equation vanishes; i.e., a symmetric boundary condition does not change the average energy of a fluxon. Inserting Eq. (3) in Eqs. (9) and (10) and following perturbative analysis [17], we get

$$(1-u^2)^{-3/2}\frac{du}{dt} = -\alpha\frac{u}{\sqrt{1-u^2}} - \frac{\pi}{4}\left\{b\,\mathrm{sech}\left[\frac{\pi^2\sqrt{1-u^2}}{2l}\right]\sin(\omega t)\sin(kx_0) - \gamma\right\}. \quad (11)$$

This expression describes the effect of perturbations on the fluxon velocity. In the above equation, the first term in the right-hand side represents the energy dissipation due to the internal damping, the second term accounts for the energy change associated with the external field, and the third term represents the input power from the bias current.

The effects of a dc current on the fluxon dynamics in the presence of an external field is studied using Eq. (11). The zero-voltage state exists in the junction (flux-free state) when the dc bias is below its threshold value. By varying the soliton position x_0, we find from Eq. (11) the largest possible bias current of the zero-voltage state ($u = 0$) to be [18]

$$\gamma_1 = b\,\mathrm{sech}(\pi^2/2l). \quad (12)$$

This is the threshold value of the applied bias, below which the flux propagation is impossible in the junction. This threshold value depends on the magnetic field and is directly proportional to the field.

Numerical methods. To solve Eq. (1) with boundary conditions given by Eq. (2), we use an explicit method treating φ_{xx} using a five-point, φ_{tt} with a three-point, and φ_t with a two-point finite-difference method. A time step of 0.0125 and a space step of 0.025 are used for the discretization. Details of the simulation can be found in [18]. After the simulation of the phase dynamics for a transient time, we calculate the average voltage V at the load over a period of the field T as

$$\langle V\rangle = \frac{1}{T}\int_0^T \varphi_t(l)dt = \frac{\varphi(T) - \varphi(0)}{T}.$$

The average velocity attained by the fluxons during the transit can be calculated from the average voltage using the relation $\langle u\rangle = (l/2\pi)\langle V\rangle = (l/2\pi)\langle\varphi_t\rangle$. Thus, the mean voltage in the junction is proportional to the average velocity of the fluxons. Voltage rectification can be clearly demonstrated using the time-domain snapshots of the instantaneous voltages, $v(t) = \varphi_t(l, t)$, in the junction. These voltage pulses are measured at intervals of $t = 4$ time units, and, to get smooth curves, we additionally averaged the pulses in those intervals. The time period of the ac signals is taken much larger than the typical response time of the system. In the following simulations, we assumed the dissipation parameter $\alpha = 0.1$.

Properties of the junction under a static field. It is important in practical applications to know the behavior of the junction under a static magnetic field, especially the dependence of critical current (I_c) on the applied field (H) [19]. In weak static magnetic fields, long JJs behave like weak superconductors and show the Meissner effect. In this regime, the critical current decreases linearly with the external field. This behavior exists up to a critical field H_c. At this critical field, magnetic flux in the form of fluxons overcomes the edge barrier effects and can penetrate the junction [20]. For long JJs, the first critical field is $H_c = \Phi_0/\pi\Lambda\lambda_J$, where Λ is the effective magnetic thickness of the junction and $\Phi_0 = h/2e = 2.064 \times 10^{-15}$ Wb is the flux quantum. The

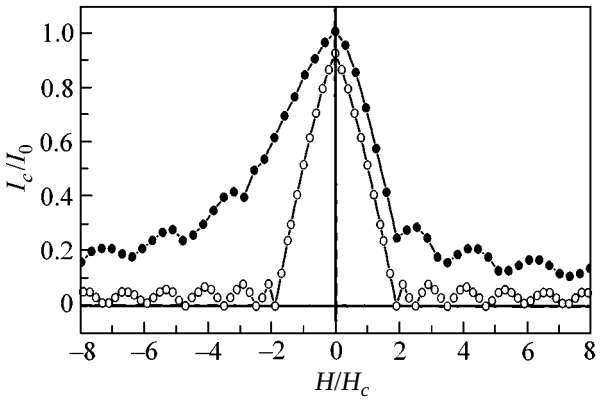

Fig. 2. Normalized critical current (I_c/I_0) vs. static magnetic field (H/H_c) of a (●) semicircular JJ and (○) rectangular JJ.

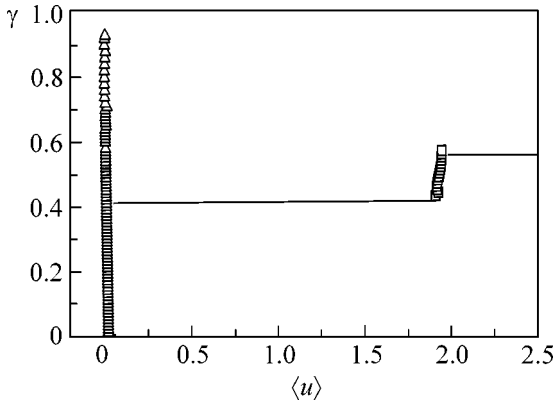

Fig. 3. Applied dc bias γ vs. average normalized velocity $\langle u \rangle = -(l/2\pi)\langle \varphi_t \rangle$ of a semicircular junction with $l = 20$ for the static field b = (□) +0.15 and (△) –0.15.

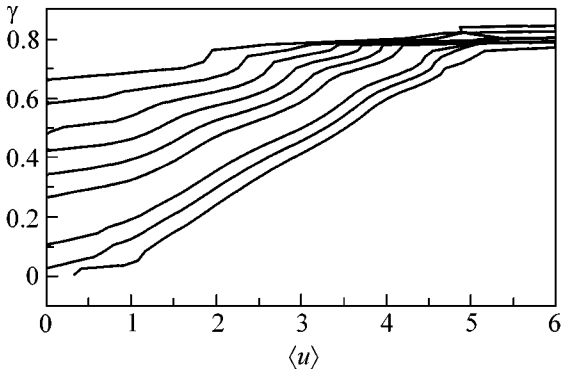

Fig. 4. Applied dc bias γ vs. average normalized velocity $\langle u \rangle$ for different values of the applied rf field. The parameters are $l = 10$ and $\omega = 0.1$. The applied field strength increases from the top to the bottom curve from 0.50 to 1.50 in steps 0.1.

dependence of I_c (normalized to the maximum Josephson current I_0) on a static magnetic field (H/H_c) applied to a semicircular JJ with $l = 10$ is shown in Fig. 2 (solid circles). For comparison, the critical current vs. magnetic field pattern of a standard rectangular JJ is presented (open circles). In positive magnetic fields, the $I_c(H)$ pattern in semicircular JJ shows that static fluxons can exist in the junction and a minimum critical current is required to induce flux motion in the junction. In negative fields, the junction behaves differently; the critical current pattern is displaced and indicates that higher critical currents are required to induce flux motion in the junction.

In the absence of an external field ($b = 0$), the fluxon dynamics in semicircular JJ is the same as in any ordinary rectangular junction. When an external static magnetic field is applied, due to the opposite polarities of the flux linked to the ends of the junction, the opposite-polarity fluxons can enter the junction from the ends in a properly biased state. In the junction, fluxons and antifluxons move in opposite directions under the influence of the dc bias. When they reach the junction ends after a transit, they exit from the junction due to the nonreflecting boundary conditions. When the direction of the external field is reversed, fluxon penetration is possible due to the repulsive Lorentz force of the dc bias, and zero voltage corresponding to the flux-free state exists in the junction. This typical characteristic demonstrates that the semicircular junctions offer the advantage of rectifying alternating magnetic fields. The rectification property of the junction can be observed from Fig. 3, where we plot the IVC of a semicircular junction of length $l = 20$ with a static magnetic field of strength $b = +0.15$ (squares) and -0.15 (triangles). To get these plots, we calculate the average voltage for a current γ, then the current γ is increased in steps $\delta\gamma = 0.01$ to calculate the voltage at the next point of the IVC. We use the distribution of phases and their derivatives achieved in the previous point of the IVC as the initial distribution for the following point. For positive values of b, flux propagation is possible, and we get finite average voltage across the junction. In this regime, the junction behaves as a forward-biased diode. At small positive bias values, a fluxon–antifluxon pair is found to take part in dynamics and the dynamics of this pair gives an average velocity $\langle u \rangle \simeq 2$. The pair executes stable dynamics in a range of bias values. At higher values of the bias, a large number of fluxons enter the junction, resulting in a switch to high-voltage states. For negative values of b, the flux penetration and propagation is impossible and a zero-voltage state exists in the junction, which is equivalent to the reverse-biased state of a diode.

IVC in rf fields. An oscillating magnetic field is applied parallel to the dielectric barrier of the junction with a constant dc bias. In the positive half cycles of the applied field, flux penetration and propagation is possible and finite voltages are observed across the junction. In the negative half cycles of the field, fluxons (or antifluxons) cannot enter the junction due to the repulsive Lorentz force, and a zero voltage exists in the junction. Simulations are started with $\varphi = 0$ on a junction of $l = 10$. Figure 4 shows the IVC of the junction for different

values of oscillating field amplitudes and at a constant frequency ($\omega = 0.1$). In the figure, the applied magnetic field increases from the top to the bottom curve in the range from 0.50 to 1.50 with steps 0.1. At lower magnetic fields, critical currents for fluxon penetration are large and the critical current gradually decreases on increasing the field strength.

Rectification of alternating fields. To demonstrate the rectification properties of the junction, we show a series of plots showing the time-domain snapshots of voltage pulse shapes $v(t)$ as a function of time t. The field magnitude should be sufficiently large to introduce fluxons into the junction. At small magnetic fields, fluxons cannot enter the junction and zero voltage exists. For sufficiently higher amplitudes (e.g., $b = 1.0$), fluxon penetration is possible in the positive half cycles, and we get a finite voltage in the junction (see Fig. 5). The rectification takes place in the following way. In the first half (positive part) of the alternating field, fluxons enter from the left end and antifluxons enter from the right end, and they move in opposite directions under the influence of the dc bias. The fluxon motion in opposite directions produces a finite voltage across the junction. During the second half (negative part) of the magnetic field, antifluxon (or fluxon) penetration is impossible due to the repulsive Lorentz force, and a zero voltage (flux-free state) exists in the junction. Thus, effective rectification of the field can be achieved in semicircular Josephson junctions. The number of fluxons involved in the dynamics (and, therefore, the output voltage) can be controlled by controlling the magnetic field strength.

In Fig. 6, we plot the average velocity (averaged over the field period) as a function of the field magnitude for different lengths of the junctions. A constant dc bias is applied to the junction in order to maintain flux motion in the alternate half cycles. In the figure, the average voltage increases from zero and then increases linearly at higher values of the external field. Thus this device gives output that is linearly proportional to the input.

By reversing the dc bias (i.e., γ to $-\gamma$), the positive part of the alternating field can be suppressed. In this case, fluxons cannot enter the junction during positive half cycles of the field due to the repulsive Lorentz force, while flux penetration and propagation are possible in the negative half cycles. In Fig. 7, we show rectification in a junction with $l = 20$ and $\gamma = -0.5$. Thus, by choosing the appropriate dc bias, either the positive part or the negative part of the alternating field can be rectified.

In conclusion, this letter contains theoretical predictions of the rectification of harmonically oscillating rf fields using fluxons in semicircular JJs. This device may find important applications in submillimeter radio wave astronomy, SQUID magnetometers, SIS mixers, etc. The main advantages of the proposed diode are that (i) it is very simple to produce, (ii) the output of the

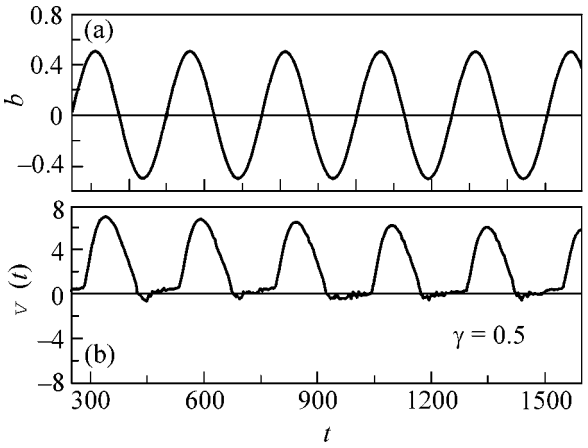

Fig. 5. Rectification of an rf field with $\gamma = 0.5$ on a junction of $l = 10$. (a) Applied field of amplitude $b = 1.0$ and frequency $\omega = 0.05$. (b) Output pulse form $v(t)$ as a function of time t.

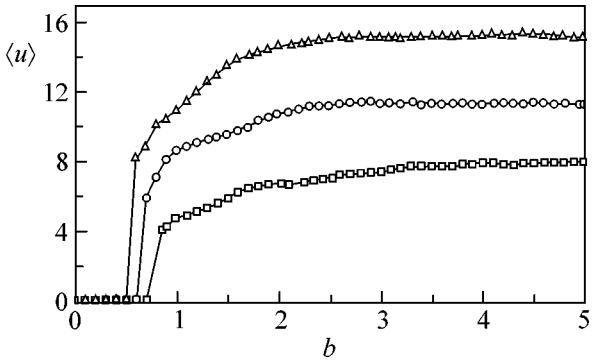

Fig. 6. Magnetic-field amplitude b vs. average velocity $\langle u \rangle$ for different junctions. The parameters are $\omega = 0.05$, $\gamma = 0.5$, and $l = (\square)$ 10, $(\circ)$ 15, and $(\triangle)$ 20.

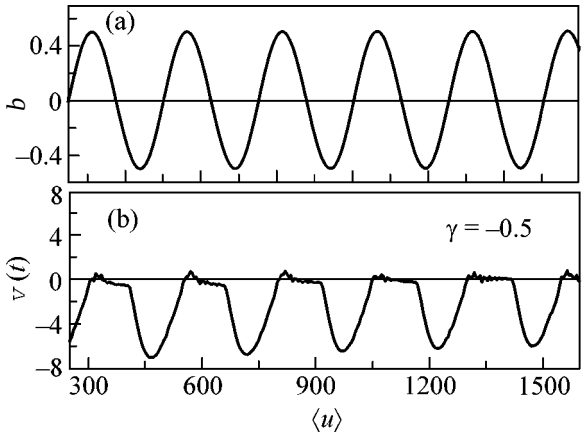

Fig. 7. Rectification on a junction of $l = 10$ with $\gamma = -0.5$. (a) Applied field of amplitude $b = 1.0$ and frequency $\omega = 0.05$. (b) Output pulse shape showing negative pulses.

device is linearly proportional to the applied field, (iii) the flux motion takes place only in alternate half cycles so that heating and energy losses associated with flux motion can be reduced, and (iv) they are independent of external perturbations. In the proposed JJ diode, the fluxon velocity is proportional to the voltage, and a nonzero average velocity over a period of the rf field means rectification of the field. By properly selecting junction parameters and the dc bias, it is possible to rectify fields in different amplitude and frequency ranges. This geometry can also be used for the rectification of ac currents with the help of a static magnetic field.

The authors thank A.V. Ustinov, G. Carapella, and E. Goldobin for helpful discussions. One of the authors (PDS) is grateful to UGC, New Delhi, for financial support in the form of a Teacher Fellowship, and VCK replaced by acknowledges the Associateship of IUCAA, Pune.

REFERENCES

1. B. D. Josephson, Rev. Mod. Phys. **36**, 216 (1964).
2. A. V. Ustinov, Physica D (Amsterdam) **123**, 315 (1998).
3. *Nonlinear Superconducting Devices and High-Tc Materials*, Ed. by R. D. Parmentier and N. F. Pedersen (World Scientific, Singapore, 1995); A. V. Ustinov, H. Kohlstedt, and P. Henne, Phys. Rev. Lett. **77**, 3617 (1996).
4. G. Carapella and G. Costabile, Phys. Rev. Lett. **87**, 077002 (2001); G. Carapella, Phys. Rev. B **63**, 054515 (2001).
5. P. D. Shaju and V. C. Kuriakose, Physica C **322**, 163 (1999); P. D. Shaju and V. C. Kuriakose, Phys. Lett. A **267**, 420 (2000).
6. A. Davidson, B. Dueholm, B. Kryger, and N. F. Pedersen, Phys. Rev. Lett. **55**, 2059 (1985).
7. A. Davidson, B. Dueholm, B. Kryger, and N. F. Pedersen, Phys. Rev. Lett. **55**, 2059 (1985); A. V. Ustinov, T. Doderer, R. P. Huebener, *et al.*, Phys. Rev. Lett. **69**, 1815 (1992).
8. T. A. Fulton and R. C. Dynes, Solid State Commun. **12**, 57 (1973); K. Nakajima, T. Yamashita, and Y. Onodera, J. Appl. Phys. **45**, 3141 (1974); Yu. S. Kivshar and B. A. Malomed, Rev. Mod. Phys. **61**, 763 (1989).
9. J. Clarke, *The New Superconducting Electronics*, Ed. by H. Weinstock and R. W. Ralston (Kluwer, Dordrecht, 1993), p. 123.
10. J. R. Tucker and M. J. Feldman, Rev. Mod. Phys. **57**, 1055 (1985).
11. M. T. Levinsen, R. Y. Chiao, M. J. Feldman, and B. A. Tucker, Appl. Phys. Lett. **31**, 776 (1977); R. J. Kautz, C. A. Hamilton, and F. J. Lloyed, IEEE Trans. Magn. **23**, 883 (1987).
12. I. Zapata, R. Bartussek, F. Sols, and P. Hänggi, Phys. Rev. Lett. **77**, 2292 (1996); S. Weiss, D. Koelle, J. Muller, *et al.*, Europhys. Lett. **51**, 499 (2000); E. Trias, J. J. Mazo, F. Falo, and T. P. Orlando, Phys. Rev. E **61**, 2257 (2000).
13. K. K. Likharev and V. K. Semenov, IEEE Trans. Appl. Supercond. **1**, 3 (1991); A. V. Rylyakov, IEEE Trans. Appl. Supercond. **7**, 2709 (1997).
14. J. F. Wambaugh, C. Reichhardt, C. J. Olson, *et al.*, Phys. Rev. Lett. **83**, 5106 (1999).
15. E. Goldobin, A. Sterck, and D. Koelle, Phys. Rev. E **63**, 031111 (2001); F. Falo, P. J. Martinez, J. J. Mazo, and S. Cilla, Europhys. Lett. **45**, 700 (1999).
16. N. Grønbech-Jensen, P. S. Lomdahl, and M. R. Samuelsen, Phys. Lett. A **154**, 14 (1991); M. Salerno, M. R. Samuelsen, G. Filatrella, *et al.*, Phys. Lett. A **137**, 75 (1989); M. Salerno, M. R. Samuelsen, G. Filatrella, *et al.*, Phys. Rev. B **41**, 6641 (1990); N. F. Pedersen and A. Davidson, Phys. Rev. B **41**, 178 (1990); J. C. Fernandez, R. Grauer, K. Pinnow, and G. Reinisch, Phys. Lett. A **145**, 333 (1990).
17. D. W. McLaughlin and A. C. Scott, Phys. Rev. A **18**, 1652 (1978).
18. P. D. Shaju and V. C. Kuriakose, Mod. Phys. Lett. B **12**, 1217 (1998).
19. A. Barone and G. Paternó, *Physics and Applications of the Josephson Effect* (Wiley, New York, 1982; Mir, Moscow, 1984).
20. C. S. Owen and D. J. Scalapino, Phys. Rev. **164**, 538 (1967).

JETP Letters, Vol. 76, No. 1, 2002, pp. 17–20. From Pis'ma v Zhurnal Éksperimental'noĭ i Teoreticheskoĭ Fiziki, Vol. 76, No. 1, 2002, pp. 20–24.

Fluctuation Conductivity in Superconducting MgB_2¶

A. S. Sidorenko[1, 2], L. R. Tagirov[1, 3], A. N. Rossolenko[4], N. S. Sidorov[4], V. I. Zdravkov[2, 4], V. V. Ryazanov[4], M. Klemm[1], S. Horn[1], and R. Tidecks[1]

[1]*Institut für Physik, Universität Augsburg, D-86159 Augsburg, Germany*

e-mail: anatoli.sidorenko@physik.uni-augsburg.de

[2]*Institute of Applied Physics, Academy of Sciences of Moldova, Chisinau, 2028 Moldova*

[3]*Kazan State University, Kazan, 420008 Tatarstan, Russia*

[4]*Institute of Solid State Physics, Russian Academy of Sciences, Chernogolovka, Moscow region, 142432 Russia*

Received April 1, 2002; in final form, May 28, 2002

Abstract—According to the crystal structure of MgB_2 and band structure calculations, quasi-two-dimensional (2D) boron planes are responsible for the superconductivity. We report on critical-field and resistance measurements of 5.6-μm-thick MgB_2 films grown on a sapphire single-crystal substrate. Resistivity measurements yield a temperature dependence of the fluctuation conductivity above the critical temperature, which agrees with the Aslamazov–Larkin and Maki–Thompson theory of fluctuations in layered superconductors, indicating a quasi-two-dimensional nucleation of superconductivity in MgB_2. © *2002 MAIK "Nauka/Interperiodica".*

PACS numbers: 74.62.Bf; 74.70.Ad; 74.76.Db

Recent discovery [1] of superconductivity in magnesium diboride (MgB_2) raised questions about the origin and properties of superconductivity in this compound. MgB_2 has a hexagonal crystal structure with boron layers interleaved by magnesium layers. Band structure calculations [2, 3] indicate that electrons at the Fermi level are predominantly derived from boron atoms. MgB_2 can be regarded as a layered compound having sheets of metallic boron with strong covalent intralayer bonding, separated by Mg layers with ionic interlayer B–Mg bonding. The strong B–B bonding induces enhanced electron–phonon interaction, so that the superconductivity in MgB_2 is mainly due to the charge carriers in the boron planes.

Experimental investigations on single crystals and *c*-oriented epitaxial and textured films (see, e.g., the review [4] and references therein) give evidence for a highly anisotropic superconducting gap. Measured critical magnetic fields usually show a pronounced anisotropy for *c*-oriented films and single crystals [4]. Applying the anisotropic Ginzburg–Landau model to these measurements, authors derive an effective mass anisotropy for the charge carriers of $\gamma = \sqrt{m_{ab}/m_c} \approx 0.15$–$0.3$. Thus, the band structure calculations and experimental measurements strongly suggest that superconductivity nucleates at the quasi-two-dimensional (2D) boron planes and then extends through the magnesium layers by a nanoscale proximity effect forming an anisotropic 3D superconducting state in the material.

In this letter, we present experimental evidence for the quasi-2D nucleation of superconductivity in a 3D magnesium diboride film. To demonstrate this, we measured the temperature dependence of the excess conductivity caused by fluctuations above the critical temperature, T_c. If quasi-2D boron planes are responsible for the superconductivity, then the excess conductivity should exhibit 2D-like behavior, although measured in a 3D sample. We found that the temperature dependence of the excess conductivity agrees with the Aslamazov–Larkin (AL) [5] and Maki–Thompson (MT) [6] theory of superconducting fluctuations in layered superconductors [7].

The MgB_2 films were prepared by DC magnetron sputtering on a single-crystal (100)-oriented sapphire substrate according to the procedure described in [8]. To compensate losses of magnesium due to its oxidation in plasma, a composite target was used which contained MgB_2 and metallic magnesium in approximately equal amounts. A Mg–MgB_2 target was sputtered in a 99.999% purity argon atmosphere at a pressure of 3 Pa. The substrate temperature during sputtering was held at 200°C and than raised to 600°C for several seconds at the final stage. At this final *in situ* annealing, the plasma discharge was not switched off. Next, the films were annealed *ex situ* in a saturated Mg vapor atmosphere for 1 hour at 850°C. X-ray studies revealed a textured (101)-oriented structure of our polycrystalline films. The MgB_2 film thickness was about 5.6 μm. For the resistance and critical field measurements, 1.5-mm-wide stripes were cut by a diamond cutter.

¶This article was submitted by the authors in English.

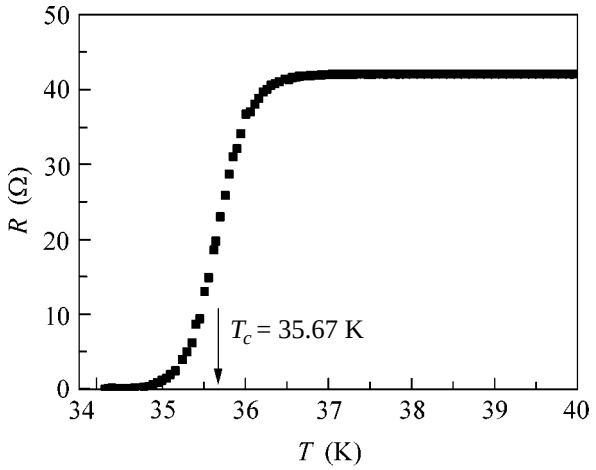

Fig. 1. Resistive transition $R(T)$ for a 5.6-μm-thick MgB_2 film in a zero magnetic field.

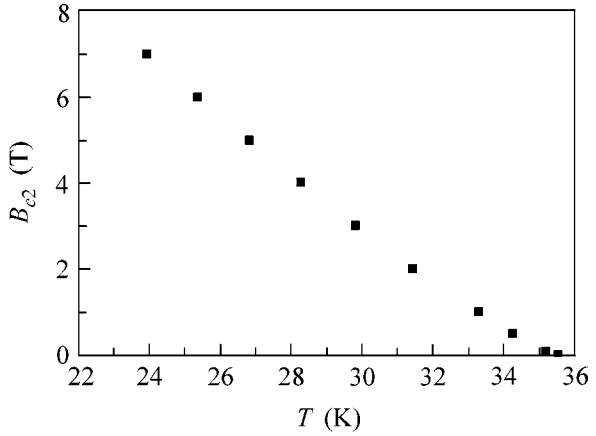

Fig. 2. The temperature dependence of the critical magnetic field $B_{c2}(T)$ perpendicular to the film plane obtained from the midpoints of $R(T)$.

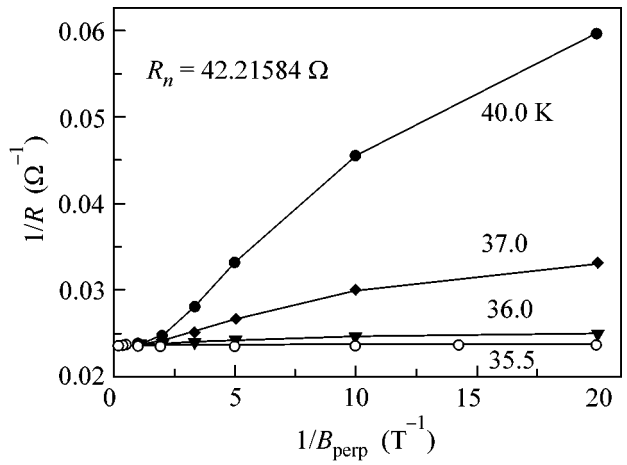

Fig. 3. Illustration of the procedure for determining the normal-state resistance of the MgB_2 film. Temperatures of measurements are indicated near the curves. Further reduction of the temperature gives results coinciding with the 35.5 K data.

The superconducting transition temperature T_c^{MP}, taken as the midpoint of the transition curve obtained by a conventional four-probe resistive method in the absence of an applied magnetic field, was about 35.7 K. The upper critical field perpendicular to the film plane was measured using the 7 T superconducting magnet of a Quantum Design MPMS-7 SQUID magnetometer.

The resistive transition, $R(T)$, in a zero magnetic field for one of the investigated samples is plotted in Fig. 1. The transition width according to a (10–90)% R_n criterion is about 0.8 K and slightly increases in a stronger magnetic field to about 1.5 K at 6 T. The temperature dependence of the critical field perpendicular to the film plane is displayed in Fig. 2. The temperature dependence of $B_{c2}(T)$ is linear except for temperatures very close to the critical temperature, where a slight positive curvature is observed. Several reasons may be responsible for the positive curvature such as anisotropy of the energy gap and proximity effect due to the weakly superconducting Mg interlayers in the MgB_2 compound [9, 10]. This nonlinear behavior of the perpendicular critical field is commonly observed in MgB_2 (see [4]).

Usually, a linear behavior of $B_{c2}(T)$ oriented parallel to the planes of a layered structure is used as an indicator of 3D superconductivity [11, 12], whereas a square-root behavior indicates 2D superconductivity. Since the MgB_2 film, according to X-ray data, is (101)-textured, the boron planes are inclined to the direction of the applied magnetic field at roughly 40°. Therefore, we have two components of the magnetic field of a comparable magnitude; one is perpendicular to the boron planes and the other is parallel. The parallel component seems to show no square-root behavior. Otherwise this should be visible in the temperature dependence of the measured $B_{c2}(T)$. Thus, the linear behavior of $B_{c2}(T)$ shown in Fig. 3 indicates the three-dimensional nature of the superconducting state in our specimens.

To obtain the Ginzburg–Landau coherence length $\xi_{GL}(0)$ from the slope of $B_{c2}(T)$ close to the critical temperature [13], we use

$$\xi_{GL}(0) = [-(dB_{c2}(T)/dT)(2\pi T_c/\phi_0)]^{-1/2}, \qquad (1)$$

where ϕ_0 is the magnetic-flux quantum, resulting in $\xi_{GL}(0) = 3.0$ nm. According to the discussion on $B_{c2}(T)$ given above, this value can be regarded as a rough estimate.

Using our data on the temperature dependence of the resistance at zero magnetic field, we calculate the fluctuation conductivity in the Lawrence–Doniach (LD) model [15] for layered superconductors (see [7], ch. 1.7):

$$\sigma^{AL}(T) = \frac{e^2}{16\hbar d}\frac{1}{[\varepsilon(\varepsilon + r)]^{1/2}}, \qquad (2)$$

$$\sigma^{MT}(T) = \frac{e^2}{4\hbar d(\varepsilon-\delta)}\ln\left[\frac{\varepsilon^{1/2}+(\varepsilon+r)^{1/2}}{\delta^{1/2}+(\delta+r)^{1/2}}\right], \quad (3)$$

where d is the interlayer spacing, $\varepsilon = (T - T_c^{AL})/T_c^{AL}$, and T_c^{AL} is the Aslamazov–Larkin critical temperature [5]. We use a simple estimation for the pair-breaking parameter $\delta = (T_{c0} - T_c^{AL})/T_{c0}$, where T_c^{AL} is the real superconducting transition temperature of the sample (but not the midpoint T_c^{MP} quoted above), and T_{c0} is the transition temperature for negligible pair-breaking [14]. The Lawrence–Doniach anisotropy parameter r is given by ([7], § 1.2.4, Eq. (1.63))

$$r(T) = 4\xi_z^2/d^2$$

$$= \frac{J^2}{k_BT}\begin{cases}\dfrac{\pi\tau}{4\hbar}, & k_BT\tau/\hbar \ll 1, \quad \text{“dirty” limit,}\\[2ex] \dfrac{7\xi(3)}{8\pi^2 k_BT}, & k_BT\tau/\hbar \gg 1, \quad \text{“clean” limit.}\end{cases} \quad (4)$$

It characterizes the strength of interlayer coupling. Here, ξ_z *i*s the interlayer tunneling coherence length; $J = \hbar W$ is the energy of interplanar tunneling, with W being the electron tunneling rate; and τ is the in-plane electron mean free time. We note that for $T \approx T_c$, $k_BT_c\tau/\hbar = 0.18l/\xi_{BCS}$, where ξ_{BCS} is the BCS coherence length and l is the electron mean free path.

The interlayer coupling strength r, according to Eq. (1), is strongly temperature dependent. When the temperature decreases, the interlayer coupling $r(T)$ increases, so that the effective dimensionality of fluctuations changes from 2D to 3D.

Taking into account that, in Eqs. (2) and (3), the parameter $\varepsilon \ll 1$ and that our samples correspond to the “dirty” case, we used the first line in Eq. (1) in the form

$$r(T) = r_0(1-\varepsilon) \quad (5)$$

with $r_0 = r(T_c^{AL})$.

The excess conductance due to superconducting fluctuations should be calculated from the temperature dependence of the resistance by the relation

$$\sigma'(T) = \frac{1}{R(T)} - \frac{1}{R_n}. \quad (6)$$

For this purpose, the normal-state resistance R_n of our samples was determined with high accuracy as the asymptotic convergence point of the $R^{-1}(1/B)$ dependence at $B \longrightarrow \infty$, according to the procedure given in [14], as shown in Fig. 3. Figure 4 shows the temperature dependence of the inverse excess conductance σ' normalized to the normal-state conductance $\sigma_n = R_n^{-1}$.

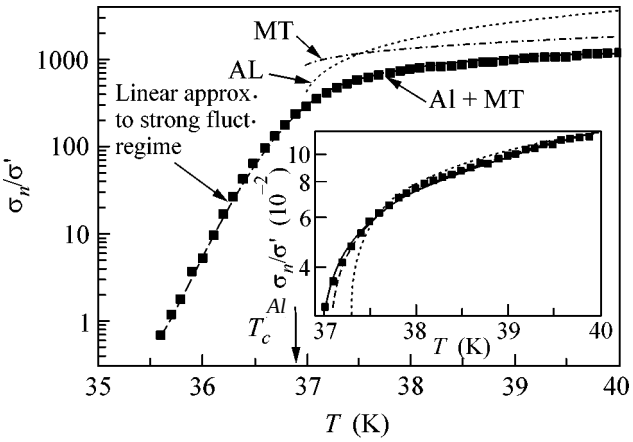

Fig. 4. The temperature dependence of the inverse fluctuation conductance $[\sigma'(T)]^{-1}$ normalized to the normal-state value σ_n for the resistive transition in zero field (data of the curve from Fig. 1). The solid line is the fit of experimental data by the sum of Eqs. (2) and (3) valid for layered superconductors. At about 37.5 K, the AL and MT contributions become equal. In the inset, the dashed line shows the result of a free fit of the 3D model to the experiment. The dotted line shows the fit of the 3D model with fixed parameter $\delta = 0.09$.

We fit the experimental data with the sum of the Aslamazov–Larkin, Eq. (2), and Maki–Thompson, Eq. (3), terms. As fitting parameters we used T_c^{AL}, δ, r_0, and the amplitude $a = 4\hbar dL/e^2R_nS$, where S is the cross section of the stripe-shaped sample and L is the distance between the voltage probes. The result of the free fitting with an unconstrained range of parameters is shown in Fig. 4 by the solid line. The fitting shows fairly good agreement between the experiment and the theory of weak superconducting fluctuations in layered superconductors (see [7] and references therein) with anisotropy parameter $r_0 \sim 0.06$, parameter $\delta \simeq 0.09$, and $T_c^{AL} \simeq 36.9$ K.

To discuss the above values of parameters it should be remembered that the Lawrence–Doniach model of layered superconductors, Eqs. (2) and (3), used for the fitting exactly reproduces the limit of a 2D superconductor for $r = 0$ and an isotropic 3D superconductor for $r \gg 1$ [5, 6]. Our value $r_0 = 0.064$ indicates a highly anisotropic superconductor with weak interlayer coupling, because, according to Eq. (1), in this case the interplanar coherence length ξ_z is much smaller than the interlayer spacing d.

In comparison, an analysis of fluctuation conductivity for the YBCO superconductor [16] yielded the anisotropy parameter $r_0 \sim 0.06$–0.09 for well oxygenated samples. Recent analysis of fluctuation-induced diamagnetism in optimally doped YBCO [17] gave the value $r_0 \simeq 0.1$. From these data we conclude that, at least concerning fluctuations, the anisotropy of super-

conducting properties of MgB_2 is very close to that of YBCO.

To demonstrate the highly anisotropic nature of MgB_2, we fitted our experimental data also using pure 3D expressions for the fluctuation conductivity [i.e., the $r \gg \varepsilon, \delta$ limit of Eqs. (2) and (3)]. The result of free fitting of all the parameters is shown in the inset of Fig. 4 by the dashed line. The fit with a 3D model seems to be reasonable. However, careful observation reveals two inconsistencies.

First, due to Eq. (5), $r(T)$ increases upon lowering the temperature, shifting the theoretical description of the fluctuation conductivity towards the 3D limit. Therefore, the 3D model should fit better the low-temperature part of the σ_n/σ' measurements than the high-temperature regime. However, the 3D model deviates systematically from the experimental points in the range 37–37.3 K.

Second, the pair-breaking parameter $\delta \simeq 0.0053$ from the 3D fit is too small to meet physical expectations. From the transition temperature of our samples and the bulk value $T_{c0}^{MP} \simeq 39.5$ K [4], both determined using the same midpoint criteria, we get $\delta^{MP} = (T_{c0}^{MP} - T_c^{MP})/T_{c0}^{MP} \simeq 0.09$. The parameter δ^{MP} estimated from the T_c suppression agrees with $\delta = 0.089$, as received from our fit of the LD model. If we fix the parameter δ at $\delta = 0.09$, the fit of our experimental data by the 3D model (the dotted curve in the inset of Fig. 4) shows an obvious discrepancy between the theory and the experiment.

Finally, the fitting parameter $T_c^{AL} \simeq 36.91$ K (for the free fit of the 3D model it is $T_c^{AL} \simeq 37.03$ K) is the transition temperature, which may be treated as the true value of the superconducting transition temperature in our sample. It does not coincide with T_c^{MP} determined by the midpoint transition criteria. The midpoint T_c^{MP} can be regarded as a "technical" value of the superconducting transition temperature, which contains all extrinsic shifts and the intrinsic shift of the critical temperature due to fluctuations. Consistent free fitting of fluctuation conductivity provides a much more sophisticated and refined determination of the superconducting transition temperature as true physical characteristics of a material.

Below T_c^{AL}, the fluctuation regime changes to strong fluctuations with the exponential temperature behavior of resistance similar to that observed in thin-film superconductors [18].

In summary, we have measured the resistance and critical fields of MgB_2 films prepared on sapphire substrates. From the linear temperature dependence of the critical magnetic field, we established the three-dimensional superconductivity of our films. From resistivity measurements, we showed that the temperature dependence of fluctuation conductivity above the critical temperature agrees with the Lawrence–Doniach theory for layered superconductors. According to the resulting anisotropy parameter, an experimental indication of almost two-dimensional nucleation of the superconductivity in MgB_2 was established.

We are grateful to Prof. A. Varlamov for discussions on superconducting fluctuation phenomena and on the experimental data reported in this work. This work was supported in part by INTAS (A.S.S. grant no. 99-00585) and BRHE (L.R.T. grant no. REC-007).

REFERENCES

1. J. Namagatsu, N. Nagakawa, T. Muranaka, *et al.*, Nature **410**, 63 (2001).
2. J. M. An and W. E. Pickett, Phys. Rev. Lett. **86**, 4366 (2001).
3. J. Kortus, I. I. Mazin, K. D. Belashchenko, *et al.*, Phys. Rev. Lett. **86**, 4656 (2001).
4. T. Buzea and T. Yamashita, Supercond. Sci. Technol. **14**, R115 (2001).
5. L. G. Aslamazov and A. I. Larkin, Fiz. Tverd. Tela (Leningrad) **10**, 1104 (1968) [Sov. Phys. Solid State **10**, 875 (1968)]; Phys. Lett. A **26A**, 238 (1968).
6. K. Maki, Prog. Theor. Phys. **39**, 897 (1968); **40**, 193 (1968); R. S. Thompson, Phys. Rev. B **1**, 327 (1970).
7. A. I. Larkin and A. A. Varlamov, in *Handbook on Superconductivity: Conventional and Unconventional Superconductors*, Ed. by K. H. Bennemann and J. B. Ketterson (Springer-Verlag, Berlin, 2002); cond-mat/0109177.
8. S. N. Ermolov, M. V. Indenbom, A. N. Rossolenko, *et al.*, Pis'ma Zh. Éksp. Teor. Fiz. **73**, 626 (2001) [JETP Lett. **73**, 557 (2001)].
9. A. Sidorenko, C. Sürgers, T. Trapmann, and H. v. Löhneysen, Phys. Rev. B **53**, 11751 (1996).
10. A. Sidorenko, C. Sürgers, and H. v. Löhneysen, Physica C (Amsterdam) **370**, 197 (2002).
11. V. I. Dediu, V. V. Kabanov, and A. S. Sidorenko, Phys. Rev. B **49**, 4027 (1994).
12. N. Ya. Fogel, O. G. Turutanov, A. S. Sidorenko, and E. I. Buchstab, Phys. Rev. B **56**, 2372 (1997).
13. M. Tinkham, *Introduction to Superconductivity* (McGraw Hill, New York, 1996, 2nd ed.).
14. K. Kajimura, *Fluctuations in the Resistive Transition in Superconducting Al Films*, Research Report No. 720 (Electrotechnical Laboratory, Agency of Industrial Science and Technology of Japan, Tokyo, 1971).
15. W. E. Lawrence and S. Doniach, in *Proceedings of the Twelfth International Conference on Low Temperature Physics, Kyoto, Japan, 1971*, Ed. by E. Kanda, p. 361.
16. M. Putti, M. R. Cimberle, C. Ferdeghini, *et al.*, Physica C (Amsterdam) **314**, 247 (1999).
17. A. Lascialfari, A. Rigamonti, L. Romano, *et al.*, Phys. Rev. B **65**, 144 523 (2002).
18. A. S. Sidorenko, N. Ya. Fogel, and I. M. Dmitrenko, Fiz. Tverd. Tela (Leningrad) **23**, 724 (1981) [Sov. Phys. Solid State **23**, 411 (1981)].

JETP Letters, Vol. 76, No. 1, 2002, pp. 21–25. Translated from Pis'ma v Zhurnal Éksperimental'noĭ i Teoreticheskoĭ Fiziki, Vol. 76, No. 1, 2002, pp. 25–30.

The Quantum Control of Electron States in a Double Quantum Dot under Coulomb Blocking Conditions

V. A. Burdov

Nizhni Novgorod State University, Nizhni Novgorod, 603950 Russia

Received May 16, 2002

Abstract—The possibility of providing for a quantum control of electron states by means of a weak electric field (constant or alternating) acting upon a system is studied in a nondissipative approximation for a system of two electrons in a double quantum dot (QD) under Coulomb blocking conditions. It is shown that the Coulomb repulsion facilitates controlled transition of the system from a symmetric (one electron in each QD) to asymmetric (both electrons in one QD) electron configuration under the action of a resonance alternating field or a slowly varying (quasi-constant) field. In the absence of Coulomb repulsion, two electrons can be localized in the same QD only under the action of a strong electric field. *© 2002 MAIK "Nauka/Interperiodica".*

PACS numbers: 73.21.La

The term "quantum control" means a combination of various (tunneling, optical, etc.) phenomena in heterostructures, whereby the quantum electron dynamics of a system is directly controlled by external fields applied to this system. For example, in application to a system of quantum dots or wells coupled by tunneling, quantum control implies the possibility of constructing stable electron states with a preset charge density distribution and ensuring transitions between these states under the action of constant or alternating electric fields [1–3]. The controlled dynamics of such electron states can serve as a basis for operation of the new generation of nanoelectronic devices, including quantum computers [4, 5].

The development of systems with controlled quantum states is closely related to the phenomenon of "dynamic localization of electron wave packets in nanostructures" (to our knowledge, the term was introduced by Dunlap *et al.* [6, 7] considering this phenomenon in superlattices and lattices of finite dimensions). The phenomenon of dynamic localization consists in confining an electron wave packet in one of a set (of two [8–11] or more [6, 7]) identical tunneling-coupled quantum wells or quantum dots (QDs). Upon such confinement, ensured by an external alternating electric field, the electron density can be transferred from one to another quantum well (or QD) by slowly varying the amplitude of either the alternating field [1, 2] or a quasi-constant dc voltage [3] applied to the system.

As was demonstrated for double quantum wells [1, 2, 8–10] and double QDs [11], dynamic localization is possible only in a sufficiently strong electric field, in which the electron potential energy is significantly greater than the tunneling splitting of electron energy levels. It is important to note that all the investigations cited above employed a one-electron approximation and ignored the effects of Coulomb blocking playing an essential role in real systems (especially in QDs). Indeed, overcoming the Coulomb blocking in small-size QDs (with dimensions of 10 nm and below) requires strong constant electric fields [12, 13] with a strength exceeding that of the blocking field, which is typically on the order of 10^4–10^5 V/cm. For this reason, we may expect that the Coulomb interaction between electrons in a system of tunneling-coupled QDs containing more than one electron will hinder their localization and make impossible dynamic quantum control in the system.

However, the opposite conclusion follows from a theoretical analysis presented below showing that the Coulomb blocking can actually help electrons to localize in the region of one QD. Moreover, this can be achieved under the action of weak (constant or alternating) electric fields in which the electron potential energy is comparable with the tunneling splitting of electron energy levels in the system of coupled QDs.

This effect will be illustrated for a system of two electrons in a symmetric double QD occurring in the layer of a wide-bandgap material. The energy of dimensional quantization in the QD is assumed to be the greatest energy parameter of the problem. Another energy parameter is the splitting Δ of the ground-state level as a result of a weak tunneling coupling between the two QDs, which can be rendered arbitrarily small by increasing the distance between QDs. The energy of the Coulomb interaction between electrons is assumed to be much greater than Δ and much smaller than the energy of dimensional quantization. For QDs with dimensions on the order of ten nanometers, the energy of dimensional quantization is about several tenths of an electronvolt. This is about ten times as large as the

Coulomb interaction energy, which, in turn, is greater by least one order of magnitude than the energy splitting Δ.

It should be noted that the aforementioned relation between the energies of dimensional quantization and Coulomb interaction is better obeyed in systems with smaller effective electron masses and greater dielectric permittivities of the QD semiconductors. For example, in gallium arsenide—a semiconductor with an effective electron mass amounting to about 7% of the free electron mass and a permittivity of about 12—the dimensional quantization and Coulomb interaction energies for a 10-nm QD are approximately 0.1 and 0.01 eV, respectively, which conforms well to the above condition.

Both constant and alternating external fields will be assumed sufficiently small, so that the electron potential energy in these fields is on the same order of magnitude as the level splitting Δ (and, hence, much lower compared to the Coulomb interaction energy). Finally, the quantum energy $\hbar\omega$ of the external alternating field will be considered comparable with the Coulomb energy. Once all these energy relations are obeyed, the consideration can be restricted to an analysis of electron dynamics on the lowest pair of split energy levels, while the higher levels can be ignored.

With neglect of various dissipative processes, the Hamiltonian of a two-electron system in an external electric field can be written in the following form:

$$\hat{H}(\mathbf{r}_1, \mathbf{r}_2) = \sum_{j=1}^{2} (\hat{H}_0(\mathbf{r}_j) + W(\mathbf{r}_j) + U(\mathbf{r}_j)\cos\omega t) + V(\mathbf{r}_1, \mathbf{r}_2), \quad (1)$$

where $\hat{H}_0(\mathbf{r})$ is the one-electron Hamiltonian of a double QD in the two-level approximation, the eigenfunctions $\chi_{0,1}(\mathbf{r})$ of which are symmetric and asymmetric in the coordinate z (the z axis coincides with the axis of the double QD system), respectively; $W(\mathbf{r})$ and $U(\mathbf{r})\cos\omega t$ are the electron potential energies in the constant and alternating fields (also directed along the axis of the system); and $V(\mathbf{r}_1, \mathbf{r}_2)$ is the electron interaction operator which is symmetric, as well as the whole operator (1), with respect to the permutation of particles.

In the absence of an alternating field, solving the eigenvalue problem yields four energies and four wave functions of stationary two-electron states [13]. The wave functions of the ground state and the second and third excited states, symmetric with respect to the permutation of particles (we are speaking of the coordinate part of the wave function, omitting the spin part), can be described by the common expression

$$\Psi_j(\mathbf{r}_1, \mathbf{r}_2) = \frac{(\varepsilon_j + V)[(\varepsilon_j - V - 2W)\Psi_L(\mathbf{r}_1)\Psi_L(\mathbf{r}_2) + (\varepsilon_j - V + 2W)\Psi_R(\mathbf{r}_1)\Psi_R(\mathbf{r}_2)]}{\sqrt{2}\sqrt{(\varepsilon_j^2 - V^2)^2 + \Delta^2(\varepsilon_j - V)^2 + 4W^2(\varepsilon_j + V)^2}} - \frac{\Delta(\varepsilon_j - V)[\Psi_L(\mathbf{r}_1)\Psi_L(\mathbf{r}_2) + \Psi_R(\mathbf{r}_1)\Psi_L(\mathbf{r}_2)]}{\sqrt{2}\sqrt{(\varepsilon_j^2 - V^2)^2 + \Delta^2(\varepsilon_j - V)^2 + 4W^2(\varepsilon_j + V)^2}}, \quad j = 0, 2, 3. \quad (2)$$

Here, ε_j are the energies measured from a certain common initial level; in a weak field, these energies are given by the formulas

$$\varepsilon_0 = -V - \frac{\Delta^2}{2V} - \frac{\Delta^2(W^2 - \Delta^2/4)}{2V^3},$$
$$\varepsilon_{2,3} = V + \frac{\Delta^2}{4V} \mp \sqrt{4W^2 + \left(\frac{\Delta^2}{4V}\right)^2}, \quad (3)$$

where V and W are the nondiagonal matrix elements of operators of the Coulomb interaction and the interaction with the constant electric field:

$$V = \langle\chi_0(\mathbf{r}_1)\chi_0(\mathbf{r}_2)|V(\mathbf{r}_1, \mathbf{r}_2)|\chi_1(\mathbf{r}_1)\chi_1(\mathbf{r}_2)\rangle,$$
$$W = \langle\chi_0(\mathbf{r})|W(\mathbf{r})|\chi_1(\mathbf{r})\rangle.$$

For estimation purposes, we can assume that $V \sim e^2/\epsilon R$ (where e is the electron charge, ϵ is the permittivity of a semiconductor, and R is the QD size) and $W \sim eER$, where E is the applied field strength. In Eq. (2), the $\Psi_{L,R}(\mathbf{r})$ functions are constructed from the wave functions $\chi_{0,1}(\mathbf{r})$,

$$\Psi_L(\mathbf{r}) = \frac{\chi_0(\mathbf{r}) - \chi_1(\mathbf{r})}{\sqrt{2}}, \quad \Psi_R(\mathbf{r}) = \frac{\chi_0(\mathbf{r}) + \chi_1(\mathbf{r})}{\sqrt{2}}$$

and localized almost completely in the left and right QDs, respectively.

In contrast to the functions of type (2), the wave function of the first excited state is antisymmetric with respect to the permutation of particles [13]. The operator of a periodic perturbation is symmetric and, hence, cannot couple the states with different symmetries. Therefore, the first excited state exhibits no evolution with time and virtually does not participate in the electron dynamics. For this reason, expressions for the wave function and energy of the first excited state are not presented here and omitted in subsequent considerations, as if the level were initially not populated.

Once the wave functions (2) of the stationary states are known, we can determine the probabilities of the

spatial distribution of electrons between the QDs. In a relatively weak (in the sense considered above) electric field such that $W \sim \Delta \ll V$ (parameter V playing the role of the effective Coulomb interaction energy), electrons in the ground state most probably exhibit a symmetric distribution (i.e., each QD contains one electron); in the second and third excited states, both electrons occur at an almost 100% probability in the left and right QDs, respectively:

$$P_S^{(0)} = \left(1 + \frac{\Delta^2}{4V^2} + \frac{\Delta^2(6W^2 - \Delta^2)}{8V^4}\right)^{-1},$$

$$P_L^{(2)} = P_R^{(3)} = \frac{1}{2} + \frac{W}{\sqrt{4W^2 + (\Delta^2/4V)^2}}.$$

The probabilities $P_L^{(2)}$ and $P_R^{(3)}$ drop sharply from about unity to 1/2 in the region of very weak fields on the order of $W \leq \Delta^2/8V$. In the ground state, the probability of the symmetric distribution $P_S^{(0)}$ is virtually independent of the applied field parameter W (a significant dependence appears only in the fourth order with respect to the small ratio Δ/V) and is very close to unity (a difference from unity being of the second order in Δ/V).

In order to solve the Schrödinger equation for the system in a weak electric field, let us expand the wave function in the stationary basis set (2):

$$\Psi(\mathbf{r}_1, \mathbf{r}_2, t) = \sum_{j \neq 1} C_j(t)\Psi_j(\mathbf{r}_1, \mathbf{r}_2) \times \exp\left\{-i\left(\frac{\varepsilon_j}{\hbar}t + \frac{U_{jj}}{\hbar\omega}\sin\omega t\right)\right\}, \quad (4)$$

where $C_j(t)$ are the unknown expansion coefficients and $U_{jj} = \langle\Psi_j|(U(\mathbf{r}_1) + U(\mathbf{r}_2))|\Psi_j\rangle$. In the region of fields such that $W \sim \Delta$, we may assume that $U_{00} = 0$, $U_{22} = -U_{33} = -2U$, where $U = \langle\chi_0|U(\mathbf{r})|\chi_1\rangle$.

It should be recalled that we assume $U \sim W \sim \Delta$. In this case, the expansion coefficients $C_j(t)$ obey the following set of equations:

$$\begin{aligned}
i\frac{dC_0}{dt} &= \sum_{m=-\infty}^{\infty} \mu_m (C_2 \exp\{i(m\omega - \omega_{20})t\} \\
&\quad + C_3 \exp\{-i(m\omega + \omega_{30})t\}), \\
i\frac{dC_2}{dt} &= \sum_{m=-\infty}^{\infty} (\mu_m C_0 \exp\{-i(m\omega - \omega_{20})t\} \\
&\quad + \lambda_m C_3 \exp\{-i(m\omega + \omega_{32})t\}), \\
i\frac{dC_3}{dt} &= \sum_{m=-\infty}^{\infty} (\mu_m C_0 \exp\{i(m\omega + \omega_{30})t\} \\
&\quad + \lambda_m C_2 \exp\{i(m\omega + \omega_{32})t\}),
\end{aligned} \quad (5)$$

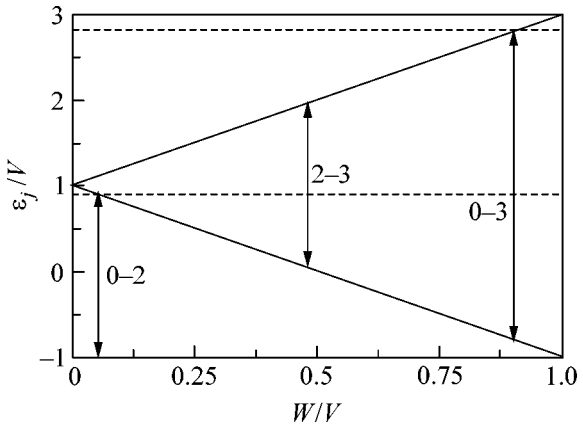

Fig. 1. Schematic diagram showing the sequence of resonances appearing with an increase in the constant field parameter W. Horizontal dashed lines indicate the levels of quantum energies spaced by $\hbar\omega \sim 1.9V$, counted from the ground-state energy level $\varepsilon_0 = -V$. Solid lines represent energies of the stationary excited states. Double arrows show resonance transitions between the indicated levels.

where ω_{20}, ω_{30}, and ω_{32} are the frequencies of transitions between the corresponding levels (3),

$$\mu_m = \frac{\omega\Delta m}{2\sqrt{2}V} J_m(2U/\hbar\omega), \quad \lambda_m = \frac{\omega\Delta^2}{16WV} J_m(4U/\hbar\omega),$$

and $J_m(x)$ is the mth order Bessel function of x. Note that the parameters μ_m and λ_m are always small in comparison with ω, which allows the system of Eqs. (5) to be solved in a resonance approximation (see, e.g., [14, p. 180]).

In the three-level system under consideration, there are three resonance transitions and, depending on the W value, one of these will be observed under the condition that $2V \neq N\hbar\omega/2$ (where N is any integer). Figure 1 shows the pattern of resonance manifestations in the course of monotonic increase in the applied constant field parameter W. When $2V = N\hbar\omega/2$, either all three transitions are resonance for a certain W value or only one transition between the second and third levels becomes resonant. This situation is not considered below.

Let us assume that, as the constant field increases, the first resonance with $\omega_{20} = \omega$ appears between the ground and second excited states (Fig. 1). Then, retaining only the resonance terms with $m = 1$ in Eqs. (5) and assuming that $C_3 \approx$ const, we obtain an expression of type (4) for the wave function,

$$\Psi(\mathbf{r}_1, \mathbf{r}_2, t) = \sum_{\sigma=1}^{3} A_\sigma \Phi_\sigma(\mathbf{r}_1, \mathbf{r}_2, t), \quad (6)$$

where A_σ are constant coefficients completely determined by the initial conditions and $\Phi_\sigma(\mathbf{r}_1, \mathbf{r}_2, t)$ are the

quasi-energy wave functions [15]. In our case, the latter functions can be expressed as

$$\Phi_1(\mathbf{r}_1, \mathbf{r}_2, t) = \Psi_0(\mathbf{r}_1, \mathbf{r}_2)$$
$$\times \sqrt{\frac{1}{2}\left(1 + \frac{\delta}{2\nu}\right)} \exp\left\{-i\left(\frac{\varepsilon_0}{\hbar} + \frac{\delta}{2} - \nu\right)t\right\}$$
$$- \Psi_2(\mathbf{r}_1, \mathbf{r}_2)\sqrt{\frac{1}{2}\left(1 - \frac{\delta}{2\nu}\right)}$$
$$\times \exp\left\{-i\left(\frac{\varepsilon_2}{\hbar} - \frac{\delta}{2} - \nu\right)t + i\frac{2U}{\hbar\omega}\sin\omega t\right\},$$
$$\Phi_2(\mathbf{r}_1, \mathbf{r}_2, t) = \Psi_3(\mathbf{r}_1, \mathbf{r}_2)$$
$$\times \exp\left\{-i\left(\frac{\varepsilon_3}{\hbar}t + \frac{2U}{\hbar\omega}\sin\omega t\right)\right\}, \quad (7)$$
$$\Phi_3(\mathbf{r}_1, \mathbf{r}_2, t) = \Psi_0(\mathbf{r}_1, \mathbf{r}_2)\sqrt{\frac{1}{2}\left(1 - \frac{\delta}{2\nu}\right)}$$
$$\times \exp\left\{-i\left(\frac{\varepsilon_0}{\hbar} + \frac{\delta}{2} + \nu\right)t\right\}$$
$$+ \Psi_2(\mathbf{r}_1, \mathbf{r}_2)\sqrt{\frac{1}{2}\left(1 + \frac{\delta}{2\nu}\right)}$$
$$\times \exp\left\{-i\left(\frac{\varepsilon_2}{\hbar} - \frac{\delta}{2} + \nu\right)t + i\frac{2U}{\hbar\omega}\sin\omega t\right\},$$

where $\delta = \omega_{20} - \omega$ is a small deviation from the resonance and $\nu = \sqrt{\mu_1^2 + \delta^2/4}$.

If the system at the initial time instant occurred in the ground state Ψ_0 (corresponding to the symmetric distribution of electrons) and the constant electric field was significantly below the resonance value ($\delta > 0$ and $\delta \gg \mu_1$), the application of a periodic electric field will drive the system with a probability of almost unity into a quasi-energy state Φ_1 coinciding with Ψ_0 at $t = 0$ to within a small value on the order of μ_1/δ. Therefore, all terms except A_1 in expansion (6) will be close to zero, while $A_1 \approx 1$. As demonstrated in [3], both the expansion coefficients and the quasi-energy functions proper remain virtually unchanged as compared to the case of W = const in the case of adiabatic variation of the constant field parameter W with time, so that the expansion coefficients can be considered as constant.

Thus, in the course of a slow variation of W, the system will stay in a quasi-energy state Φ_1. Upon passing through the resonance and gradually going away ($\delta < 0$, $|\delta| \gg \mu_1$), the quasi-energy state Φ_1 will coincide, to within a phase factor and small terms on the order of $\mu_1/|\delta|$, with the other stationary state Ψ_2. While the initial state Ψ_0 corresponded to the symmetric distribution of electrons between QDs, the final state Ψ_2 is characterized by a maximum asymmetry of the charge distribution, whereby both electrons occur in the left QD. The total charge in the left QD upon this transition is given by the formula

$$Q = -e\left[1 + \frac{1}{2}\left(1 - \frac{\delta}{2\nu}\right)\right].$$

As can be seen, upon going through the resonance, the ratio $\delta/2\nu$ changes from 1 to –1 and the total charge Q changes by one unit (electron charge). Therefore, the resonance action of even a weak alternating field on the background of an adiabatically varied constant field is capable of overcoming a strong Coulomb blocking and localizing electrons in one of the two QDs. The role of a weak constant field reduces to driving the system through a resonance interaction point and, moving it away from the resonance, fixing the system in a stable state close to the stationary state.

As noted above, the dynamic localization of an electron wave packet in a weak field ($W \sim U \sim \Delta$) cannot be ensured in the absence of the Coulomb repulsion. The reason is that the stationary one-particle states in a symmetric double QD at $W \sim \Delta$ are not strongly localized (the localized state is attained only at $W \gg \Delta$). Since the electron density in the one-particle states is distributed between the two QDs, the adiabatic transition through the resonance (driving the system from one to another stationary state) is not accompanied by localization of the wave function in any of the two QDs. On the contrary, in the case of a strong Coulomb repulsion, both electrons in the excited two-electron states are localized in one of the two QDs at a nearly unity probability. Therefore, driving the system by a weak resonance field from the ground stationary state into an excited state (within the same quasi-energy state) leads to an almost complete localization of the electron density in one QD.

It should be noted that the further adiabatic increase in the constant field parameter W, while leading the system out of the resonance $\omega_{20} = \omega$ and localizing both electrons in the left QD, drives the system to another resonance $\omega_{32} = \omega$. As can be readily demonstrated, a slow passing through this resonance will drive the system from the second to the third excited state, whereby both electrons will be transferred from left to right QD. By continuing to increase the constant field parameter, it is possible to return the system to the ground state upon going through the resonance $\omega_{30} = 2\omega$, thus completing the cycle. The total charge in the left QD upon this transition is given by the approximate formula

$$Q = -e + \frac{e}{2}\left\{\frac{\delta'}{\nu'} + \frac{1}{2}\left(\frac{\delta\nu}{-}\frac{\delta''}{\nu''}\right)\right\},$$

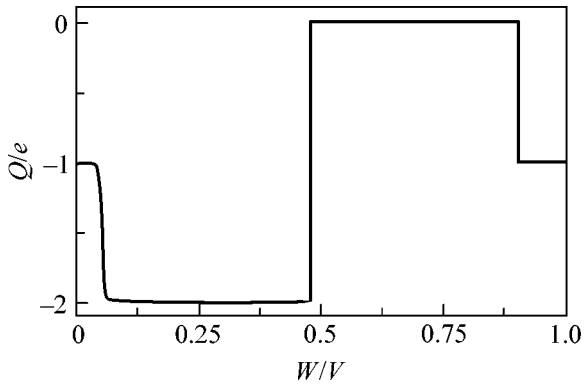

Fig. 2. Variation of the amount of charge with the constant field W in the left QD for $\Delta/V = 0.1$, $\hbar\omega/V = 1.9$, and $U = \Delta$. On the passage through each next resonance, the charge in the left QD changes in a jumplike manner by a multiple of unit (electron) charge. After the transition $3 \longrightarrow 0$, corresponding to $W/V = 0.9$, the population of the left QD accomplishes the cycle and returns to the initial value.

where δ', ν', and δ'', ν'' are the values of δ and ν for the resonances $2 \longrightarrow 3$ and $3 \longrightarrow 0$, respectively.

Figure 2 shows a diagram of Q versus W corresponding to the complete cycle of charge transfer as described above. The characteristic resonance widths are determined by the Fourier coefficients μ_1 (for the $0 \longrightarrow 2$ resonance), λ_{-1} ($2 \longrightarrow 3$), and μ_{-2} ($3 \longrightarrow 0$). For the values of parameters indicated in the legend to Fig. 2, we obtain $\mu_1/\omega = 0.00186$, $\lambda_{-1}/\omega = -0.00014$, and $\mu_{-2}/\omega = -0.0001$. Therefore, the first resonance has a maximum width and, hence, the first resonance charge transfer from the ground state to the second excited state ($0 \longrightarrow 2$) proceeds more gradually than the other two transitions (as shown in Fig. 2).

It should be noted that the two other transitions ($2 \longrightarrow 3$ and $3 \longrightarrow 0$) require much higher values of the constant field parameter W (comparable with the Coulomb energy V) than that featuring the first resonance ($0 \longrightarrow 2$). Indeed, for $\hbar\omega/V = 1.9$, the resonance values of W for the three sequential transitions are 0.05, 0.475, and $0.9V$, respectively. Nevertheless, all these values are still below the threshold constant field W capable of overcoming the Coulomb blocking without additional action of the variable field component. According to [13], this threshold field is precisely equal to V.

Note also that such a controlled transfer of the electron density requires that the electron lifetime in the excited states be sufficiently long, exceeding the time required for the system to pass from one to another state. According to estimates, the width of energy levels in the excited states must not exceed 10^{-4} eV.

This study was supported by the Russian Foundation for Basic Research (project no. 01-02-16569) and by the Ministry of Education of the Russian Federation (project UR.01.01.057).

REFERENCES

1. R. Bavli and H. Metiu, Phys. Rev. A **47**, 3299 (1993).
2. A. A. Gorbatsevich, V. V. Kapaev, and Yu. V. Kopaev, Zh. Éksp. Teor. Fiz. **107**, 1320 (1995) [JETP **80**, 734 (1995)].
3. V. A. Burdov, Zh. Éksp. Teor. Fiz. **116**, 217 (1999) [JETP **89**, 119 (1999)].
4. K. A. Valiev and A. A. Kokin, *Quantum Computers: Hopes and Reality* (RKhD, Moscow, 2001).
5. D. F. Zaretskiĭ and S. B. Sazonov, Zh. Éksp. Teor. Fiz. **121**, 521 (2002) [JETP **94**, 446 (2002)].
6. D. H. Dunlap and V. M. Kenkre, Phys. Rev. B **34**, 3625 (1986).
7. S. Raghavan, V. M. Kenkre, D. H. Dunlap, *et al.*, Phys. Rev. A **54**, R1781 (1996).
8. F. Grossmann, T. Dittrich, P. Jung, and P. Hanggi, Phys. Rev. Lett. **67**, 516 (1991).
9. F. Grossmann and P. Hanggi, Europhys. Lett. **18**, 571 (1992).
10. Y. Dakhnovskii and R. Bavli, Phys. Rev. B **48**, 11 010 (1993).
11. C. A. Stafford and N. S. Wingreen, Phys. Rev. Lett. **76**, 1916 (1996).
12. G. Bryant, Phys. Rev. B **48**, 8024 (1993).
13. V. A. Burdov, Fiz. Tverd. Tela (St. Petersburg) **43**, 1110 (2001) [Phys. Solid State **43**, 1152 (2001)].
14. L. D. Landau and E. M. Lifshitz, *Course of Theoretical Physics*, Vol. 3: *Quantum Mechanics: Non-Relativistic Theory* (Nauka, Moscow, 1989, 4th ed.; Pergamon, New York, 1977, 3rd ed.).
15. Ya. B. Zel'dovich, Zh. Éksp. Teor. Fiz. **51**, 1492 (1966) [Sov. Phys. JETP **24**, 1006 (1967)].

Translated by P. Pozdeev

JETP Letters, Vol. 76, No. 1, 2002, pp. 26–29. Translated from Pis'ma v Zhurnal Éksperimental'noĭ i Teoreticheskoĭ Fiziki, Vol. 76, No. 1, 2002, pp. 31–34.

Low-Temperature Anomalies of the Hall Coefficient for a Magnetic Kondo Lattice of $CeAl_2$

N. E. Sluchanko*, A. V. Bogach*, V. V. Glushkov*, S. V. Demishev*, N. A. Samarin*, G. S. Burkhanov, and O. D. Chistyakov****

** Institute of General Physics, Russian Academy of Sciences, ul. Vavilova 38, Moscow, 119991 Russia*
e-mail: nes@lt.gpi.ru

*** Baikov Institute of Metallurgy and Materials Technology, Russian Academy of Sciences, Leninskiĭ pr. 49, Moscow, 119991 Russia*

Received May 16, 2002; in final form, May 24, 2002

Abstract—The Hall coefficient R_H and magnetoresistance of a magnetic Kondo lattice of $CeAl_2$ were investigated over a wide temperature range from 1.8 to 300 K in magnetic fields of up to 80 kOe. Analysis of the measured angular dependences $R_H(\varphi, T, H)$ made it possible to separate the contributions of skew scattering and anomalous magnetic scattering to the anomalous Hall effect. The results obtained were compared with the existing theoretical models. *© 2002 MAIK "Nauka/Interperiodica".*

PACS numbers: 72.15.Qm

1. Mixed-valence compounds and concentrated Kondo systems based on Ce, Yb, and other rare-earth elements are characterized by low-temperature anomalies of their transport properties [1]. The manifestation of the anomalous contributions to the Hall coefficient is one of the most interesting and poorly understood features of low-temperature transport in these intermetallic compounds. Until now, only a qualitative theoretical description of the Hall effect in systems with strong electron correlations has been proposed by Coleman *et al.* [2] and Hadzic-Leroux *et al.* [3]. This approach is based on the inclusion of the mechanisms of skew scattering of band charge carriers by localized magnetic moments of rare-earth ions. Since the currently available experimental data on the anomalous Hall effect in mixed-valence compounds and concentrated Kondo systems are very scarce, it is difficult to analyze the physical properties of these objects and to develop approaches to their adequate description. At the same time, the sign and the magnitude of the anomalous Hall effect contain extremely important information on the mechanisms of formation of a heavy-fermion ground state [2].

2. The purpose of the present work was to obtain detailed data on the behavior of the transport properties in concentrated Kondo systems. We analyzed the angular and field dependences of the Hall resistance and magnetoresistance for polycrystalline samples of the $CeAl_2$ compound—a classical example of magnetic Kondo lattices [4]. The experimental results obtained allowed us to separate and identify the anomalous components of the Hall effect. It turned out that the observed activation behavior of the dependence $R_H(T)$ for the $CeAl_2$ intermetallic compound is inconsistent with the conclusion drawn in [2, 3], according to which the scattering effects play a decisive role in the anomalies of the Hall coefficient of concentrated Kondo systems.

The angular dependences of the Hall coefficient and the magnetoresistance were measured in a constant magnetic field with strengths as high as 80 kOe over a wide temperature range from 1.8 to 300 K. The measurements were performed using a unique quantized-motor-operated device, which provided the sample rotation in a cryogenic medium. The angular accuracy of the sample positioning was $\varphi = (\hat{\mathbf{Hn}}) = 1.8°$, where $\mathbf{n}$ is the vector normal to the sample surface. The rotation and temperature were controlled with a personal computer through an automatic unit of original design with a serial interface. Weak signals were recorded on a Keithley 2182 two-channel nanovoltmeter.

3. Figure 1 shows the temperature dependence of the Hall coefficient $R_H(T)$ measured by a rotating sample method in a magnetic field $H \approx 3.4$ kOe and the temperature dependences of the resistivity $\rho(T)$ and the Hall mobility $\mu_H = R_H(T)/\rho(T)$. The data presented in Fig. 1 in the $\ln R_H$–$1/T$ coordinates (see inset a in Fig. 1) allow us to separate two activation portions which are characterized by an increase in the Hall coefficient R_H with a decrease in the temperature. The activation energies corresponding to these portions are as follows: $E_{a1} = 30.3 \pm 0.8$ K and $E_{a2} = 9.2 \pm 0.1$ K. At temperatures close to the liquid-helium temperature, the dependence $R_H(T)$ exhibits two features: a relatively broad maximum of the Hall coefficient at $T \approx 4$ K (see also [5]) and a narrow peak in $R_H(T)$ at $T = T_N \approx 3.85$ K,

whose position corresponds to a transition to the antiferromagnetic state of $CeAl_2$ [6].

Let us consider in more detail the experimental angular dependences of the galvanomagnetic characteristics studied in this work. The observed dependence of the Hall resistance $R_h(\varphi, T = 4.2\ \text{K})$ at $H = 3.4$ kOe slightly deviates from a sinusoidal shape (Fig. 2a). The deviation increases with a decrease in the temperature below the transition point to the antiferromagnetic state ($T < T_N \approx 3.85$ K). The fitting of the experimental data presented in Fig. 2 demonstrated that the distortions observed in the curve $R_h(\varphi) \sim \sin\varphi$ can be adequately described by adding a second harmonic of the type $R_{h2}\sin 2\varphi$. It should be emphasized that we carried out a combined analysis of the angular dependences of the Hall resistance $R_h(\varphi, H)$ and the magnetoresistivity $\rho(\varphi, H)$ in magnetic fields of up to 80 kOe. As a result, the effect of an asymmetric arrangement of Hall contacts on the sample was excluded from the factors responsible for the complex shape of the angular dependences of the Hall resistance (Fig. 2). (Note that the asymmetric arrangement of Hall contacts leads to the appearance of a spurious contribution from $\rho(\varphi, H)$ to the Hall signal.) Therefore, the families of curves that correspond to different temperatures in the range $T \le 4.2$ K (Fig. 2a, $H = 3.4$ kOe) and different magnetic fields $H \le 80$ kOe (Fig. 2b, $T = 4.17$ K) characterize the behavior of only the Hall component of the resistance.

Moreover, the experimental data presented in Fig. 2 and the results obtained from the measured dependences $R_h(\varphi, T < 10\ \text{K}, H < 80\ \text{kOe})$ were used to separate different contributions to the Hall coefficient of $CeAl_2$. The curves $R_h(\varphi, T_0, H_0)$ were approximated by the analytical relationship

$$R_h(\varphi, T_0, H_0) = R_0 + R_{h1}\sin(\varphi - \varphi_{01}) + R_{h2}\sin 2(\varphi - \varphi_{02}). \quad (1)$$

The obtained parameters R_{h1} and R_{h2} in relationship (1) were then used to determine the low-temperature contributions R_H^a and R_H^{am} (Fig. 3) to the Hall coefficient of the magnetic Kondo lattice of $CeAl_2$. In addition to the coefficients R_H^a and R_H^{am}, the appropriate analysis of the experimental data in terms of relationship (1) made it possible to determine the phase shift $\Delta\varphi = \varphi_{01} - \varphi_{02}$ between the harmonics in relationship (1) (see inset in Fig. 3).

4. Now, we turn to the discussion of the results presented in Figs. 1–3. First and foremost, it should be noted that the anomalous components R_H^a and R_H^{am} of the Hall coefficient exhibit a significantly different behavior in the magnetically ordered and paramagnetic phases of $CeAl_2$. The anomalous positive contribution R_H^a to the Hall coefficient $R_H(T, H)$ is observed over a wide temperature range from 1.8 to 300 K (Fig. 1). In the concentrated Kondo system, this contribution is associated with the mechanism of skew scattering of conduction electrons by localized magnetic moments of cerium ions [2, 3]. The specific features of the com-

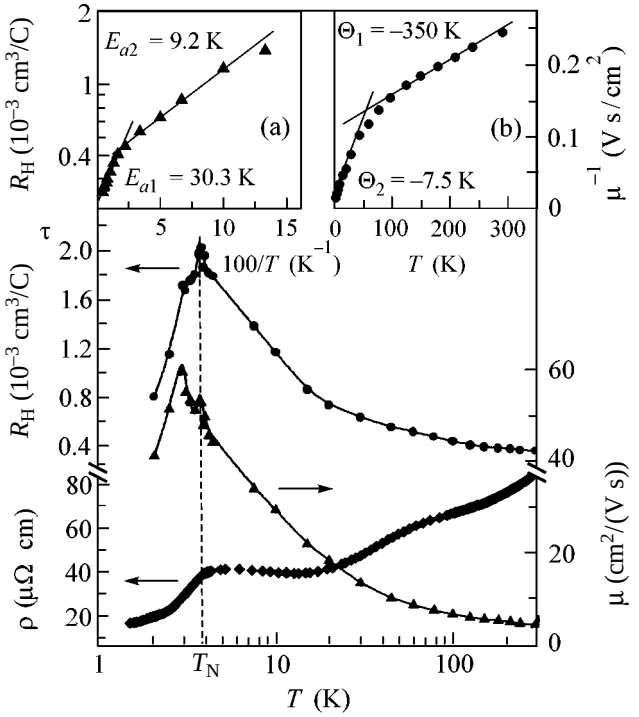

Fig. 1. Temperature dependences of the Hall coefficient R_H, the resistivity ρ, and the Hall mobility $\mu_H = R_H/\rho$ for $CeAl_2$. The insets show the temperature dependences of (a) the Hall coefficient R_H in the $\log R_H$–$1/T$ coordinates and (b) the Hall mobility μ_H in the μ_H^{-1}–T coordinates (see text).

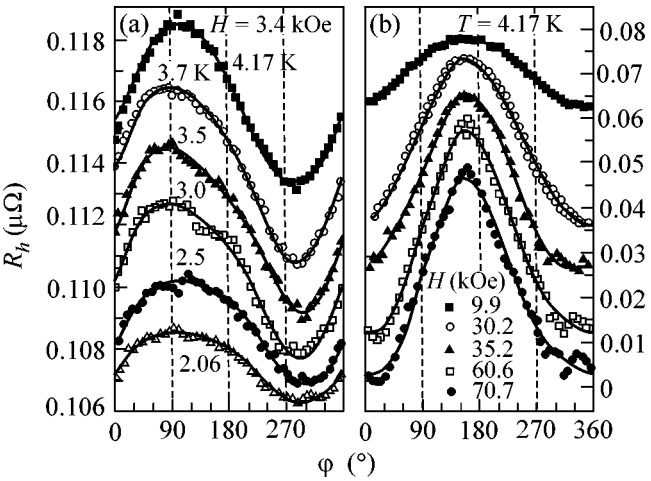

Fig. 2. Angular dependences of the Hall resistance for $CeAl_2$: (a) at different liquid-helium temperatures in the magnetic field $H = 3.4$ kOe and (b) in different magnetic fields $H < 80$ kOe at the temperature $T = 4.17$ K.

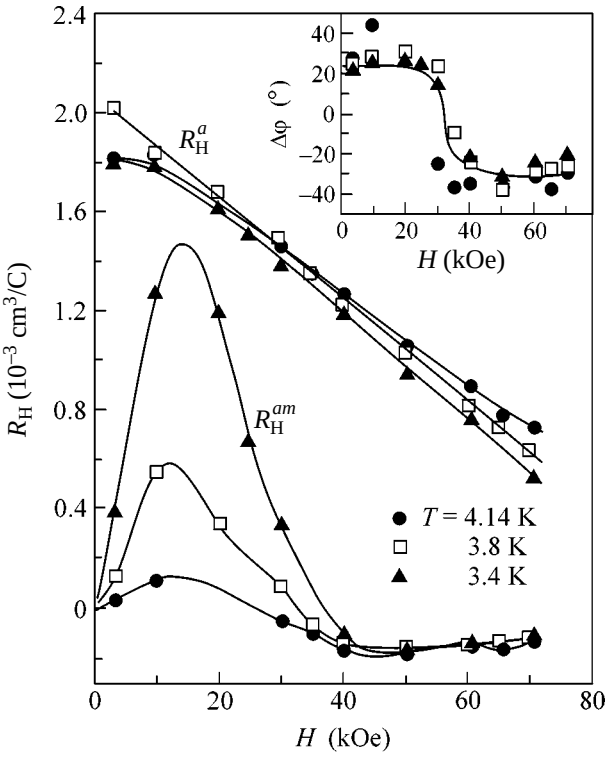

Fig. 3. Field dependences of the anomalous contributions R_H^a and R_H^{am} (see text) to the Hall coefficient of $CeAl_2$. The inset shows the field dependence of the phase shift $\Delta\varphi = \varphi_{01} - \varphi_{02}$ between the harmonics of the Hall signal in relationship (1).

ponent R_H^a of the Hall signal are as follows: (i) a broad maximum in the vicinity of the Kondo temperature ($T_K(CeAl_2) \approx 5$ K [4]) and (ii) a strong suppression of the Hall effect in the magnetic field. It can be seen from Fig. 3 that the magnitude of R_H^a drastically decreases with an increase in the magnetic field. As a result, the anomalous component R_H^a in a magnetic field $H \approx 80$ kOe is approximately three times less than its initial value. Such a significant decrease in the component R_H^a with an increase in the magnetic field H can be explained by the suppression of the Kondo compensation of localized magnetic moments in a magnetic field $H \approx k_B T_K/\mu_B \approx 80$ kOe (where k_B is the Boltzmann constant and μ_B is the Bohr magneton). Similar dependences $R_H^a(H)$ observed at $T \geq T_N$ and $T \leq T_N$ (Fig. 3) confirm the inferences made in [4] regarding the coexistence of the Kondo scattering of conduction electrons and magnetic ordering in the low-temperature phase of $CeAl_2$.

The presence of two activation portions of increase in the anomalous component R_H^a of the Hall coefficient (see inset 0 in Fig. 1) has defied simple explanation in the framework of the skew scattering models [2, 3], according to which the dependence $R_H^a(T) = \rho\mu_H \sim \rho\chi(1 - \chi T)$ (where χ is the reduced magnetic susceptibility) should be observed in the temperature range $T \gg T_K \approx 5$ K. It should be emphasized that the activation energies E_{a1} and E_{a2} determined in the present work for the Hall coefficient appear to be substantially less than the crystalline splitting $\Delta_{CF1} \approx 100$ K [4]. Moreover, the activation energy $E_{a2} = 9.2 \pm 0.1$ K for the paramagnetic phase is in good agreement with the specific feature revealed by Steglich *et al.* [4] in the neutron inelastic scattering spectra of $CeAl_2$ at $h\nu \approx 0.7 \pm 0.4$ meV. Note that the temperature dependence of the Hall mobility $\mu_H(T) = R_H(T)/\rho(T)$ (Fig. 1, inset (b)), to some extent, is consistent with the predictions made in [2, 3]. In actual fact, the dependence $\mu_H(T)$ is characterized by a drastic change in its behavior and involves two portions, which can be linearized in the coordinates $\mu_H^{-1} \sim (T - \theta_i) \sim \chi^{-1}$ at $\theta_1 = -350 \pm 20$ K and $\theta_2 = -7.5 \pm 0.5$ K. However, ignoring the effect of the crystalline splitting of the Ce $^2F_{5/2}$ state on the behavior of the anomalous component of the Hall coefficient and the Hall mobility in [2, 3] makes a quantitative analysis of the experimental results difficult. At lower temperatures, the dependence $\mu_H(T)$ shows two narrow maxima in the vicinity of $T_{N1} \approx 3.85$ K and $T_{N2} \approx 3.00$ K. These maxima suggest the occurrence of two magnetic phase transitions with close critical temperatures, which were also revealed by Schefzyk *et al.* [7] in the investigation of the thermodynamic properties of $CeAl_2$.

In turn, the anomalous magnetic component R_H^{am} of the Hall coefficient is characterized by two features: (i) a narrow maximum in the curve $R_H(T)$ in the vicinity of the Néel temperature (Fig. 1) and (ii) a substantially nonmonotonic behavior of the second harmonic of the Hall signal in the magnetic field with a maximum in the vicinity of $H_m \approx 15$ kOe (Fig. 3). As the temperature decreases in the range $T < T_N \approx 3.85$ K, the anomalous magnetic contribution R_H^{am} sharply increases and becomes equal to R_H^a at $T \leq 3.4$ K. In the vicinity of $H \approx 35$ kOe, the phase shift $\Delta\varphi = \varphi_{01} - \varphi_{02}$ between the components R_H^a and R_H^{am} of the Hall signal jumpwise changes by 65° (see inset in Fig. 3). For the sake of clarity, this is represented as the inversion of the sign of the anomalous magnetic component R_H^{am} in Fig. 3.

The anomalous magnetic scattering and, correspondingly, the anomalous magnetic component R_H^{am} of the Hall coefficient in magnetic fields $H < 20$ kOe (Fig. 3) can, most likely, be associated with the magnetization reversal of magnetic domains. Earlier, this phenomenon was observed by Croft *et al.* [8, 9], who studied the thermodynamic properties of $CeAl_2$. Moreover,

it was found that short-range ferromagnetic correlations occur in the $CeAl_2$ matrix in the paramagnetic state in the immediate vicinity of the transition to the antiferromagnetic state [4, 7, 9]. In our opinion, similar effects can be responsible for the anomalies in the Hall signal R_H^{am} in magnetic fields $H > 30$ kOe (Fig. 3). However, the specific features of the magnetic phase diagram and the character of magnetic interactions in the Kondo lattice of $CeAl_2$ call for further investigation.

5. The detailed data obtained in measuring the galvanomagnetic parameters for the magnetic Kondo lattice of $CeAl_2$ permitted us to separate and identify the contributions to the anomalous Hall effect $R_H(H, T)$ in this compound with heavy fermions. It was demonstrated that the temperature dependence of the anomalous component R_H^a for this Kondo lattice exhibits a complex activation character. The observed behavior of the dependence $R_H^a(T)$ for $CeAl_2$ is inconsistent with the conclusions drawn in the framework of the models proposed in [2, 3], according to which scattering effects play a decisive role in the anomalies of the Hall coefficient in concentrated Kondo systems.

This work was supported by the Russian Foundation for Basic Research (project nos. 01-02-16601 and 02-02-06720), INTAS (project no. 00-807), and the 6th Competition of Research Projects of Young Scientists of the Russian Academy of Sciences (project no. 16).

REFERENCES

1. P. Wachter, in *Handbook on the Physics and Chemistry of Rare Earths*, Ed. by K. A. Gschneidner, Jr., L. Eyring, G. H. Lander, and G. R. Choppin (Elsevier, Amsterdam, 1994), Vol. 19, Chap. 132.
2. P. Coleman, P. W. Anderson, and T. V. Ramakrishnan, Phys. Rev. Lett. **55**, 414 (1985).
3. M. Hadzic-Leroux, A. Hamzic, A. Fert, *et al.*, Europhys. Lett. **1**, 579 (1986).
4. F. Steglich, C. D. Bredl, M. Loewenhaupt, *et al.*, J. Phys. (Paris), Colloq. **40**, C5-301 (1979).
5. N. B. Brandt, V. V. Moshchalkov, N. E. Sluchanko, *et al.*, Fiz. Nizk. Temp. **10**, 940 (1984) [Sov. J. Low Temp. Phys. **10**, 490 (1984)].
6. B. Barbara, M. F. Rossignol, J. X. Boucherle, *et al.*, Phys. Rev. Lett. **45**, 938 (1980).
7. R. Schefzyk, W. Lieke, and F. Steglich, Solid State Commun. **54**, 525 (1985).
8. M. Croft, I. Zoric, and R. D. Parks, Phys. Rev. B **18**, 345 (1978).
9. M. Croft, I. Zoric, and R. D. Parks, Phys. Rev. B **18**, 5065 (1978).

Translated by O. Borovik-Romanova

JETP Letters, Vol. 76, No. 1, 2002, pp. 30–32. From Pis'ma v Zhurnal Éksperimental'noĭ i Teoreticheskoĭ Fiziki, Vol. 76, No. 1, 2002, pp. 35–37.

Long-Range and Short-Range Magnetic Order in New Compound $NaVGe_2O_6$¶

A. N. Vasiliev, T. N. Voloshok, O. L. Ignatchik, M. Isobe[1], and Y. Ueda[1]

Low Temperature Physics Department, Moscow State University, Moscow, 119992 Russia

[1] Materials Design and Characterization Laboratory, Institute for Solid State Physics, University of Tokyo, Kashiwa, Chiba 277-8581, Japan

Received May 17, 2002

Abstract—New metal oxide pyroxene compound $NaVGe_2O_6$ containing isolated edge-sharing VO_6 (S = 1) chains undergoes transition into a long-range antiferromagnetic state at T_N = 16 K. The broad maximum in the temperature dependence of magnetic susceptibility at T_M = 26 K indicates the low-dimensional character of the magnetic subsystem. Even though the antiferromagnetic ordering is accompanied by a sharp peak of specific heat, significant magnetic entropy is released above the Néel temperature. *© 2002 MAIK "Nauka/Interperiodica".*

PACS numbers: 75.40.Cx; 75.60.Ej; 75.50.Gg; 61.66.Fn; 65.40.-b

The search for compounds containing integer or half-integer spin chains is motivated by their intriguing properties at low temperatures. The magnetic excitation spectrum of integer spin chains is gapped, so that the lowest lying excited states are separated by a finite energy gap from the ground state [1]. This is in contrast to the case of half-integer spin chains, where the magnetic excitation spectrum is gapless [2]. The gap in the magnetic excitation spectrum of the half-integer spin chain can be introduced through the dimerization of uniform chains. This dimerization, known as the spin-Peierls transition, occurs due to magnetoelastic coupling in an intrinsically unstable quantum spin chain [3]. Recently, it was conjectured [4] that the $LiVGe_2O_6$ pyroxene represents a remarkable example of a compound that combines the properties of both integer and half-integer quantum spin chains. The idea was that an anomalously large biquadratic exchange interaction closes the Haldane gap in the S = 1 spin chain, and this now gapless integer spin chain undergoes a spin-Peierls phase transition. However this idea was not supported by neutron diffraction experiment; it was concluded that $LiVGe_2O_6$ undergoes at low temperatures a transition into a commensurate antiferromagnetic long-range ordered state [5]. The realization of either spin-Peierls or Néel ground state depends on tiny variations of structure and magnetic subsystem parameters. These variations occur with isovalent chemical substitutions within a given structure. Here, we present the results of an investigation of structural, magnetic, and thermal properties of a new member of the pyroxene compounds family, $NaVGe_2O_6$.

The crystal structure of $NaVGe_2O_6$, shown in Fig. 1, is monoclinic with space group $P2_1/c$ [6]. This structure contains isolated chains of VO_6 edge-sharing octahedra running along the *c* axis. These chains are separated by the double chains of distorted GeO_4 tetrahedra. In the crystal structure of pyroxenes, the valence state of vanadium is 3+ and V ions have the integer spin S = 1.

The solid-state synthesis of $NaVGe_2O_6$ was carried out at 900°C in an evacuated silica tube for several days from the stoichiometric mixture of $Na_4Ge_9O_{20}$, GeO_2, V, and V_2O_3. $Na_4Ge_9O_{20}$ was prepared by heating mixtures of $NaCO_3$ and GeO_2 at 800°C in air. An olive-colored product of synthesis was obtained. The purity and phase composition of the sample were checked by powder X-ray diffraction at room temperature. It was confirmed that the powder was single-phase with the crystal structure of pyroxene. The crystal lattice parameters of $NaVGe_2O_6$ at room temperature are given in the table.

The magnetization in the range 2–350 K was measured by a Quantum Design SQUID magnetometer at 0.1 T. The temperature dependence of magnetic susceptibility χ for $NaVGe_2O_6$ is shown in Fig. 2. This dependence shows a broad maximum at T_M characteristic of quasi-one-dimensional magnetic compounds. Below T_M, $\chi(T)$ has an inflection point at T_N, which can be seen as a sharp peak in $\partial\chi/\partial T$. A weak upturn at the lowest temperatures is probably due to a small amount of magnetic impurities and deviations from stoichiometry.

The specific heat *C* in the range 6–300 K was measured in a Termis quasi-adiabatic calorimeter. The peak in the $C(T)$ curve is seen at the same temperature where $\partial\chi/\partial T$ has a maximum.

¶This article was submitted by the authors in English.

The temperature dependences of $\chi(T)$ and $C(T)$ obtained on $NaVGe_2O_6$ are qualitatively similar to those measured for $LiVGe_2O_6$ [4, 7], but the temperatures of short-range and long-range magnetic ordering are significantly lower in the former compound. While the magnetic structure of $NaVGe_2O_6$ at low temperatures can be unambiguously determined only in the neutron scattering measurements, the experimental data obtained strongly suggest that the ground state of this pyroxene is antiferromagnetic.

The Weiss temperature Θ and the effective magnetic moment μ_{eff} were determined from the $\chi(T)$ dependence at high temperature in accordance with the Curie–Weiss law

$$\chi = \mu_{eff}^2 N_A / 3k_B(T + \Theta), \quad (1)$$

where N_A is the Avogadro number and k_B is the Boltzmann constant.

The temperature T_M of the broad maximum in the $\chi(T)$ curve is related to the value of in-chain exchange interaction $J_\parallel$ [8]:

$$T_M = 1.282 J_\parallel. \quad (2)$$

The inflection point for $\chi(T)$ corresponds to the Néel temperature T_N. An analysis, as in [9], of the Néel temperature T_N and the in-chain exchange interaction $J_\parallel$ yields the value of exchange interaction between the chains:

$$J_\perp = T_N / 1.28n[\ln(5.8J_\parallel / T_N)]^{1/2}, \quad (3)$$

where $n = 4$ is the number of nearest neighboring chains.

The parameters of the magnetic subsystem of $NaVGe_2O_6$, defined by Eqs. (1)–(3), are summarized in the table. The ratio $J_\perp/J_\parallel$ characterizes the "one-dimensionality" of the magnetic subsystem. As compared with $LiVGe_2O_6$, the low-dimensional character of the new compound is less pronounced; i.e., the ratio $J_\perp/J_\parallel$ in $NaVGe_2O_6$ is twice that in $LiVGe_2O_6$ and also the temperatures of short-range T_M and long-range T_N magnetic orderings are much closer to each other in $NaVGe_2O_6$ than in $LiVGe_2O_6$.

The $C(T)$ dependences at low temperatures are well fitted by a cubic term βT_3. However, the value of β cannot be used for the determination of the Debye temperature, since both the phonon and magnetic subsystems of an antiferromagnet give cubic terms in the specific heat at low temperatures. Moreover, the magnetic con-

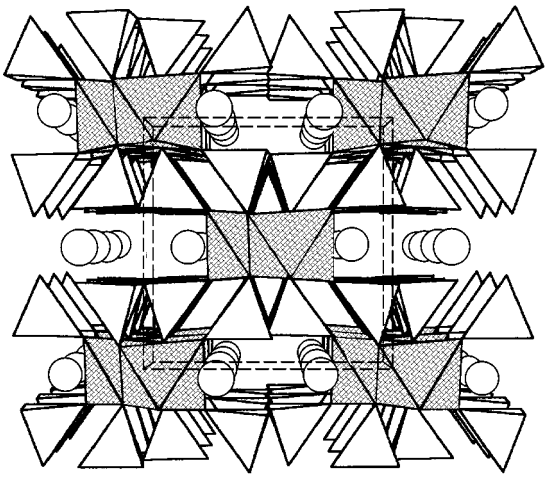

Fig. 1. The crystal structure of $NaVGe_2O_6$ pyroxene. The unit cell is shown by dotted lines, Na^+ ions are represented by dark circles, V^{3+} ions are situated within gray VO_6 octahedrons, and Ge^{4+} ions are situated within light-colored GeO_4 tetrahedrons.

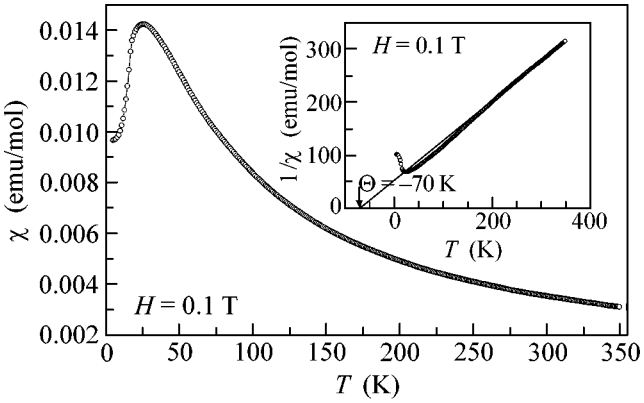

Fig. 2. The temperature dependence of magnetic susceptibility χ of $NaVGe_2O_6$. The inset shows inverse susceptibility $1/\chi$. The straight line represents the linear fit of the high-temperature part by the Curie–Weiss law.

Structural, thermal, and magnetic parameters of $NaVGe_2O_6$

Structural parameters	a, A	b, A		c, A		β'	
	9.62(5)	8.72(3)		5.28(8)		106.8(7)	
Thermal parameters	β, J/(mol K^4)	E_1, K	E_2, K	E_3, K	Q, J/mol	ΔS_{magn}, J/(mol K)	ΔS_{AF}, J/(mol K)
	3.13×10^{-3}	166	417	956	117	9	4.1
Magnetic parameters	Θ, K	μ_{eff}, μ_B	T_M, K	T_N, K	$J_\parallel$, K	$J_\perp$, K	$J_\perp/J_\parallel$
	–70	3.16	26	16	20	2.2	0.11

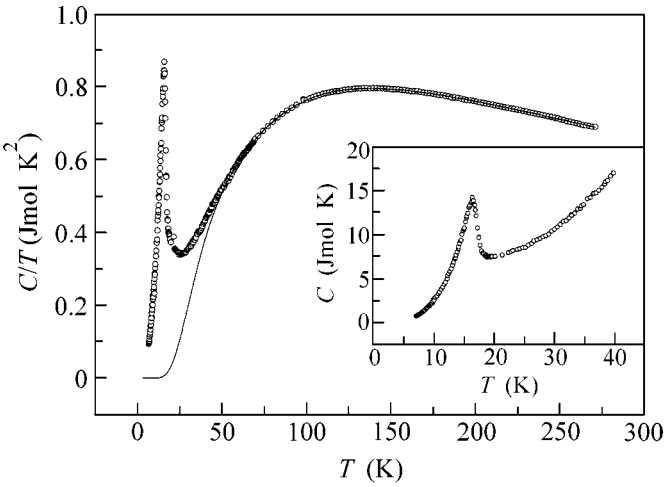

Fig. 3. The temperature dependence of normalized specific heat C/T of $NaVGe_2O_6$. The solid line represents the fit by three Einstein modes. The inset shows $C(T)$ dependence at low temperatures.

tribution to the specific heat in low-dimensional magnetic systems is smeared over a wide temperature range, at least up to double T_M. The low values of T_N and T_M in $NaVGe_2O_6$ allow, however, the fitting of the experimental data at high temperatures by the Einstein model. This fitting in the range 50–280 K was done using three Einstein modes, as given in the table. The extrapolation of the calculated curve to low temperatures allows the subtraction of the lattice contribution. The experimental C/T vs. T curve, as well as the curve obtained from the fitting procedure are shown in Fig. 3. The area between the experimental and calculated curves determines the magnetic entropy ΔS_{magn} released upon the ordering of the magnetic subsystem. The experimental value of $\Delta S_{magn} = 9$ J/mol K is slightly less than the theoretical estimate $\Delta S_{magn} = R\ln(2S + 1) = 9.13$ J/(mol K). Less than half of magnetic entropy ΔS_{AF} in $NaVGe_2O_6$ is released below the Néel temperature, which is typical of low-dimensional magnetic systems.

In summary, a study of the structural, thermal, and magnetic properties of a new low-dimensional metal oxide compound $NaVGe_2O_6$ with a pyroxene structure has been performed. On substitution of Na for Li in this structure, the quasi-one-dimensional character of the pyroxene magnetic subsystem becomes less pronounced. The in-chain exchange interaction parameter $J_\parallel$ decreases while the value of interchain exchange interactions $J_\perp$ does not change significantly. A long-range three-dimensional antiferromagnetic order is established in $NaVGe_2O_6$ at low temperatures.

This work was partially supported by INTAS grant no. 99-0155 and NWO grant no. 008-012-047.

REFERENCES

1. F. D. M. Haldane, Phys. Lett. A **93A**, 463 (1983).
2. H. A. Bethe, Z. Phys. **71**, 205 (1931).
3. M. Hase, I. Terasaki, and K. Uchinokura, Phys. Rev. Lett. **70**, 3651 (1993).
4. P. Millet, F. Mila, F. C. Zhang, *et al.*, Phys. Rev. Lett. **83**, 4176 (1999).
5. M. D. Lumsden, G. E. Granroth, D. Mandrus, *et al.*, Phys. Rev. B **62**, R9244 (2000).
6. M. Isobe *et al.*, in preparation.
7. J. L. Gavilano, S. Mushkolaj, H. R. Ott, *et al.*, Phys. Rev. Lett. **85**, 409 (2000).
8. J. C. Bonner and M. E. Fisher, Phys. Rev. A **135**, 640 (1964).
9. H. J. Schulz, Phys. Rev. Lett. **77**, 2790 (1996).

JETP Letters, Vol. 76, No. 1, 2002, pp. 33–36. Translated from Pis'ma v Zhurnal Éksperimental'noĭ i Teoreticheskoĭ Fiziki, Vol. 76, No. 1, 2002, pp. 38–42.

On the Possibility of Experimentally Testing Some Predictions of the Theory of Localization

A. G. Groshev and S. G. Novokshonov

Physicotechnical Institute, Ural Division, Russian Academy of Sciences, ul. Kirova 132, Izhevsk, 426001 Russia

e-mail: nov@otf.fti.udmurtia.su

Received May 20, 2002

Abstract—Spatial nonlocality (dispersion) of transport equations leads to a nonlinear dependence of the voltage drop U on the distance between the points of voltage measurement. For this reason, the results of conventional two-probe measurements of conductivity substantially depend on the relationship between the linear dimensions of the sample L and the characteristic length of spatial dispersion R of the generalized diffusion coefficient $D(q, \omega)$. This makes it possible to obtain information on the character of spatial nonlocality of $D(q, \omega)$ in the vicinity of the Anderson transition and, in particular, on the magnitude of the correlation multifractal dimension D_2 of electron wave functions near the mobility edge. *© 2002 MAIK "Nauka/Interperiodica".*

PACS numbers: 72.15.Rn; 71.30.+h

1. In recent years, great attention has been paid to the problem of the spatial dispersion (nonlocality) of the kinetic coefficients of disordered systems in the vicinity of the Anderson transition [1–6]. The reason is the understanding that the character of the $q\omega$ dependence of the generalized diffusion coefficient $D(q, \omega)$ near the mobility edge is closely related to the critical behavior of electron wave functions and is ultimately determined by the scenario of the metal–insulator transition [1, 3]. Indeed, the Berezinskiĭ–Gor'kov criterion of localization [7] requires that $D(q, 0)$ simultaneously (at all values of the wave vector q) vanish in the localized phase, whereas, according to the hypothesis of one-parametric scaling, the following relation should be fulfilled [8]:

$$D(t; q, \omega) = b^{2-d} D(b^{1/\nu} t; bq, b^d \omega), \quad 2 < d < 4. \tag{1}$$

Here, $t = (\mathscr{E} - \mathscr{E}_c)/\mathscr{E}_c$ is the distance to the mobility edge $\mathscr{E}_c$, b is the scaling factor, d is the dimensionality of space, and ν is the critical exponent of the correlation length.

Two qualitatively different variants of critical behavior of $D(q, \omega)$ satisfy these general requirements.

(i) According to Chalker's hypothesis [1], the multifractal nature of electron wave functions near the mobility edge ($t \longrightarrow 0$ or $\omega \longrightarrow 0$) leads to an anomalously *strong* spatial dispersion of the generalized diffusion coefficient with a characteristic length $R = \min(\xi, L_\omega) \longrightarrow \infty$, where $\xi \propto |t|^{-\nu}$ is the correlation length and $L_\omega \propto \sqrt{D(\omega)/\omega} \propto \omega^{-1/d}$ is the diffusion length of an electron per time $\sim 1/\omega$ [1, 2]. Depending on the relation between ξ, L_ω, and q, Chalker [1] distinguishes four main asymptotics:

$$D(q, \omega) = D_0 \left(\frac{l}{R}\right)^{d-2} \begin{cases} 1, & qR \ll 1, \\ (qR)^{d-2-\eta}, & qR \gg 1, \end{cases} \tag{2}$$
$$R = \min(\xi, L_\omega).$$

Here, D_0 is the Drude diffusion coefficient, l is the mean free path, and η is the anomalous critical exponent related to the multifractal dimension of wave functions D_2 ($\eta = d - D_2$) [2].

(ii) At the same time, Suslov's symmetry approach [4] to the localization theory predicts *suppression* (up to atomic scales, $R \sim \lambda_F$) of the spatial dispersion of the diffusion coefficient in the vicinity of the Anderson transition. Later, this conclusion was confirmed in terms of the generalized formulation [5, 6] of the self-consistent Vollhardt–Wölfle theory [9]. According to [5, 6], we have in the regime of Anderson's localization

$$D(q, \omega) = \frac{D(t, \omega)}{1 + (qR)^2}, \quad qR \ll 1, \tag{3}$$

where the nonlocality scale is $R \propto \sqrt{D_0 \tau}\, |D(t, \omega)/D_0|$ and decreases as $D(t, \omega) \propto [\min(\xi, L_\omega)]^{2-d}$ down to saturation at $R \sim \lambda_F$.

In his review [3], Suslov notes that the absence of anomalously strong spatial dispersion in the generalized diffusion coefficient in the vicinity of the mobility edge by no means contradicts the concept of the multifractality of electron wave functions but only indicates that the equality $\eta = d - 2$ (or $D_2 = 2$) should

be satisfied. The well-known Wegner's result $\eta = 2\epsilon$ ($\epsilon = d - 2 \ll 1$) [10] in reality directly concerns the critical behavior of the "inverse participation fraction" (see [10]). At the same time, the relation of this quantity (used in [1, 2, 11]) to $D(q, \omega)$ cannot be considered to be correct for a number of reasons[1]; therefore, in our opinion, the contradiction is here only apparent. The same may be said of the results of the numerical simulation of η ($\eta = 1.2 \pm 0.15$, 1.3 ± 0.2, and 1.5 ± 0.3 [2] and 1.3 ± 0.2 [11]) obtained by various methods at $d = 3$.

This dilemma, which touches on the fundamental concepts of Anderson's localization, requires independent (both theoretical and experimental) solution. In this paper, we only derive the constitutive equation that relates (in a spatially inhomogeneous case) the current with the measured difference of chemical electrochemical potentials and suggest a measuring scheme that permits one to obtain information on the degree of nonlocality of the coefficient of diffusion of charge carriers.

2. The voltage drop measured in a spatially inhomogeneous case is equal to the difference of electrochemical potentials $\Delta U = \Delta\zeta/e = \Delta\varphi + \Delta\mu/e$ between corresponding points of a conductor. Consequently, when calculating the current density, we should take into account the response of the system on both the mechanical disturbance (electrical potential φ) and the thermal one (chemical potential μ) caused by the inhomogeneous distribution of electrons in the conductor.[2]

By applying the general equations of the theory of linear isothermal response [12, 13] to the problem under consideration, we obtain a constitutive equation that relates the total-current density to the gradient of the electrochemical potential. Its Fourier transform at $q \ll k_F$ has the following form:

$$\begin{aligned} j(q, \omega) &= -iqen_F D(q, \omega)\xi(q, \omega) \\ &= -iq\sigma(q, \omega)U(q, \omega)/e, \end{aligned} \tag{4}$$

where n_F is the density of states at the Fermi level and $\sigma(q, \omega)$ is the measured electrical conductivity related to $D(q, \omega)$ by the Einstein relation. It should be emphasized that $\sigma(q, \omega)$ is not the Kubo kinetic coefficient

$$\tilde{\sigma}(q, \omega) = e^2 n_F \frac{D(q, \omega)}{1 + i(q^2/\omega)D(q, \omega)}, \tag{5}$$

which, in contrast to $\sigma(q, \omega)$ (see Eq. (4)), relates the total-current density to the electric field operating in the system. Only in the homogeneous case ($q = 0$) have we $\sigma(0, \omega) = \tilde{\sigma}(0, \omega)$, and Eq. (5) coincides with the Einstein relation.

[1] A detailed discussion of the basic pros and cons of the $\eta = d - 2$ hypothesis can be found in [3].

[2] The inhomogeneous spatial distribution of electrons leads not only to a disturbance of the electric field in the conductor, which is supposed to be taken into account in φ, but also to the appearance of a diffusion component in the measured density of the total current. It is this latter current that represents the response of the system to the thermal disturbance.

Equations (4) and (5) describe the nonlocal linear response of the spatially unbounded homogeneous system. In general, the nonlocality of the constitutive equations has a more complex character. In the geometry typical of an experiment, the sample has the shape of a plane-parallel layer of thickness L. In this case, the diffusion propagator of charge carriers $\tilde{G}(x, x'; \omega)$ is a solution to the equation

$$\begin{aligned} &-i\omega\tilde{G}(x, x'; \omega) \\ &-\frac{\partial}{\partial x}\int_{-L/2}^{L/2} \tilde{D}(x, y; \omega)\frac{\partial}{\partial y}\tilde{G}(y, x'; \omega)dy = \delta(x - x') \end{aligned} \tag{6}$$

with open boundary conditions

$$\tilde{G}(x, x'; \omega)\big|_{x, x' = \pm L/2} = 0. \tag{7}$$

The integral kernel of this equation (the nonlocal diffusion coefficient) enters into the constitutive equation that relates the electric current to the gradient of the electrochemical potential (voltage drop)

$$I(x) = -e^2 n_F S \int_{-L/2}^{L/2} \tilde{D}(x, x'; \omega)\frac{\partial}{\partial x'}U(x')dx', \tag{8}$$

where $S \propto L^{d-1}$ is the cross-sectional area of the sample. The solution to the boundary problem (6), (7) in the absence of spatial dispersion ($\tilde{D}(x, x'; \omega) = D(\omega)\delta(x - x')$) can be obtained by the well-known image method [14]

$$\begin{aligned} \tilde{G}(x, x'; \omega) &= \sum_{n=-\infty}^{+\infty} [G(x - x' + 2nL; \omega) \\ &\quad - G(x + x' + (2n + 1)L; \omega)], \end{aligned} \tag{9}$$

$$G(x; \omega) = \frac{1}{L}\sum_q \frac{\exp(iqx)}{-i\omega + q^2 D(\omega)}.$$

Here, $G(x, \omega)$ is the diffusion propagator for an unbounded spatially homogeneous system. We assume that solution (9) remains valid even in the presence of spatial dispersion if its characteristic length is small as compared to the sample dimensions ($R \ll L$). In this case, the integral kernel of the constitutive equation (8) is expressed (by analogy with Eq. (9)) through the generalized diffusion coefficient $D(q, \omega)$ of the unbounded spatially homogeneous system

$$\begin{aligned} \tilde{D}(x, x'; \omega) &= \frac{2}{L}\sum_{n=0}^{+\infty} [D(\bar{q}_n, \omega)\sin\bar{q}_n x \sin\bar{q}_n x' \\ &\quad + D(q_n, \omega)\cos q_n x \cos q_n x'], \end{aligned} \tag{10}$$

where $\bar{q}_x = 2\pi n/L$ and $q_n = \pi(2n + 1)/L$ are discrete values of wave numbers.

Taking into account that the voltage drop $U(x)$ is an odd function of x and the current strength $I(x) = I$ is constant along the sample under consideration, we represent them in the form of corresponding Fourier expan-

sions. Then, after substituting Eq. (10) into the constitutive equation (8), we can easily find the expression for the Fourier coefficients U_n. Finally, the x dependence of the voltage drop can be represented in the form of the following Fourier series:

$$U(x) = \frac{4I}{LSe^2 n_{\mathrm{F}}} \sum_{n=0}^{+\infty} \frac{(-1)^{n+1}}{q_n^2 D(q, \omega)} \sin q_n x, \quad |x| < L/2. \tag{11}$$

3. If the diffusion coefficient is independent of the wave number q_n, series (11) yields (for a conductor of finite dimensions) the conventional definition of the conductance $g(L, \omega) = L^{d-2} e^2 n_{\mathrm{F}} D(0, \omega) = L^{d-2}\sigma(\omega)$ and describes the linearly varying voltage drop $U(x) \propto x$ inside the sample ($|x| < L/2$). In the presence of spatial nonlocality of the generalized diffusion coefficient $D(q_n, \omega)$, the conductance is defined as

$$\frac{1}{g(L, \omega)} = \frac{8}{LSe^2 n_{\mathrm{F}}} \sum_{n=0}^{+\infty} \frac{1}{q_n^2 D(q_n, \omega)} \tag{12}$$

so that the x dependence of voltage drop (11) becomes nonlinear. Therefore, the information about the spatial dispersion of the generalized charge-carrier diffusivity $D(q, \omega)$ can be obtained by measuring the nonlinear part of $U(x)$ (11):

$$\frac{1}{g(L, \omega)} = \frac{8}{LSe^2 n_{\mathrm{F}}} \sum_{n=0}^{+\infty} \frac{1}{q_n^2 D(q_n, \omega)} \tag{13}$$

Consider a sample in the form of a plane-parallel layer of thickness $L \gg R$ (R is the scale of the spatial nonlocality) with ideal ohmic contacts on the opposite surfaces and two potential (measuring) probes located symmetrically at a distance x from the middle plane of the sample (see Fig. 1a). It is expedient to place the measuring probes near points $x_{\max}$, where $\Delta U(x)$ reaches maximum values $\Delta U_{\max}$. To measure the nonlinear part of the voltage drop (13), one more pair of potential probes is required; in our case, the ohmic probes are used to this end.

The substitution of Eq. (3) into (11) and (13) yields $\Delta U(x) = 0$. Strictly speaking, this equality is fulfilled only if the linear part of the voltage drop is compensated ideally. But in any case, the measured signal is small in terms of the parameter $R/L \ll 1$. The nonzero contribution to $\Delta U(x)$ comes only from the nontrivial q-dependent parts of the generalized diffusion coefficient in (2). Figure 1b displays typical $\Delta U(x)$ dependences calculated using linear interpolations between various Chalker's asymptotics (2) for the inverse diffusion coefficient $1/D(q, \omega)$ at $qR \ll 1$ and $qR \gg 1$. In this case, $x_{\max}$ is independent of the scales of the spatial nonlocality of $D(q, \omega)$ and, at $\eta = 1.1$–1.5, takes on values from the interval $x_{\max} \approx (0.70$–$0.76)L/2$. The values of $\Delta U_{\max}$ calculated at these points have the following asymptotics:

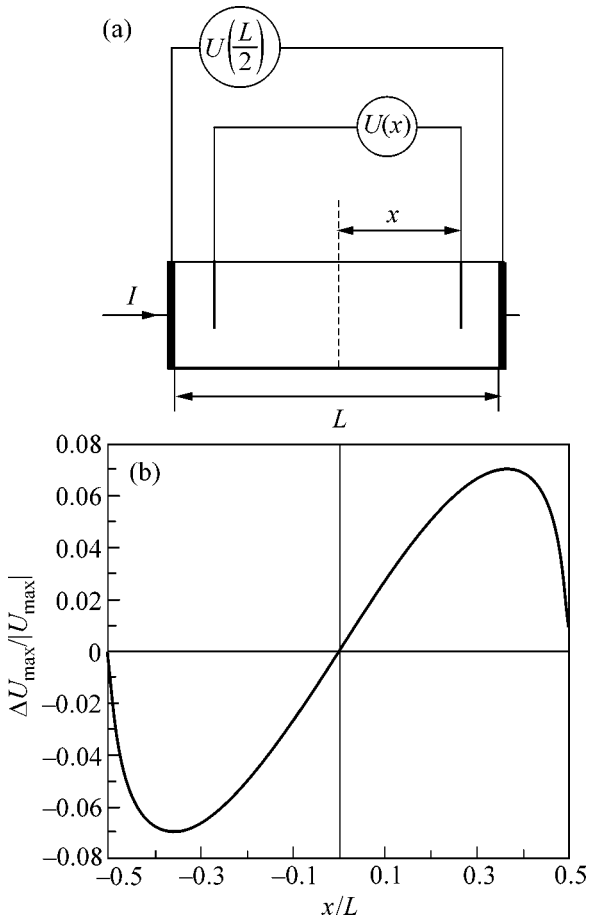

Fig. 1. (a) Schematic of measuring the nonlinear part of the voltage drop (the longitudinal section of the sample is shown). (b) Typical variation of the nonlinear part of the voltage drop as a function of the position x of the measuring probes. The curve was calculated using Chalker's asymptotics (2) for $\eta = 1.3$ and $R/L = 0.1$.

$$\Delta U_{\max} \propto \left(\frac{R}{L}\right)^{\eta} \propto \begin{cases} \omega^{-\eta/d}, & L_\omega \ll \xi, \\ \xi^n \propto |t|^{-\nu\eta}, & L_\omega \gg \xi, \end{cases} \quad L_\omega, \xi \ll L. \tag{14}$$

Two variants of measuring signal (14) can be suggested. In the first case, the frequency dependence $\Delta U_{\max}(\omega)$ is studied in a sample with a fixed level of disorder in a sufficiently small vicinity of the mobility edge on the metallic side of the transition ($|t| \ll 1$). According to (14) and to predictions of [1], $\Delta U_{\max} \propto \omega^{-\eta/d}$ should increase upon lowering frequency ($\omega \gg \omega_c$), up to the saturation, which is reached at $\Delta U_{\max} \propto (\xi/L)^{\eta}$ ($\omega \ll \omega_c$). The critical frequency ω_c is determined by the condition $L_{\omega_c} = \xi$ or $\hbar\omega_c = \lambda_{\mathrm{F}}^{-d} n_{\mathrm{F}}^{-1} |t|^{\nu d}$, where λ_{F} is the de Broglie wavelength at the Fermi level.

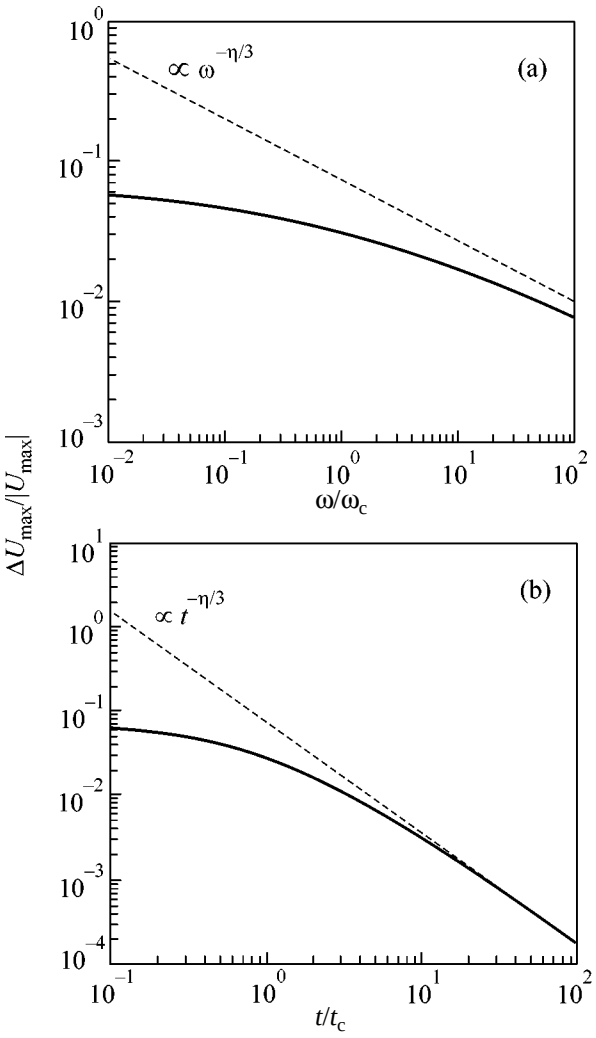

Fig. 2. Typical dependences of ΔU_{max} on (a) the frequency ω and (b) the dimensionless distance to the mobility edge t calculated using Eqs. (11) and (13) and Chalker's asymptotics (2) for $\eta = 1.3$. Dashed lines show the asymptotic behavior predicted by Eq. (14).

In the second variant, the ΔU_{max} dependence on the dimensionless distance t to the mobility edge $\mathscr{E}_c$ is measured at a fixed value of the frequency ω. The simplest way of changing t in the vicinity of $\mathscr{E}_c$ appears to be controlling the Fermi level by varying pressure [15]. A very suitable material for such measurements is Si:P, in which the use of this technique permits one to obtain changes in $|t| \approx 10^{-3}$ [15]. According to (14) and to predictions in [1], a decrease in t should be accompanied by a growth of ΔU_{max} proportional to $t^{-\nu\eta}$ ($t \gg t_\omega$) up to saturation, which is reached at $\Delta U_{max} \propto (L_\omega/L)^\eta$ ($t \ll t_\omega$). Here, the critical value t_ω is determined by the condition $L_\omega = \xi$ or $\lambda_F^d n_F \hbar\omega \approx |t_\omega|^{\nu d}$.

Figure 2 displays the dependences obtained from Eqs. (11) and (13) using the interpolation formula $R^{-1} = \xi^{-1} + L_\omega^{-1}$ for the nonlocality scale. Since in a sufficiently small vicinity of the mobility edge the nonlocality scale of $D(q, \omega)$ (2) takes on anomalously large values $R = \min(L_\omega, \xi)$, the signal ΔU_{max} (14) is well accessible for measurements. Estimates show that for Si:P samples with typical concentrations of phosphorus $n_P \approx 10^{18}$ cm^{-3} at realizable values of $|t| \approx 10^{-2}$–10^{-3}, the ΔU_{max} dependences predicted in this paper (see Eq. (14) and Fig. 2) should be observed in a range of frequencies ω accessible for probe measurements. For example, at $t \approx 10^{-3}$, the critical value of the frequency is $\omega_c \approx 10^3$–10^4 s^{-1} (see Fig. 2a) and the corresponding correlation lengths are on the order of $L_{\omega_c} \sim \xi \sim 10^{-3}$–$10^{-2}$ cm.

Thus, the fact of the existence [1, 2] or suppression [4–6] of anomalous spatial dispersion of the generalized diffusion coefficient near the Anderson transition is of fundamental importance for the understanding of the microscopic mechanism of the phenomenon of localization and, in our opinion, can be tested experimentally.

We are grateful to I.M. Suslov, who called our attention to this problem. We are also grateful to him for fruitful discussions and for the constant interest in our work. The work was supported by the INTAS (grant no. 99-1070).

REFERENCES

1. J. T. Chalker, Physica A (Amsterdam) **167**, 253 (1990).
2. T. Brandes, B. Huckestein, and L. Schweitzer, Ann. Phys. **5**, 633 (1996).
3. I. M. Suslov, Usp. Fiz. Nauk **168**, 503 (1998) [Phys. Usp. **41**, 441 (1998)].
4. I. M. Suslov, Zh. Éksp. Teor. Fiz. **108**, 1686 (1995) [JETP **81**, 925 (1995)].
5. A. G. Groshev and S. G. Novokshonov, Zh. Éksp. Teor. Fiz. **111**, 1787 (1997) [JETP **84**, 978 (1997)].
6. S. G. Novokshonov and A. G. Groshev, Zh. Éksp. Teor. Fiz. **114**, 711 (1998) [JETP **87**, 388 (1998)].
7. V. L. Berezinskiĭ and L. P. Gor'kov, Zh. Éksp. Teor. Fiz. **77**, 2498 (1979) [Sov. Phys. JETP **50**, 1209 (1979)].
8. E. Abrahams and P. A. Lee, Phys. Rev. B **33**, 683 (1986).
9. D. Vollhardt and P. Wölfle, Phys. Rev. B **22**, 4666 (1980).
10. F. Wegner, Z. Phys. B **36**, 209 (1980).
11. K. Slevin and T. Ohtsuki, Phys. Rev. Lett. **82**, 382 (1999).
12. D. N. Zubarev, in *Modern Problems in Mathematics* (VINITI, Moscow, 1979), Vol. 15, p. 131.
13. V. P. Kalashnikov, Preprint No. R4-7803, OIYaI (Joint Inst. for Nuclear Research, Dubna, 1974).
14. V. S. Vladimirov, *Equations of Mathematical Physics* (Nauka, Moscow, 1981; Dekker, New York, 1971).
15. M. A. Paalanen, S. Sachdev, R. N. Bhatt, and A. E. Ruckenstein, Phys. Rev. Lett. **57**, 2061 (1986).

Translated by S. Gorin

JETP Letters, Vol. 76, No. 1, 2002, pp. 37–39. Translated from Pis'ma v Zhurnal Éksperimental'noĭ i Teoreticheskoĭ Fiziki, Vol. 76, No. 1, 2002, pp. 43–46.

Pressure-Induced Dislocation Amorphization of Crystals

P. N. Timonin

Institute of Physics, Rostov State University, Rostov-on-Don, 344090 Russia

e-mail: timonin@icomm.ru.

Received March 21, 2002; in final form, May 23, 2002

Abstract—In terms of the isotropic elastic crystal model, it is shown that the formation of planar layers consisting of edge dislocation pileups is advantageous in energy if the shear modulus of the crystal is far lower than the bulk modulus. As pressure rises, the dislocation radius decreases, which can destroy the crystal structure. © *2002 MAIK "Nauka/Interperiodica".*

PACS numbers: 62.50.+p; 64.70.Kb

The destruction of a crystal lattice (amorphization) under a sufficiently high hydrostatic pressure of 1–100 GPa is observed in many crystals (see surveys [1, 2]). The physical reasons behind this phenomenon remain unclear in many respects. Several amorphization mechanisms have been advanced: the mechanical instability of a crystal [3, 4], chemical degradation [5], and structural constraints on packing of molecular complexes [6]. The most popular interpretation of pressure-induced amorphism is the following: it is suggested that a first-order structural phase transition occurring under a certain pressure generates nuclei of a new phase in the crystal and that their growth is inhibited by the slow kinetics of the compressed crystal [1]. Presumably, the resulting amorphous phase is a chaotic mixture of meso clusters of two stable crystalline phases.

The existing approaches to explain amorphization are qualitative, which in most cases keeps one from quantitatively predicting the properties of an amorphous phase. Most theoretical investigation of amorphization is confined to numerical simulations of the molecular dynamics or crystal dynamics under high pressures; see, e.g., [1, 7, 8].

Another drawback of most amorphization models is their nonspecificity for a compressed crystal. For example, mechanical instability can likewise be caused by a change in temperature, resulting in ordinary structural transition, and two-phase states with slow kinetics can likewise be observed upon cooling in the region of low-temperature structural transitions. In addition, the existence of a denser, high-pressure polymorph has not been discovered in many crystals that experience a transition to an amorphous state. Therefore, it is of interest to consider other amorphization mechanisms that are not related to the occurrence of structural transitions but are specific to a compressed crystal.

There seems to be no doubt that amorphism is related to the necessity of reducing the volume, and thereby decreasing the energy, of interaction of the crystal with the external pressure [2]. In the absence of a denser crystalline phase, a crystal can reduce its volume by creating structural defects, which can be more advantageous in energy than homogeneous compression. For example, in an isotropic elastic crystal in which bulk modulus K is far higher than shear modulus μ, homogeneous hydrostatic compression can be less advantageous than compression due to the generation of dislocations, whose energy is controlled by μ.

The compressibility of a crystal by means of dislocation generation was clearly demonstrated in numerical experiments on the impact compression of copper [8]. The initially appearing dislocation loops rapidly grow in number; they merge to cause the complete destruction of the crystal order. A crystal with a high dislocation density seems to be in an intermediate state *en route* to an amorphous phase.

Such an intermediate dislocation-compression phase can be easily described in terms of the isotropic elastic crystal model. According to [9], displacements of atoms caused by planar dislocation loops at distances far larger than the loop size are defined by

$$\begin{aligned} u_i(\mathbf{r}) &= -d_{jk}\partial_j G_{ik}(\mathbf{r}), \\ d_{jk} &= c_{jklm} n_l b_m S. \end{aligned} \tag{1}$$

Here, S *i*s the loop surface area, $\mathbf{n}$ is the vector normal to the loop surface, $\mathbf{b}$ is the Burgers vector, G_{ik} is the Green function from elasticity theory equations, and c_{jklm} is the tensor of elastic moduli.

Since $G_{ik} \propto r^{-1}$, displacements (1) are similar to an electric charge field. Therefore, a dense, planar layer of dislocation loops will create a constant displacement of atoms nearby. Indeed, for the displacements generated by such a layer, we have

$$u_i(\mathbf{r}) = -\partial_j \int\limits_{|z|<l/2} d\mathbf{r}'\rho(\mathbf{r}')d_{jk}(\mathbf{r}')G_{ik}(\mathbf{r}-\mathbf{r}') \approx -\rho\langle d_{jk}\rangle\partial_j \int\limits_{|z|<l/2} d\mathbf{r}'G_{ik}(\mathbf{r}-\mathbf{r}'). \quad (2)$$

Here, we set that the dislocation density is constant: $\rho(\mathbf{r}) = \text{const}$. We also ignored fluctuations in tensor d_{jk}, replacing it by a volume-average value $\langle d_{jk}\rangle$:

$$\langle d_{jk}\rangle = c_{jklm}\langle Sn_lb_m\rangle.$$

If the layer size D is great compared to its thickness, $D \gg l$, then, setting $S = \text{const}$, for $l/2 < |z| \ll D$ from Eq. (2) we have

$$u_i(\mathbf{r}) = \frac{S\rho l}{2} \times\left(\delta_{i,z}\frac{\sigma\langle n_jb_j\rangle - \langle n_zb_z\rangle}{1-\sigma} + \langle n_ib_z\rangle + \langle n_zb_i\rangle\right)\text{sgn}(z), \quad (3)$$

where $\sigma = \frac{1}{2}[(3K-2\mu)/(2K+\mu)]$ is the Poisson coefficient.

Thus, the formation of a dislocation loop layer leads to homogeneous (to random fluctuations) displacements of atoms in the nearby regions of the crystal. Substantial strain is experienced only by the dislocation layer, so that the energy consumed in this process is controlled by the energy dislocations. Depending on the sign at sgn(z) in Eq. (3), this expression describes either the compression or stretching of a crystal. The largest compression occurs in the case of purely edge dislocations with $\mathbf{b} = -\mathbf{n}b$ and $\mathbf{n}$ parallel to axis z. Here, we will consider their isotropic orientation distribution (and $b = \text{const}$) when

$$\langle b_jn_k\rangle = b\delta_{j,k}/3.$$

The average energy of dislocation interaction in this case is zero. Indeed, for the average interaction energy density, we have

$$W_{\text{int}} = -\left(\frac{\rho^2}{2V}\right)\langle d_{ij}\rangle\langle d_{kl}\rangle \int\limits_{|\mathbf{r}-\mathbf{r}'|>b} d\mathbf{r}d\mathbf{r}'\partial_i\partial_kG_{jl}(\mathbf{r}-\mathbf{r}') \propto \int\limits_{|\mathbf{r}-\mathbf{r}'|>b} d\mathbf{r}d\mathbf{r}'\Delta|\mathbf{r}-\mathbf{r}'|^{-1} = 0. \quad (4)$$

For the isotropic edge-dislocation orientation distribution, expression (3) reads

$$u_i(\mathbf{r}) = -\frac{Sb\rho l(1+\sigma)}{6(1-\sigma)}\delta_{i,z}\text{sgn}(z). \quad (5)$$

Let us consider the uniaxial compression of a crystal under pressure p along axis z that involves the formation of such edge dislocations. The energy density of a crystal containing a set of dislocation layers with thickness l separated at distance l' is defined by

$$W = (\rho lU_d + iW_{\text{int}} - 2|u_z|p)/(l+l'). \quad (6)$$

Here, U_d is the intrinsic energy of a single dislocation, $W_{\text{int}} = 0$ according to Eq. (4), and u_z is defined from Eq. (5).

In the case of edge dislocations of radius R [9],

$$U_d = \frac{\mu b^2R}{2(1-\sigma)}\ln\frac{R}{b}. \quad (7)$$

Therefore, estimating the highest density of randomly oriented dislocations at $(2R)^{-3}$, from Eqs. (4)–(7), we have

$$W = \frac{l}{l+l'}\frac{\mu}{16(1-\sigma)}\left(\frac{b^2}{R^2}\ln\frac{R}{b} - \frac{2bp}{Rp_0}\right), \quad p_0 \equiv 3\mu/\pi(1+\sigma). \quad (8)$$

The applicability of Eq. (8) is constrained by the validity conditions for formulas (1), (3), and (7), namely, $D \gg (l, l') \gg R \gg b$. The W value is the least for dislocations with the radius satisfying the relationship

$$\frac{b}{R}\ln\frac{R}{\sqrt{e}b} = \frac{p}{p_0}. \quad (9)$$

For $p \ll p_0$, a solution to this equation exists with $R \gg b$:

$$R \approx \frac{bp_0}{p}\ln\frac{p_0}{\sqrt{e}p}. \quad (10)$$

The W value corresponding to this R is

$$W \approx -\frac{l}{l+l'}\frac{\mu}{16(1-\sigma)}\frac{p^2}{p_0^2\ln\frac{p_0}{\sqrt{e}p}} = \frac{l}{l+l'}\frac{\alpha p^2}{2E\ln\frac{p_0}{\sqrt{e}p}}, \quad \alpha \equiv \frac{\pi^2(1+\sigma)^3}{36(1-\sigma)},$$

where E is the Young modulus. Comparing this W for $l' \ll l$ to the energy density of a homogeneously compressed crystal $W_0 = -p^2/2E$, we find that dislocation compression is more advantageous for $p > p_c$:

$$p_c = p_0e^{-\alpha-1/2}.$$

The critical pressure conforms to the condition $p_c \ll p_0$ if α is close to its maximal value

$$\alpha_c = \frac{3\pi^2}{16} \approx 1.85,$$

which is reached when $\mu \ll K$ and $\sigma = 1/2$. Therefore, in crystals with $\mu \ll K$, dislocation layers can form when the pressure is higher than

$$p_c = p_0e^{-\alpha_c-1/2} \approx 0.1p_0 \approx 0.06\mu.$$

For typical μ of about 10–100 GPa, p_c is on the order of 1–10 GPa, which is close to experimental values [1, 2]. With this, the average radius of layer-forming dislocations (see Eq. (9)) is

$$R_c = \alpha_c e^{\alpha_c + 1/2} b \approx 20b.$$

Macroscopic strain in the dislocation phase

$$\varepsilon_{zz} = -2|u_z|/(l + l') \approx -\frac{\pi}{8}\frac{b}{R} = -\frac{\pi}{8}\frac{p}{p_0 \ln\frac{p_0}{\sqrt{e}p}}$$

coincides, when $p = p_c$, with homogeneous strain $-p_c/E \approx -0.02$, so that the volume is continuous at the point of dislocation-layer formation.

The effective Young modulus for the dislocation phase is

$$E_a \equiv -p/\varepsilon_{zz} = \frac{E}{\alpha_c}\ln\frac{p_0}{\sqrt{e}p}.$$

It equals E for $p = p_c$ and decreases as pressure rises. This means that the dislocation phase has a higher density and a lower energy than a homogeneously compressed crystal under the same pressure.

The increasing pressure also causes a monotonic decrease in the equilibrium dislocation radius until reaching the critical pressure

$$p_a = e^{-3/2} p_0 \approx 0.22 p_0 \approx 0.13\mu,$$

under which

$$R = e^{3/2} b \approx 4.5b.$$

For $p > p_a$, Eq. (10) has no solution, and the minimum in W occurs only when $R = 0$. Thus, when $p > p_a$, nonhomogeneous layers cannot be described as a dislocation pileup, and it is natural to suggest that they become amorphous. Indeed, because in the dislocation distribution in question distances between the dislocation centers are on the order of R, when R is on the order of b, practically all crystal sites appear near dislocation cores and experience random nonhomogeneous displacements comparable to the lattice constant. It seems very probable that these strong nonhomogeneities will completely spoil long-range order. With this, the high-pressure amorphous phase will qualitatively differ from glassy phases forming in undercooled liquids, the latter having lower densities and higher energies than crystals [2].

The amorphization mechanism seems very likely in real crystals with elastic anisotropy: in this case, too, planar dislocation layers will cause homogeneous (on average) displacements, and dislocation compression can be advantageous under high pressures, at least when anisotropy is not very high, so that $W_{\text{int}} < \rho U_d$.

The formation of planar layers of an amorphous phase under a uniaxial impact load or slow hydrostatic compression was observed in many crystals at 5–20 GPa: quartz [1, 10, 11], berlinite $AlPO_4$ [11, 12], fayalite Fe_2SiO_4 [13], and forsterite Mg_2SiO_4 [2, 13]. The amorphous layers observed may well form as a result of the evolution of newly formed dislocation pileups. Quartz, where moduli c_{33} and c_{11} are several times shear moduli c_{44} and c_{66} for $p > 12$ GPa [4], offers an especially high probability for the realization of the mechanism in question.

The intermediate dislocation phase considered here is clearly not the only energetically advantageous phase under high pressures. Layers can form from dislocations of various types and shapes with various S and b distributions, various orientations, and various l/l' values. Since such state have different energies, they will be separated from a homogeneous state by different energy barriers, which are the sum of the energies of the nascent dislocations. The probability of the occurrence of various phases in experimentally achievable times will be a significant function of the barrier height and of the occurrence of defects that could serve as dislocation sources.

This work was supported by the Switzerland Foundation for Scientific Research, project SCOPE no. 2000-7SUPJO62362.

REFERENCES

1. S. M. Sharma and S. M. Sikka, Prog. Mater. Sci. **40**, 1 (1996).
2. P. Richet and P. Gillet, Eur. J. Mineral. **9**, 907 (1997).
3. L. L. Boyer, Phase Transitions **5**, 1 (1990).
4. E. Gregoryanz, R. J. Hemley, H. K. Mao, *et al.*, Phys. Rev. Lett. **84**, 3117 (2000).
5. A. K. Arora, Solid State Commun. **115**, 665 (2000).
6. R. R. Winters, G. C. Serghiou, and W. S. Hammack, Phys. Rev. B **46**, 2792 (1992).
7. N. Binggeli and J. R. Chelikowsky, Phys. Rev. Lett. **69**, 2220 (1992).
8. J. Schiotz, T. Leffers, and B. N. Singh, cond-mat/0008336 (2000).
9. J. P. Hirth and J. Lothe, *Theory of Dislocations* (McGraw-Hill, New York, 1968; Atomizdat, Moscow, 1972).
10. K. J. Kingma, C. Meade, H. K. Mao, *et al.*, Science **259**, 666 (1993).
11. P. Cordier, J. C. Doukhan, and J. Peyronneau, Phys. Chem. Miner. **20**, 176 (1993).
12. P. Cordier, A. J. Gratz, J. C. Doukhan, *et al.*, Phys. Chem. Miner. **21**, 133 (1993).
13. F. Guyot and B. Reynard, Chem. Geol. **96**, 411 (1992).

Translated by O. Fedorova

JETP Letters, Vol. 76, No. 1, 2002, pp. 40–43. Translated from Pis'ma v Zhurnal Éksperimental'noĭ i Teoreticheskoĭ Fiziki, Vol. 76, No. 1, 2002, pp. 47–50.

New Manifestation of the Statistical Nature of Orientation Ordering in Impure Nematics

E. M. Aver'yanov[1,*] and V. G. Rumyantsev[2]

[1] *Kirenskiĭ Institute of Physics, Siberian Division, Russian Academy of Sciences, Akademgorodok, Krasnoyarsk, 660036 Russia*

**e-mail: aver@iph.krasn.ru*

[2] *Research Institute of Organic Intermediate Products and Dyes, Dolgoprudnyĭ, Moscow region, 141700 Russia*

Received May 27, 2002

Abstract—It is found that the splitting of polarized electron absorption bands of impurity dye molecules is inverted with temperature in a nematic liquid-crystal matrix. This effect is caused by the statistical nature of orientation ordering of impurity molecules and by the manifestation of higher order moments of the orientation distribution function. © *2002 MAIK "Nauka/Interperiodica".*

PACS numbers: 61.30.Gz; 61.30.Gd; 42.70.Df

1. The orientation ordering of uniaxial molecules relative to the director **n** in a nematic liquid crystal (LC) has a statistical nature and is characterized by the moments $\langle P_n(\cos\theta)\rangle$ of the orientation distribution function $f(\theta)$. Here, θ is the angle between the longitudinal axis **l** of the molecule and **n**, $P_n(\cos\theta)$ are the odd Legendre polynomials; the brackets $\langle\ldots\rangle$ stand for statistical averaging. The parameter $\langle P_2\rangle = S$ determines the degree of molecular ordering, and the inhomogeneity of orientation distribution of molecules is characterized by the dispersions $\Delta_{mq} = \langle P_m P_q\rangle - \langle P_m\rangle\langle P_q\rangle$ depending on the parameters $\langle P_n\rangle$ with $n \geq 4$. The manifestations of the latter in the physical properties of LCs are of great interest for the elucidation of the nature of an LC state, for the development of molecular statistical theory, and for practical applications. The relation between S and $\langle P_4\rangle$ determines the ratio K_{33}/K_{11} of elastic moduli in a nematic phase [1], the anisotropy of Leslie viscosities α_i [2], the intensities of polarized Raman bands [3], the two-photon absorption dichroism [4], the splitting of polarized absorption bands of impurity molecules in a nematic matrix [5], and other properties of LCs. This stimulated much work on measuring $\langle P_{2,4}\rangle$ by various methods, together with work devoted to the theoretical interpretation of the observed dependences of $\langle P_4\rangle$ on S.

Recently, interest has grown in the manifestations of the $\langle P_n\rangle$ moments with $n \geq 6$ in anisotropic statistically ordered molecular media, because the dependence of $\langle P_n\rangle$ or Δ_{mq} on S is a sensitive indicator of fine structural distinctions associated with the structural anisotropy appearing in a medium as a result of external action or molecular self-organization [6]. Recently, first neutron diffraction measurements of $\langle P_{2-6}\rangle$ have been carried out in different LC phases [7]. However, no physical effects caused by the $\langle P_n\rangle$ moments with n = 2–6 were observed in LCs. This work reports the first effect associated with the manifestation of the $\langle P_n\rangle$ moments with n = 2–8 in a nematic phase.

2. To observe the effects caused by the moments $\langle P_n\rangle$ with $n \geq 4$, one should consider the LC property which depends entirely on the dispersions Δ_{2n} with $n \geq 2$, because Δ_{2n} contains the contributions from the terms $\sim\langle P_n\rangle$ and $\langle P_{n\pm2}\rangle$. The difference (splitting) $\Delta\nu = \nu_\parallel - \nu_\perp$ in the maxima ν_j of electron absorption bands $D_j(\nu)$ of uniaxial impurity molecules excited by the light polarized parallel ($j = \parallel$) and perpendicular ($j = \perp$) to **n** in a nematic matrix is such a property [8]. For impurity absorption with the dipole transition moment $\mathbf{d} \parallel \mathbf{l}$, ν_j is given by the expression [8]

$$\nu_j = \nu_i - S_m \sum_{n\geq 2} A_n(S_m)\left[\langle P_n\rangle + \frac{C_j\Delta_{2n}}{1 + C_j S}\right], \qquad (1)$$

where the summation goes over odd n, $C_\parallel = 2$, $C_\perp = -1$, ν_i corresponds to the maximum of impurity band $D_i(\nu)$ in the isotropic LC phase, and S_m is the orientation ordering parameter of the matrix molecules. The coefficients $A_n(S_m) = A_{n0} + A_{n1}S_m$ [5] characterize a change in the energy of anisotropic impurity–matrix interaction upon the electronic excitation of impurity, and the magnitudes and signs of parameters $A_{n0,1}$ are determined by the contributions from different types of intermolecular interaction.

The splitting $\Delta\nu$ reflects the statistical character of molecular orientation ordering in a nematic phase, and its value

$$\Delta\nu = -\frac{3S_m}{(1-S)(1+2S)}\sum_{n\geq 2} A_n(S_m)\Delta_{2n} \qquad (2)$$

depends on the balance of contributions from the dispersions Δ_{2n} and the parameters $\langle P_q \rangle$ with $q \geq 4$. Since the parameters Δ_{2n} vary with mesophase temperature and depend to varying degrees on S [6], the temperature curves for ν_j should exhibit some features such as the temperature-induced sign inversion of $\Delta\nu$ due to the cancellation of contributions from Δ_{2n} to $\Delta\nu$, which can occur only if the terms with at least $n = 2$, 4 and the $\langle P_{2-6} \rangle$ quantities are taken into account. At the inversion point, $\nu_\parallel = \nu_\perp \neq \nu_i$. This manifestation of moments $\langle P_n \rangle$ with $n \geq 6$ can easily be discriminated from the temperature-induced sign inversion of $\Delta\nu$ and turning A_q to zero at this point in the case where only one term with $n = q$ is taken into account in Eq. (2), because in this case the relation $\nu_j = \nu_i$ holds.

3. To provide a sizable contribution from the dispersions Δ_{2n} with different n to $\Delta\nu$, one should choose molecules whose excitation brings about a change in a variety of their properties such as the dipole moment, the anisotropy of linear and nonlinear polarizabilities, etc. Among these objects are linear molecules with a π-conjugated system containing end π-electron donor and acceptor substituents with polar conjugation via the system of molecular fragments. In our work, we used the D6 dye

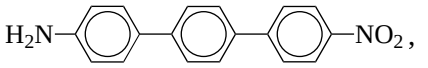

which satisfied these demands. 4-Butoxyphenyl ester of 4'-hexyloxybenzoic acid (BEHA [9]) was taken as a matrix,

Cr 50–N–102.5 I,

with known crystal–nematic–isotropic liquid (Cr–N–I) phase-transition temperatures (C) and a broad temperature interval of the nematic phase. BEHA refers to nematics with high S_m values [9], which are well approximated by the formula $S_m = S_{m0}(1 - T/T_1)^\beta$ with parameters $S_{m0} = 1.223$, $\beta = 0.177$, and $T_1 - T_{NI} = 0.314$ K.

The spectra of polarized optical-density components $D_j(\nu)$ in the electron absorption range of D6 were recorded in a plane-parallel cell of thickness $d = 40$ μm with a uniform planar director orientation and a dye weight content of 0.3% that had negligible effect on the T_{NI} value, the sample birefringence, and the degree of matrix ordering. The spectra were recorded and automatically processed on a PU-8800 spectrophotometer. For each spectral component, a weak background absorption of pure matrix at the high-frequency wing of impurity band was subtracted from the absorption of impure LC with the same d and reduced temperature $\Delta T = T - T_{NI}$. The resulting $D_j(\nu)$ spectra were used for determining $D_j(\nu_j)$ and ν_j in the nematic and isotropic phases. Figure 1 shows the $D_j(\nu)$ spectra for $\Delta T = -21.5$ K and $D_i(\nu)$ for $\Delta T = 6$ K. The isolated nondegenerate long-wavelength electronic transition in D6 is polarized along the long molecular axis, and the dichroism $N_1(\nu) = D_\parallel(\nu)/D_\perp(\nu)$ is virtually independent of ν within the absorption band, indicating its uniform polarization and the absence of hidden unresolved vibronic transitions. Hence, the observed difference between ν_j and ν_i and between $\nu_\parallel$ and $\nu_\perp$ is caused by a change in the anisotropic impurity–matrix interactions upon impurity excitation.

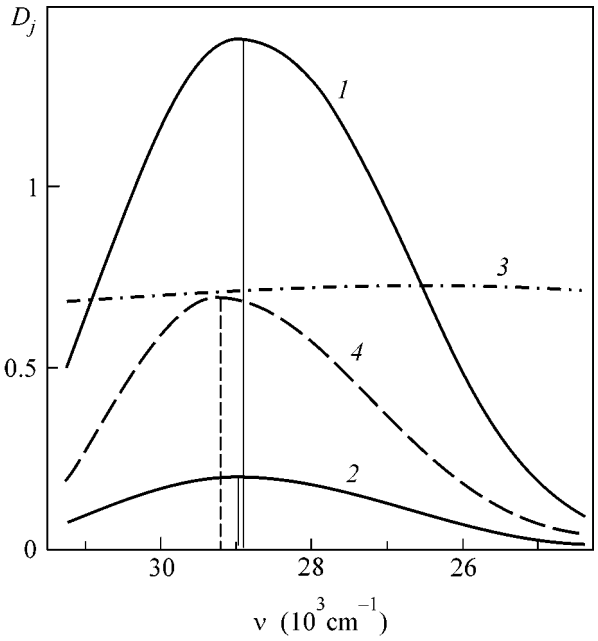

Fig. 1. Frequency dependences of the optical-density components (*1*) $D_\parallel(\nu)$, (*2*) $D_\perp(\nu)$, and (*3*) of the dichroic ratio $0.1D_\parallel(\nu)/D_\perp(\nu)$ in the nematic phase at $\Delta T = -21.5$ K and (*4*) $D_i(\nu)$ in the isotropic phase at $\Delta T = 6$ K.

The $\nu_j(\Delta T)$ curves in Fig. 2 show some features that were previously not observed for **d** ∥ **l** transitions. Over the entire mesophase range, $\nu_\perp$ is constant while $\nu_\parallel(\Delta T)$ strongly depends on temperature. At $\Delta T = \Delta T^* = -6.5$ K, $\Delta\nu$ inverts its sign, and the ratio between ν_i and $\nu_\parallel$ changes in the vicinity of T_{NI}. The $D_\parallel(\nu)$ and $D_\perp(\nu)$ bands correspond to the absorption of orthogonally polarized mutually noninteracting normal optical waves in LC, so that the observed degeneracy $\nu_\parallel = \nu_\perp$ at ΔT^* is exact. The fact that $\nu_i > \nu_j$ at ΔT^* indicates the presence of contributions from the dispersions Δ_{2n} with several values $n \geq 2$ in Eq. (2) and the cancellation of these contributions to $\Delta\nu$ at this point.

To interpret the features observed in the $\nu_j(\Delta T)$ curves at ΔT values corresponding to the experimental values of $\nu_j(\Delta T)$ in Fig. 2, Eq. (1) was used and S was determined using the expressions [10]

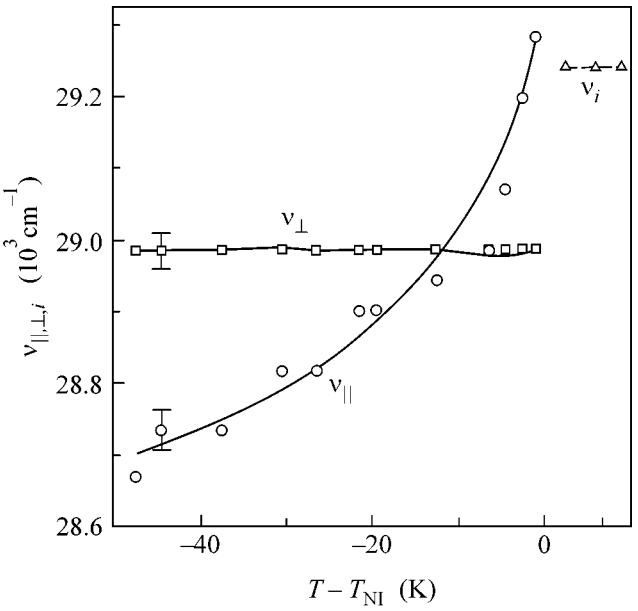

Fig. 2. Temperature dependences of the maxima $\nu_{i,j}$ of impurity bands $D_{i,j}(\nu)$ for the D6 dye in the BEHA nematic matrix. Solid lines are the ν_j interpolations calculated by Eq. (1) with parameters given in the text.

$$S = \frac{N_1 g - 1}{N_1 g + 2}, \quad g = \frac{n_{b\|} f_{b\perp}^2}{n_{b\perp} f_{b\|}^2}, \tag{3}$$

where $N_1 = D_\|(\nu_\|)/D_\perp(\nu_\perp)$, $n_{bj} = n_j(\nu_j)$ are the matrix refractive indices (background indices in the impurity absorption), and $f_{bj} = 1 + L_j(n_{bj}^2 - 1)$ are the background tensor components of the local optical wave field in the impurity band. The $n_j(\nu_j)$ values were derived from the temperature dependences of $n_j(\lambda = 546$ nm) and the dispersion relations for $n_j(\lambda)$ [9]. The components of Lorentz tensor L_j were determined by the conventional procedure [10] using the dichroic relations N_1 and $N_2 = D_\perp(\nu_\perp)/D_i(\nu_i)$, the $n_j(\nu_j)$ values, and the densities ρ and ρ_i of the nematic and isotropic phase, respectively [9]. It was established that, over the entire range of the nematic phase, the ratio $f_{b\perp}/f_{b\|} = 1 \pm 0.02$ and the correction to S for the anisotropy of tensor f_b is insignificant in the D6 absorption. The temperature dependences of the parameters N_1, $n_j(\nu_j)$, L_j, and S and the details of the procedure will be published elsewhere. Note that the $N_1(\Delta T)$ and $S(\Delta T)$ curves show no specific features in the vicinity of the ΔT^* point. The experiment was interpreted using the experimental values of S, which are well approximated by the formula $S = S_0(1 - T/T_2)^\beta$ with parameters $S_0 = 1.026$, $\beta = 0.124$, and $T_2 - T_{NI} = 0.18$ K. For the same ΔT, the parameters S and S_m are close to each other.

The parameters $\langle P_n \rangle$ and dispersions Δ_{2n} in Eq. (1) were calculated using the distribution function

$$f(\theta) = (1/Z)\exp[\lambda_2(S)P_2(\cos\theta)],$$
$$Z = \int_{-1}^{1} \exp[\lambda_2(S)P_2(\cos\theta)]d\cos\theta, \tag{4}$$

which corresponds to the experiment in [5–7] with high S values for the host and impurity molecules without end chains. The parameters $\lambda_2(S)$ were determined from the equation $S = \partial \ln Z/\partial\lambda_2$. Analysis showed that the inclusion of the $n = 2$ and 4 terms in Eq. (1) and the determination of fitting parameters $A_{n0,1}$ from the ν_j values at two ΔT points or the $\nu_\perp$ values at four ΔT points yield a linear dependence $\nu_\|(\Delta T)$ with the sign inversion for $\Delta\nu$ at ΔT close to the midpoint of the mesophase temperature interval.

The inclusion of the $n = 2$–6 terms in Eq. (1) substantially improves the agreement between theory and experiment. Figure 2 displays the $\nu_j(\Delta T)$ curves corresponding to the smallest standard deviation of the calculated $\nu_j(\Delta T)$ from their experimental values. The fitting parameters were found to be $A_{20} = 2518$, $A_{21} = 2456$, $A_{40} = -20\,734$, $A_{41} = 10\,563$, $A_{60} = 38\,105$, and $A_{61} = -31\,717$ cm^{-1}. The agreement between the theory and the experiment testifies that all the above-mentioned features of $\nu_j(\Delta T)$ and their relations with ν_i are mutually self-consistent.

The discrepancy between the theoretical and experimental values of $\nu_j(\Delta T)$ is maximal at the inversion point ΔT^* and rapidly decreases upon moving away from it. For the distribution function (4), $\Delta_{22}(S)$ decreases monotonically with increasing S in the range $S = 0.503$–0.795 corresponding to the discussed system, while $\Delta_{24}(S)$ and $\Delta_{26}(S)$ change nonmonotonically and pass through the maxima at $S = 0.55$ and 0.74, respectively. Since the experimental value $S(\Delta T^*) = 0.623$ is close to 0.638, where the difference $\Delta_{22}(S) - \Delta_{24}(S)$ changes sign from positive to negative with increasing S, the discrepancy between the calculation and experiment in the vicinity of ΔT^* may be due to a small difference between the real distribution function and the model function (4).

Thus, the observed temperature-induced sign inversion of $\Delta\nu$ and other features of the $\nu_j(\Delta T)$ curves are due to the statistical nature of the orientation ordering of impurity molecules and to the manifestation of the orientation distribution function moments $\langle P_n \rangle$ with $n = 2$–8. The spectral features of polarized impurity absorption may serve as an efficient and unique indicator of the subtle structural features in statistically ordered anisotropic molecular media.

REFERENCES

1. D. A. Dunmur and K. Toriyama, in *Physical Properties of Liquid Crystals*, Ed. by D. Demus, J. Goodby, G. W. Gray, H. W. Spiess, and V. Vill (Wiley-WCH, Weinheim, 1999), Chap. 5, p. 151.

2. F. Schneider and H. Kneppe, in *Physical Properties of Liquid Crystals*, Ed. by D. Demus, J. Goodby, G. W. Gray, H. W. Spiess, and V. Vill (Wiley-WCH, Weinheim, 1999), Chap. 8, p. 352.
3. S. Jen, N. A. Clark, P. S. Pershan, and E. B. Priestley, J. Chem. Phys. **66**, 4635 (1977).
4. S. D. Durbin and Y. R. Shen, Phys. Rev. A **30**, 1419 (1984).
5. E. M. Aver'yanov, V. M. Muratov, and V. G. Rumyantsev, Opt. Spektrosk. **67**, 603 (1989) [Opt. Spectrosc. **67**, 354 (1989)].
6. E. M. Aver'yanov, Mol. Mater. **14**, 233 (2001).
7. I. W. Hamley, G. R. Luckhurst, R. M. Richardson, and F. Santos, J. Chem. Phys. **116**, 3887 (2002).
8. E. M. Aver'yanov, Opt. Spektrosk. **63**, 790 (1987) [Opt. Spectrosc. **63**, 469 (1987)].
9. L. M. Blinov, V. A. Kizel, V. G. Rumyantsev, and V. V. Titov, J. Phys. (Paris), Colloq. **36**, C1-69 (1975).
10. E. M. Aver'yanov, *Effects of Local Field in Optics of Liquid Crystals* (Nauka, Novosibirsk, 1999).

Translated by V. Sakun

JETP Letters, Vol. 76, No. 1, 2002, pp. 44–49. Translated from Pis'ma v Zhurnal Éksperimental'noĭ i Teoreticheskoĭ Fiziki, Vol. 76, No. 1, 2002, pp. 51–56.

Mirror Nesting: A Superconducting Pairing of Carriers with a Large Momentum

V. I. Belyavsky[1], V. V. Kapaev[2], and Yu. V. Kopaev[2]

[1] *Voronezh State Pedagogical University, ul. Lenina 86, Voronezh, 394043 Russia*

[2] *Lebedev Physical Institute, Russian Academy of Sciences, Leninskiĭ pr. 53, Moscow, 119991 Russia*

e-mail: kopaev@sci.lebedev.ru

Received May 27, 2002

Abstract—The coincidence of Fermi contour portions with isolines of zero kinetic energy of the relative pair motion (the pair Fermi contour) is a necessary condition for superconducting pairing of carriers with a large total pair momentum. In high-T_c cuprates, this situation can occur either due to the formation of a stripe structure or in the absence of the stripe structure when the Fermi contour satisfies the mirror nesting condition. A gradual deviation from this condition leads to a decrease in the superconducting energy gap to zero. © *2002 MAIK "Nauka/Interperiodica".*

PACS number: 74.20.Mn; 74.20.Rp; 74.72.-h

1. In our recent works [1, 2], we proposed the mechanism of superconductivity in cuprates according to which the main channel of charge carrier pairing consists in forming carrier pairs with a large total momentum $K \approx 2k_F$ (where k_F is the Fermi momentum in the direction of the pair momentum K) with a Coulomb repulsion of carriers forming a pair, i.e., the K pairing. This pairing channel is closely associated with the specific features of the phase diagram of high-T_c cuprates in which the doping regions corresponding to the superconducting and antiferromagnetic states are immediately adjacent to one another. In this respect, an attempt was made to relate the usual Cooper pairing (at $K = 0$) to antiferromagnetism within the framework of the SO(5) phenomenological model in which the two-component superconducting order parameter and the three-component antiferromagnetic order parameter are combined into a specific vector (superspin) in five-dimensional space [3]. This attempt necessitated considering not only the U(1) and SO(3) group generators (describing the Cooper d-wave pairing and antiferromagnetic ordering, respectively) but also the generators corresponding to triplet pairs with a large total momentum π/a (where a is the lattice parameter in the conducting plane)—the so-called π operators. Earlier, the above approach justified from symmetry considerations in [3] was applied within the microscopic model of the coexistence of superconductivity and antiferromagnetism [4]. In the framework of the SU(4) dynamical symmetry model proposed by Guidry *et al.* [5], the complete set of generators making up the Lie algebra contains (in addition to the operators introduced by Zhang [3]) the operators of singlet d-wave pairs associated with orbital antiferromagnetism [6]. The experimental angle-resolved photoemission spectra (ARPES) obtained by Kaminski *et al.* [7] with the use of circularly polarized light were interpreted in terms of the spontaneous breaking of time-reversal symmetry in a pseudogap state of underdoped BSCCO thin films. This is consistent with the assumption made by Chakravarty *et al.* [8], according to which the phase diagram of high-T_c cuprates contains a phase with a hidden order (from the viewpoint of the difficulties associated with its identification using the currently available experimental techniques) in the vicinity of the superconducting region. In [8], the hidden order was treated as an orbital antiferromagnetic order with $d_{x^2-y^2}$ symmetry of the order parameter, i.e., a d-density wave (DDW) similar to a charge-density wave in the case of s symmetry. In our opinion, it is quite probable that it is these K pairing and d-density waves that coexist in cuprates in an optimum manner.

The resonance peak observed in the neutron scattering spectra at energies close to 40 meV for high-temperature superconductor cuprates at temperatures below the superconducting transition point T_c was assigned by Hu and Zhang [9] to the collective mode (π mode) corresponding to the π operators. In [10], the incommensurate magnetic fluctuations are attributed to the dispersion of the π mode, whose energy reaches a maximum at a commensurate antiferromagnetic momentum. The deviation from the commensurate momentum results in a softening of the π mode; i.e., there is a tendency toward the second-order phase transition to a certain state that corresponds to a mixture of incommensurate antiferromagnetic and superconducting states and can be interpreted as a stripe state [9]. Japaridze *et al.* [12] considered the pairing of carriers with a large total pair momentum (the η-pairing mech-

anism introduced within the Hubbard model in [11]) in the one-dimensional model with due regard for the interaction between pairs located at neighboring sites (the Penson–Kolb–Hubbard model). These authors made the assumption that the formation of η pairs with a total momentum equal to π/a is accompanied by the breakdown of the one-particle band and the formation of the two-particle band of strongly correlated η-pairing states. Thus, there exists an analogy with our recent concept of the pair Fermi contour (PFC) for pairs with a large total momentum [2].

2. The momenta k and $-k$ of particles forming pairs with a zero total momentum can belong to the entire momentum space inside or outside the Fermi contour by its symmetry with respect to the transformation $k \longrightarrow -k$. In this case, the particle momentum has also a meaning of the momentum of pair relative motion and the Fermi contour is defined as a zero-energy line of the relative pair motion. At a nonzero total pair momentum K, the presence of a populated region of the momentum space inside the Fermi contour imposes certain constraints on the size and shape of the momentum space region Ξ_K, which includes the momenta k_+ and k_- of particles forming a pair with the given momentum $K = k_+ + k_-$ (K pair). For a singly connected Fermi contour, the region Ξ_K is bounded by the Fermi contour portion and its reflection from the perpendicular to the vector **K** passing through the point $K/2$ [1], as is shown in Fig. 1. Therefore, the relative motion momenta of particles forming pairs with the total pair momenta $k = (k_+ - k_-)/2$ belong to the region Ξ_K with a symmetry center at the point $K/2$, and only this region corresponds to the Fourier components involved in both the wave function for the relative pair motion and the effective energy of interaction between particles forming a pair with the given momentum K. The kinetic energy of the pair (reckoned from its chemical potential 2μ) is defined as

$$2\xi_{Kk} = \varepsilon\left(\frac{K}{2} + k\right) + \varepsilon\left(\frac{K}{2} - k\right) - 2\mu, \qquad (1)$$

where $\varepsilon(k)$ is the dispersion law of particles forming the pair. The $\varepsilon(k)$ function becomes zero at two points a and a' at the boundary of the region Ξ_K. Consequently, in contrast to the case $K = 0$, this boundary is not a zero-energy line of the relative motion of the K pair.

For the momentum space with a hyperbolic metric (at different signs of effective-mass components in an extended neighborhood of the saddle points), the above zero-energy lines exist but, in general, do not coincide with the terminal Fermi contour portions; i.e., they do not separate occupied and vacant regions, which is necessary for superconducting pairing with a large total momentum at such a weak interaction as possible.

The spatially inhomogeneous stripe structure observed in high-T_c cuprates [13] corresponds to a certain redistribution of charge carriers over the momentum space. In this case, the charge carrier transfer may

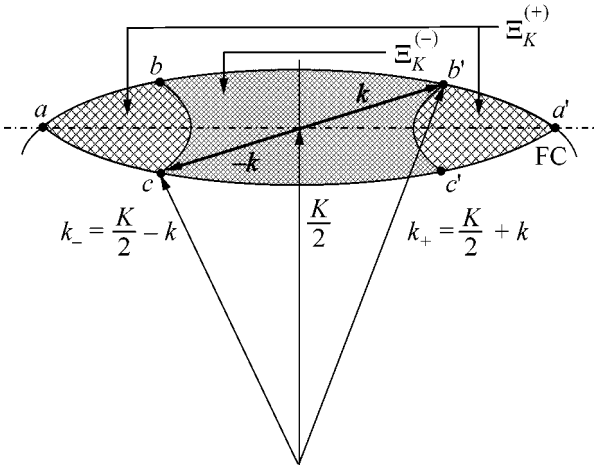

Fig. 1. Region Ξ_K (hatched) of the momentum space involving the momenta k_+ and k_- of particles forming a pair with the total momentum K. Line FC is a portion of the Fermi contour. Parts $\Xi_K^{(-)}$ and $\Xi_K^{(+)}$ of the region Ξ_K correspond to occupied and vacant states, respectively. Lines bc and $b'c'$ are the pair Fermi contour portions belonging to the region Ξ_K.

occur from the initially populated part of the momentum space region Ξ_K (in Fig. 1, the part $\Xi_K^{(+)}$ of the region Ξ_K is bounded by the $abca$ and $a'b'c'a'$ lines) to states with a higher energy [2] (not shown in Fig. 1). The resultant loss of the kinetic energy of the carriers can be compensated for by either a partial restoration of the antiferromagnetic order in the real space regions vacated by excess carriers or the emergence of another order, for example, the orbital antiferromagnetic order. The states with the lowest excitation energy (i.e., the states adjacent to the Fermi contour) inside the momentum space region Ξ_K should be depopulated first. In the case when the depopulated region $\Xi_K^{(+)}$ is formed as a result of the transfer of a carrier pair with the total momentum K to a region outside the Fermi contour in which this pair acquires a total momentum $K' > 2k_F$, the boundary between the region of newly vacated states and the region $\Xi_K^{(-)}$ of as-yet occupied states can be represented by the isolines of the relative motion energy of the K pair (lines bc and $b'c'$ in Fig. 1) on which the kinetic energy (1) of this pair becomes zero. These isolines form a pair Fermi contour providing the effective superconducting pairing of carriers with the total momentum K: for each relative K-pair motion momentum k belonging to one of the isolines of the pair Fermi contour, there is a momentum $-k$ belonging to another line of this contour (Fig. 1). According to relationship (1), this line satisfies the following condition:

$$\varepsilon\left(\frac{K}{2} + k\right) + \varepsilon\left(\frac{K}{2} - k\right) = 2\mu = \text{const}. \qquad (2)$$

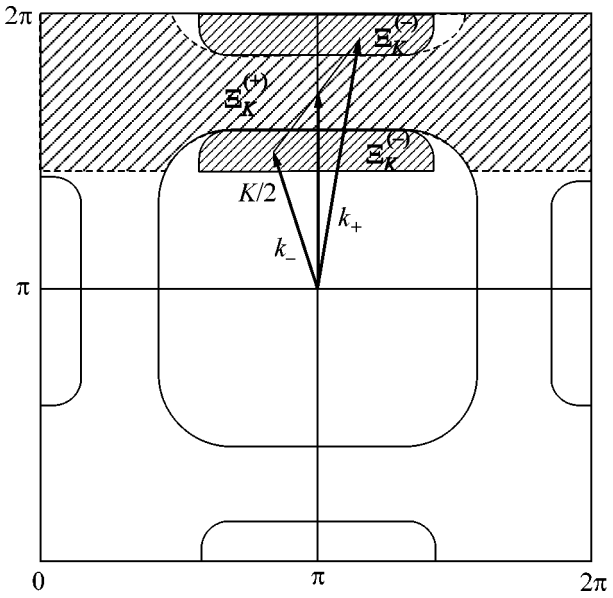

Fig. 2. Region $\Xi_K^{(-)}$ (hatched) of the momentum space involving the momenta k_+ and k_- of holes forming a pair with the total momentum K and region $\Xi_K^{(+)}$ of the momentum space including the momenta k'_+ and k'_- of electrons forming a pair with the same total momentum.

In [11], condition (2) in the form $\varepsilon(k) + \varepsilon(\pi - k) = \text{const}$ was treated as a necessary condition for η pairing. However, in the case of an ideal nesting at $K \longrightarrow 2k_F$, which was considered in [11], the surface area of the momentum space Ξ_K tends to zero. Therefore, as was shown in [12], the superconducting pairing can occur only upon a sufficiently strong interaction between carrier pairs at adjacent sites.

In actual fact, relationship (2) is a generalization of the nesting condition that is necessary for dielectric pairing upon a weak interaction when $\varepsilon(k) = -\varepsilon(k + Q)$ at any momenta k (belonging to the Fermi contour portion) and a specified momentum Q. Therefore, taking into account that, at $K \neq 0$, the range of definition of the relative motion momenta k of the K pair has a reflection symmetry with respect to the perpendicular to the vector **K** at the point $K/2$ and with respect to the vector **K** itself, equality (2) can be referred to as the condition for "mirror" nesting.

3. The above scenario of the formation of the pair Fermi contour is associated with such an interaction in the system of electrons that leads to a spatially inhomogeneous distribution of charges and spins in the conducting plane of CuO_2 and a corresponding change in the Fermi contour shape. The formation of a stripe structure can affect the Fermi contour shape to an extent that the electron motion in the conducting planes of high-T_c cuprates becomes quasi-one-dimensional in character [13]. In this respect, it can be assumed that the specific features of the crystal structure and electron–electron interactions in high-T_c cuprates can also provide the appropriate conditions for superconducting pairing of carriers with a large total pair momentum without formation of a spatially inhomogeneous structure.

An example is provided by the two-band model which is consistent with earlier calculations of the electronic structure of high-T_c compounds [14, 15]. This model allows for the interaction between electrons in the conducting plane of CuO_2 and in a certain parallel plane, for example, in the plane containing oxygen chains (as in the YBCO compound) or belonging to a reservoir (as for BiO in BSCCO, HgO in HBCCO, or TlO in TBCCO [16, 17]). Consequently, the Fermi contour is not singly connected, as is schematically shown in Fig. 2. This figure depicts a doubly connected hole-like Fermi contour centered at the point (π, π) for the BSCCO compound (a similar multiply connected structure of the Fermi contour in BSCCO was revealed by Bogdanov *et al.* [18] with the use of high-resolution angle-resolved photoemission spectroscopy). In the Fermi contour, a singly connected part that is centered at the point (π, π) and bears a resemblance in shape to a square with rounded corners [19], which is typical of high-T_c cuprates with hole doping, can be assigned primarily to the conducting plane of CuO_2. The second (smaller sized) singly connected part, which is centered at a point of the (0, π) type, is predominantly formed by electronic states corresponding to the BiO plane with metallic conductivity. Sufficiently long regions of these two parts o the Fermi contour are aligned nearly parallel to each other. This enables us to choose the total pair momentum K in such a way that the considerable portion of the boundary separating the occupied and vacant parts in the corresponding region Ξ_K will coincide with the Fermi contour. The direction of vector **K** should coincide with the direction of the nesting vector of the Fermi contour, i.e., with a direction of the [100] type (see Fig. 2). The magnitude of vector **K** is chosen so that the point $K/2$ bisects the distance between the nearly parallel regions of the two singly connected parts of the Fermi contour. As a result, the region Ξ_K consists of two regions, namely, the region $\Xi_K^{(-)}$ filled with holes and the region $\Xi_K^{(+)}$ free of holes.

In the case where only one band intersects the Fermi level, the Fermi contour is singly connected and its shape, which is determined from the experimental angle-resolved photoemission spectra of high-T_c cuprates with hole doping, corresponds to a square with rounded corners, as is schematically plotted in Fig. 2. The authors of [14] noted that the observed shape of the Fermi contour can be satisfactorily described in the tight binding approximation with appropriate fitting of hopping integrals for both nearest and several

next-to-nearest neighbor atoms. The dispersion law with allowance made for three coordination spheres can be written as

$$\varepsilon(k_1, k_2) = 2 - 2t_1(\cos k_1 a + \cos k_2 a) - 4t_2 \cos k_1 a \cos k_2 a - 2t_3(\cos 2k_1 a + \cos 2k_2 a), \quad (3)$$

where t_1, t_2, and t_3 are the hopping integrals for the first, second, and third coordination spheres, respectively. The hopping integrals are chosen in such a way as to provide the best agreement between the theoretical and experimental Fermi contour shapes. These integrals formally refer to sites of the conducting plane of CuO_2 but actually account for the interactions between this plane and the adjacent planes (belonging to the reservoir). It can be expected that this choice of the parameters t_1, t_2, and t_3 leads to a correct description of the family of isolines with energies close to the Fermi level.

Figure 3 schematically depicts the Fermi contour and zero-energy isolines for relative pair motion at $K = 0.94\pi/a$ and the following ratios between the hopping integrals in relationship (3): $t_1 = 0.5$, $t_2 = -03t_1$, and $t_3 = t_1$. As can be seen from this figure, the zero-energy isolines for the relative motion of the K pair virtually coincide with the terminal portions of the Fermi contour; i.e., the mirror nesting conditions are satisfied. It seems likely that the condition $t_3 = t_1$ is not typical of cuprates, because the fulfillment of this condition requires a considerable overlap of the orbitals centered at the third nearest neighbor atoms (copper atoms with oxygen in between and vice versa). However, it is not improbable that this condition can be satisfied in layered compounds with a different crystal chemical structure. This circumstance should be kept in mind when searching for new superconducting materials.

4. The mirror nesting is a sufficient condition for superconducting pairing at a large total pair momentum. We will restrict our consideration to the case when the sole significant interaction between particles forming the K pair is the screened Coulomb repulsion. This effective interaction gives rise to a bound state and can be approximated by a point interaction whose force is proportional to the area of the momentum space involving the initial and final relative motion momenta of the K pair [1, 2]. The matrix element of the effective interaction between particles forming the K pair depends on the part of the region Ξ_K (Fig. 2) in which scattering occurs upon the interaction: $\tilde{U}^*(k-k') \sim \Xi_K^{(-)}$ at k and $k' \in \Xi_K^{(-)}$, $\tilde{U}^*(k-k') \sim \Xi_K^{(+)}$ at k and $k' \in \Xi_K^{(+)}$, and $\tilde{U}^*(k-k') \sim \Xi_K$ at $k \in \Xi_K^{(-)}$ and $k' \in \Xi_K^{(+)}$ or, vice versa, at $k \in \Xi_K^{(+)}$ and $k' \in \Xi_K^{(-)}$. At $T = 0$, the equation for the superconducting order parameter Δ_{Kk}, which depends on the relative motion momentum k of the K pair, takes the form

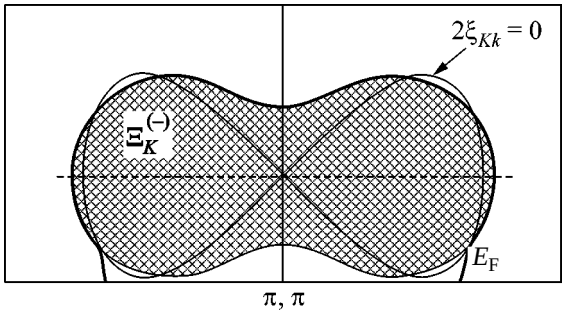

Fig. 3. Formation of the pair Fermi contour according to the one-band model (3). The thin line corresponds to $2\xi_K^{(-)} = 0$. The thick line illustrates the approximate fulfillment of the mirror nesting condition for the terminal portions of the Fermi contour. The relative K-pair motion momentum region corresponding to occupied states is hatched.

$$\Delta_{Kk} = -\frac{1}{2}\sum_{k' \in \Xi_K} \frac{\tilde{U}^*(k-k')\Delta_{Kk'}}{\sqrt{\xi_{Kk}^2 + \Delta_{Kk}^2}}. \quad (4)$$

For repulsive interaction between the particles forming the pair under investigation, Eq. (4) has no constant-sign solution similar to the Bardeen–Cooper–Schrieffer solution. In the present work, we restrict our treatment to the simplest discontinuous solution of Eq. (4) under the assumption that $\Delta_{Kk} \equiv \Delta_- > 0$ at $k \in \Xi_K^{(-)}$ and $\Delta_{Kk} \equiv +\Delta_+ < 0$ at $k \in \Xi_K^{(+)}$. In general, the change in sign of the superconducting order parameter in passing across the pair Fermi contour is characteristic of two-band models with repulsive interaction [20]. In this respect, it should be noted that, in the models considered in [16, 17], the superconducting order parameter changes sign when passing from the CuO_2 plane (in which the interaction between particles in the pair is assumed to be attractive) to the plane of oxygen chains or the reservoir plane with metallic conductivity (in which the interparticle interaction is assumed to be repulsive). Therefore, we can assume that, in the framework of the two-band models under consideration, the components of the K pair are located in different parallel planes. Note also that, in the Penson–Kolb–Hubbard one-dimensional model studied in [12], the order parameter corresponding to the η pairing changes sign when passing to every neighboring site; i.e., it is alternating and takes on constant values of opposite sign for two equivalent sublattices. Owing to quantum interference, a change in the phase of the superconducting order parameter by π upon the transfer of K pairs in the real space (and the appropriate phase change upon transfers between the regions $\Xi_K^{(-)}$ and $\Xi_K^{(+)}$ in the momentum space) results in an energy

gain due to the pair exchange contribution and is similar to the Josephson effect.

The above assumptions regarding the character of the solution to Eq. (4) permit us to rewrite this equation in the form of a system of two integral equations for the parameters Δ_- and Δ_+ [2], that is,

$$\begin{aligned}(1-\alpha)\Delta_- + \Delta_+ &= \frac{U_K h_\alpha}{2S}\sum_{k\in\Xi_K^{(-)}}\frac{\Delta_-}{\sqrt{\xi_{Kk}^2+\Delta_-^2}},\\ \Delta_- + \alpha\Delta_+ &= \frac{U_K h_\alpha}{2S}\sum_{k\in\Xi_K^{(+)}}\frac{\Delta_-}{\sqrt{\xi_{Kk}^2+\Delta_+^2}}.\end{aligned} \tag{5}$$

Here, we introduced the following notation: $\alpha \equiv \Xi_K^{(-)}$, $h_\alpha = 1 - \alpha - \alpha^2$, S is the normalization area, $U_K = (e^2 r_0/2\pi)\Xi_K a^2$ [2], and r_0 is the screening length. The quantities α and r_0 depend on the doping level; however, we will not discuss this dependence in the present work.

In the general case, we have $\Delta_- \neq \Delta_+$; however, at $\alpha = 1/2$, when the areas of the regions $\Xi_K^{(-)}$ and $\Xi_K^{(+)}$ are equal to each other, the system of equations (5) proves to be invariant with respect to the transformation $\Delta_- \longleftrightarrow \Delta_+$ and, hence, is reduced to one equation for the sole parameter $\Delta \equiv \Delta_- = \Delta_+$, that is,

$$\frac{U_K}{4S}\sum_{k\in\Xi_K^{(-)}}\frac{1}{\sqrt{\xi_{Kk}^2+\Delta^2}} = 1. \tag{6}$$

We will restrict our consideration to this special case, which, in principle, involves all the main features in the behavior of the superconducting order parameter.

5. For mirror nesting, the solution of Eq. (6) coincides in form with the standard Bardeen–Cooper–Schrieffer solution. In a real electronic system, the mirror nesting condition is satisfied only approximately, and the zero-kinetic-energy line of the relative motion of the K pair does not coincide with the boundary of the region $\Xi_K^{(-)}$ (it is within this region that the summation over the relative pair motion momentum is performed in Eq. (6)). Therefore, the deviation of the boundaries of the regions $\Xi_K^{(-)}$ and $\Xi_K^{(+)}$ from the pair Fermi contour plays the role of a specific truncation parameter in the equation for the superconducting energy gap in much the same manner as the magnetization in weak ferromagnets [21]. For a considerable deviation of the boundaries of the regions $\Xi_K^{(-)}$ and $\Xi_K^{(+)}$ from the pair Fermi contour, the state with a superconducting energy gap becomes impossible. For this reason, when changing over from summation in Eq. (6) to integration with respect to the components k_1 and k_2 of the relative pair motion momentum, proper allowance must be made for the fact that the zero-kinetic-energy of the relative pair motion [see relationship (1)] deviates from the boundary of the region $\Xi_K^{(-)}$ by the characteristic quantity Ω. It is this quantity Ω that has the meaning of the truncation parameter of integral (6) at the lower limit. Specifically, if the vector $\mathbf{k}$ runs through magnitudes corresponding to the boundary of the region $\Xi_K^{(-)}$, we obtain $\varepsilon(K/2 - k) = \mu$ and $\varepsilon(K/2 + k) - \mu \equiv 2\Omega \geq 0$, which corresponds to the effective truncation of the integral at the lower limit. The truncation parameter Ω depends on the component k_1 of the relative motion momentum. As a consequence, when integrating expression (6), it is convenient to change over from the variable k_2 to another variable that is reasonably chosen to be ξ_{Kk}. Then, expression (6) can be rewritten as

$$\frac{U_K}{4(2\pi)^2}\int_{-k_0}^{k_0}\int_{\Omega}^{\varepsilon_0}\frac{1}{\hbar v_{F2}}\frac{d\xi dk_1}{\sqrt{\xi_{Kk}^2+\Delta^2}} = 1, \tag{7}$$

where v_{F2} is the component of the Fermi velocity along the k_2 axis. This quantity only slightly depends on k within the region of integration $\Xi_K^{(-)}$; hence, it can be replaced by a mean value and factored outside the integral sign. The quantity $2k_0$ characterizes the length of the region $\Xi_K^{(-)}$ along the k_1 axis, and the quantity ε_0 determines its energy width. Let us assume that $\varepsilon_0 \gg \Delta$ (under this condition, the dependence of ε_0 on k_1 can be ignored) and perform elementary integration with respect to ξ. In order to evaluate the remaining integral over k_1, we will use the mean-value theorem and determine the truncation parameter in the form $\Omega \approx \nu\hbar^2 k_0^2/m$, where ν is the ratio between the magnitudes of the components m_1 and m_2 of the tensor of inverse effective masses ($\nu \ll 1$ for the Fermi contour shape typical of high-T_c cuprates with hole doping). Taking into account that $k_0/(2\pi)^2\hbar v_{F2} = g_k$ (where g_k is the mean density of states of the relative motion of the K pair within the region Ξ_K), for the superconducting energy gap, we obtain

$$\Delta = \sqrt{\Delta_0(\Delta_0 - 2\Omega)}, \tag{8}$$

where

$$\Delta_0 = 2\varepsilon_0\exp\left(-\frac{1}{U_K g_k}\right) \tag{9}$$

is the energy gap under the conditions of ideal mirror nesting, i.e., in the case when the boundaries of the region $\Xi_K^{(-)}$ completely coincide with the pair Fermi contour.

6. By assuming that the mirror nesting condition is best fulfilled at an optimum doping level $x = x_{opt}$, we can draw the inference that the deviation of x from x_{opt} in any direction is attended by changes in the size and

shape of the Fermi contour and should result in an increase in the effective truncation parameter $\Omega = \Omega(x)$. According to expression (8), Eq. (6) has a nontrivial solution when $2\Omega < \Delta_0$. Thus, two solutions of the equation $2\Omega = \Delta_0$, namely, x_1 and x_2, determine the doping range $x_1 < x < x_2$ in which the superconducting order parameter is nonzero.

REFERENCES

1. V. I. Belyavsky, V. V. Kapaev, and Yu. V. Kopaev, Zh. Éksp. Teor. Fiz. **118**, 941 (2000) [JETP **91**, 817 (2000)].
2. V. I. Belyavsky and Yu. V. Kopaev, Phys. Lett. A **287**, 152 (2001); V. I. Belyavsky and Yu. V. Kopaev, Zh. Éksp. Teor. Fiz. **121**, 175 (2002) [JETP **94**, 149 (2002)]; V. I. Belyavsky and Yu. V. Kopaev, cond-mat/0203138.
3. S.-C. Zhang, Science **275**, 1089 (1997).
4. Yu. V. Kopaev, in *Problems of High-Temperature Superconductivity*, Ed. by V. L. Ginzburg and D. A. Kirzhnits (Nauka, Moscow, 1977), Chap. 5.
5. M. Guidry, L.-A. Wu, Y. Sun, and C.-L. Wu, Phys. Rev. B **63**, 134 516 (2001).
6. B. I. Halperin and T. M. Rice, Solid State Phys. **21**, 115 (1968); B. A. Volkov, A. A. Gorbatsevich, Yu. V. Kopaev, and V. V. Tugushev, Zh. Éksp. Teor. Fiz. **81**, 729 (1981) [Sov. Phys. JETP **54**, 391 (1981)]; I. Afflec and J. B. Marston, Phys. Rev. B **37**, 3774 (1988).
7. A. Kaminski, S. Rosenkranz, H. M. Fretwell, *et al.*, cond-mat/0203133.
8. S. Chakravarty, R. B. Laughlin, D. K. Morr, and C. Nayak, Phys. Rev. B **63**, 094 503 (2001).
9. J.-P. Hu and S.-C. Zhang, Phys. Rev. B **64**, 100 502 (2001).
10. P. Bourges, Y. Sidis, H. F. Fong, *et al.*, Science **288**, 1234 (2000); P. C. Dai, H. A. Mook, R. D. Hunt, and F. Dogan, Phys. Rev. B **63**, 054 525 (2001).
11. C. N. Yang, Phys. Rev. Lett. **63**, 2144 (1989).
12. G. I. Japaridze, A. P. Kampf, M. Sekania, *et al.*, Phys. Rev. B **65**, 014 518 (2002).
13. J. Orenstein and A. J. Millis, Science **288**, 468 (2000).
14. J. Yu, S. Massidda, and A. J. Freeman, Phys. Lett. A **122**, 203 (1987).
15. W. E. Pickett, H. Krakauer, R. E. Cohen, and D. J. Singh, Science **255**, 46 (1992).
16. R. Combescot and X. Leyronas, Phys. Rev. Lett. **75**, 3732 (1995); Phys. Rev. B **54**, 4320 (1996).
17. R. Combescot, Phys. Rev. B **57**, 8632 (1998).
18. P. V. Bogdanov, A. Lanzara, X. J. Zhou, *et al.*, Phys. Rev. B **64**, 180 505 (2001).
19. Z.-X. Shen, W. E. Spicer, D. M. King, *et al.*, Science **267**, 343 (1995).
20. H. Suhl, B. T. Matthias, and L. R. Walker, Phys. Rev. Lett. **3**, 552 (1959); V. A. Moskalenko, Fiz. Met. Metalloved. **4**, 503 (1959).
21. P. Fulde and R. A. Ferrel, Phys. Rev. **135**, A550 (1964); A. I. Larkin and Yu. N. Ovchinnikov, Zh. Éksp. Teor. Fiz. **47**, 1136 (1964) [Sov. Phys. JETP **20**, 762 (1964)].

Translated by O. Borovik-Romanova

JETP Letters, Vol. 76, No. 1, 2002, pp. 50–52. Translated from Pis'ma v Zhurnal Éksperimental'noĭ i Teoreticheskoĭ Fiziki, Vol. 76, No. 1, 2002, pp. 57–59.

Tunneling of $6s^2$ Electrons in PbO and Bi_2O_3: XANES Spectroscopy and DFT Calculations

S. P. Gabuda[1,*], S. G. Kozlova[1], S. B. Érenburg[1, 2], N. V. Bausk[1, 2], R. L. Davidovich[3], V. V. Zyryanov[4], and Yu. M. Yukhin[4]

[1] *Nikolaev Institute of Inorganic Chemistry, Siberian Division, Russian Academy of Sciences, pr. akademika Lavrent'eva 3, Novosibirsk, 630090 Russia*

** e-mail: gabuda@casper.che.nsk.su*

[2] *Budker Institute of Nuclear Physics, Siberian Division, Russian Academy of Sciences, pr. Akademika Lavrent'eva 11, Novosibirsk, 630090 Russia*

[3] *Institute of Chemistry, Far East Division, Russian Academy of Sciences, pr. Stoletiya Vladivostoka 159, Vladivostok, 690022 Russia*

[4] *Institute of Solid-State Chemistry, Siberian Division, Russian Academy of Sciences, Novosibirsk, 630128 Russia*

Received May 29, 2002

Abstract—The results of XANES spectroscopy and DFT calculations are evidence for the occurrence of anomalous $2p_{2/3} \longrightarrow 6s_{1/2}$ electronic transitions in lead(II) and bismuth(III) oxides. The observed transitions may be due to the tunneling of outer $6s^2$ electrons. © *2002 MAIK "Nauka/Interperiodica".*

PACS numbers: 71.20.Ps; 78.70.Dm; 71.15.Mb

The mechanism of unusual structural distortions and symmetry lowering in some heavy *p*-element oxides occurring in low oxidation states is among the unresolved problems of condensed state physics [1, 2]. In particular, contrary to the majority of AB compounds with the simple cubic NaCl or CsCl structure, lead monoxide PbO crystallizes in two lower-symmetry modifications α-PbO and β-PbO [3]. Although the symmetry lowering in PbO is usually attributed to a change in the state of the outer ($6s^2$) electron shell of Pb^{2+} ion, the mechanism of this change still remains to be clarified [1, 2]. In this work, we studied the electronic structure of Pb^{2+} ions by analyzing their X-ray absorption near-edge structure (XANES). For comparison, an analogous study was carried out for the bismuth compounds. The measurement results were compared with the data of DFT (density functional theory) calculations.

The XANES experiments were conducted at the Center of Synchrotron Radiation Storage Ring VÉPP-3 (Budker Institute of Nuclear Physics, Siberian Division, Russian Academy of Sciences) at the EXAFS station. In measurements, the storage ring operated at an energy of 2.00 GeV and a current of 50–100 mA. An ionization chamber filled with Ar/He was used as a monitoring detector. A monoblock slit silicon single crystal ({111} plane) was used as a double crystal monochromator. The transmission spectra were recorded for samples pressed with an inert filler (cellulose). The preparation and analysis of the α-PbO, β-PbO, and β-PbO_2 samples (rutile structure) is described in [4]; the synthesis and properties of the cubic mixed-valence BiO_2(=$Bi^{III}Bi^{V}O_4$) oxide with fluorite structure (CaF_2) are described in [5]; and the α-B_2O_3 oxide was reagent grade. The BiOCl compound (reagent grade) and the PbClF compound obtained by interacting equimolar amounts of $Pb(NO_3)_2$, NH_4Cl, and NH_4F in an aqueous solution (both are structurally close to α-PbO) were also studied for comparison. Metallic lead and bismuth were used as a reference. All calculations were performed by the DFT method using the ADF program package with zero-order relativistic corrections [6].

The *L*(3)-edge fine structure of the X-ray absorption due to the electronic dipole transitions from the $2p_{3/2}$ core level to the unoccupied upper levels was studied. The X-ray absorption edge for metallic Pb and Bi is caused by the allowed transitions to the $6d_{5/2}$ and $7s_{1/2}$ levels. The tabulated absorption edge energies are $Pb^0L(3)$ = 13.034 keV and $Bi^0L(3)$ = 13.418 keV [7]. In the bivalent and quadrivalent lead compounds, the main peak is shifted, respectively, by 13 and 11 eV to higher energies, and a fine structure appears at lower energies. The fine structure is more clearly seen in the second derivatives of the X-ray absorption *L*(3)-edge curves for the bivalent lead compounds and PbO_2 (Fig. 1a). The results obtained for the bismuth compounds are identical (Fig. 1b).

With the aim of assigning the fine-structure components to particular electronic transitions, the transition energies Δ*E* were calculated for the Pb and Bi atoms and

ions. The results $\Delta E[Pb^0(2p_{3/2} \longrightarrow 6d_{5/2})] = 12.9036$ keV and $\Delta E[Pb^0(2p_{3/2} \longrightarrow s_{1/2})] = 12.9018$ keV differ from the experimental $Pb^0L(3) = 13.034$ keV by less than 1%. Similar results for bismuth gave $\Delta E[Bi^0(2p_{3/2} \longrightarrow 6d_{5/2})] = 13.2866$ keV and $\Delta E[Bi^0(2p_{3/2} \longrightarrow 7s_{1/2})] = 13.2948$ keV, which is also close to the experimental value $Bi^0L(3) = 13.418$ keV. The calculated and measured energy intervals in the X-ray absorption edge fine structure of the system are given in the table.

With such a good agreement between the calculated and experimental values of $\Delta E(6s_{1/2}–6p_{1/2})$, one can conclude that the $L(3)$-edge fine structure observed for PbO_2 and BiO_2 can be explained by the excitation of electronic dipole transitions $2p_{3/2} \longrightarrow 6s_{1/2}$ and $2p_{3/2} \longrightarrow 6p_{1/2}$ in the Pb^{4+} and Bi^{5+} ions, respectively. The first of these transitions is allowed, whereas the second is allowed only for the inner quantum number ($\Delta j = \pm 1$) but is forbidden by the rule $\Delta l = \pm 1$. It is likely that this forbiddenness is removed in the systems of interest by the strong spin–orbit interaction. In should also be noted that the $2p_{3/2} \longrightarrow 6s_{1/2}$-transition amplitude decreases in BiO_2 (compared to the same transition in PbO_2) because of the halving of the number of ions for which the $2p_{3/2} \longrightarrow 6s_{1/2}$ transitions can be observed. Such are only the Bi^{5+} ions ($5d^{10}$ configuration), whereas the corresponding transitions cannot occur in the Bi^{3+} ions ($5d^{10}6s^2$ configuration), because the $6s^2$ level is filled in these ions.

Likewise, the $2p_{3/2} \longrightarrow 6s_{1/2}$ transitions in the Pb^{2+} ions ($5d^{10}6s^2$ configuration) should not be observed. However, the expected behavior of X-ray absorption was observed only for PbFCl (Fig. 1a) and other bivalent lead compounds [$PbSO_4$, $Pb(NO_3)_2$, etc.] whose structure is undistorted. For these compounds, no anomalies were observed in the vicinity of the $2p_{3/2} \longrightarrow 6s_{1/2}$ transition. At the same time, the X-ray absorption in the vicinity of the $2p_{3/2} \longrightarrow 6s_{1/2}$ transition was observed for the α-PbO, β-PbO (Fig. 1a), and α-Bi_2O_3 (Fig. 1b) oxides, although, physically, it cannot occur in the free ions with filled $6s^2$ state. Unexpectedly, the Bi^{3+} ions in BiOCl showed a weak absorption peak in the vicinity of the $2p_{3/2} \longrightarrow 6s_{1/2}$ transition, although this compound is structurally and electronically analogous to PbFCl.

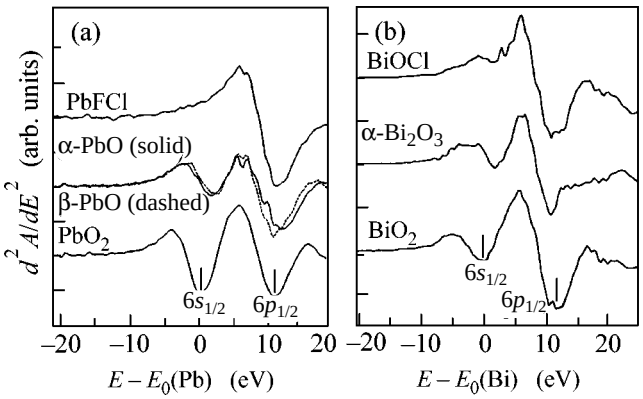

Fig. 1. Second derivatives of the X-ray absorption edge for (a) lead oxide Pb$L(3)$, (b) bismuth oxide Bi$L(3)$, and for PbFCl and BiOCl. The vertical lines indicate absorption peaks that are assigned to the $2p_{3/2} \longrightarrow 6s_{1/2}$ and $2p_{3/2} \longrightarrow 6p_{1/2}$ electronic transitions.

The appearance of anomalous X-ray absorption and $2p_{3/2} \longrightarrow 6s_{1/2}$ transitions in the ions with configuration $5d^{10}6s^2$ is evidence for a substantial change in the electronic structure of these ions in oxides, e.g., due to chemical bonding. However, the detailed band calculations did not reveal such bonding [1, 2]. An alternative mechanism for the modification of the electronic structure of the Pb^{2+} and Bi^{3+} ions may be associated with a nonzero probability of $6s^2$-electron tunneling through a potential barrier and with the formation of a virtual energy level [8]. Because of the nonzero transparency of a potential barrier, which prevents the delocalization of $6s^2$ electrons, the energy level with wave function $\Psi_{LP}(6s^2)$ splits due to tunneling. The order of magnitude for this splitting can be estimated [9] from the relation $\delta E \sim k(h^2/mD^2)$, where k is the barrier relative transparency, h is the Planck's constant, m is electron mass, and D is the tunneling distance (in α-PbO, $D_{Pb–Pb} = 3.83$ Å [3]). Therefore, the $6s^2$-pair tunneling gives rise to a nearby excited (unoc-

Calculated and experimental energy differences for the $6s_{1/2}$, $6p_{1/2}$, $6d_{5/2}$, and $7s_{1/2}$ levels (in eV)

Ion or atom	$\Delta E(6s_{1/2} - 6p_{1/2})$		$\Delta E(6s_{1/2} - 6d_{5/2})$		$\Delta E(6s_{1/2} - 7s_{1/2})$	
	calculation	experiment	calculation	experiment	calculation	experiment
Pb^{4+}	10.36	10.5 ± 0.5	26.91	27 ± 2	27.22	27 ± 2
Pb^{2+}	8.72	8.5 ± 0.5	21.68	20 ± 2	19.87	20 ± 2
Pb^0	7.29	–	15.18	–	13.45	–
Bi^{5+}	11.72	12 ± 0.5	31.52	30 ± 2	32.94	30 ± 2
Bi^{3+}	10.16	8 ± 0.5	25.29	25 ± 2	24.94	25 ± 2
Bi^0	8.33	–	17.99	–	16.18	–

cupied) $\Psi(6s_{1/2})'$ level, rendering the $2p_{3/2} \longrightarrow (6s_{1/2})'$ transitions observable.

The suggested mechanism of anomalous $2p_{3/2} \longrightarrow 6s_{1/2}$ transitions in oxides is confirmed by the well-known dependence of the barrier relative transparency on the electric field acting on atoms and ions [10]. This field is maximal precisely in the binary oxides, where the charge distribution in the cation surroundings is highly asymmetric: the cations are grouped into double layers in α-PbO and β-PbO and into cation pairs in α-Bi_2O_3 [3], while the negatively charged O^{2-} anions are situated on the outside of the layers and pairs. On the other hand, the Pb^{2+} ions in PbFCl are located at the centers of square pyramids formed by four singly charged F^- ions and one apical Cl^-. Such an arrangement corresponds to the more symmetric arrangement of the negatively charged ions in the Pb^{2+} environment and, hence, to a decrease in the electric field at the central ion. In the isostructural BiOCl, the Bi^{3+} ions are situated at the centers of similar square pyramids, but now they are formed by four doubly charged O^{2-} ions and one Cl^-. According to the above crude estimates, the electric field strength at the Bi^{3+} ions in this case is intermediate between the fields at the Pb^{2+} ions in PbFCl and the Pb^{2+} and Bi^{3+} cations in binary oxides, where these fields are maximal. Thus, the intensities of anomalous $2p_{3/2} \longrightarrow 6s_{1/2}$ transitions in the Pb^{2+} and Bi^{3+} ions correlate with the electric field strengths at these ions in the lead(II) and bismuth(III) compounds, confirming the relevance of these transitions to the tunneling of $6s^2$ electrons.

It should be noted in conclusion that the tunneling of $6s^2$ electrons with the formation of virtual levels leads to energy lowering by a value on the order of $\delta E \sim k(h^2/mD^2)$. Qualitatively, such an energy lowering can be sufficient to stabilize the distorted ion groups and to lower the symmetry in the Pb(II) and Bi(III) oxides and other crystals with closely related electronic structure. However, for a quantitative description of the symmetry lowering mechanism in ionic crystals, a more thorough consideration is needed with account taken of the mixed character of ionic $6s^2$ states in a strong field.

This work was supported by the Russian Foundation for Basic Research, project no. 02-03-32816.

REFERENCES

1. G. Watson, S. C. Parker, and G. Kresse, Phys. Rev. B **59**, 8481 (1999).
2. H. Terpsta, R. A. de Groot, and C. Haas, Phys. Rev. B **52**, 11 690 (1995).
3. A. F. Wells, *Structural Inorganic Chemistry* (Clarendon, Oxford, 1984, 5th ed.; Mir, Moscow, 1987).
4. V. V. Zyryanov and A. A. Gusev, Neorg. Mater. **37**, 323 (2001).
5. A. N. Romanov, D. P. Shashkin, and E. V. Khaula, Zh. Neorg. Khim. **45**, 570 (2000).
6. *Amsterdam Density Functional Program*, Release 2000.02 (Vrije Universteit, Amsterdam, 2000).
7. *XAFS Database International XAFS Society*, http://ixs.csrri.iit.edu/database; http://www.csrri.iit.edu/periodic-table.html.
8. J. M. Ziman, Solid State Phys. **26**, 1 (1971).
9. S. Flugge, *Practical Quantum Mechanics I* (Springer-Verlag, Berlin, 1971; Mir, Moscow, 1974), Task 20.
10. N. B. Delone and V. P. Kraĭnov, Usp. Fiz. Nauk **168**, 531 (1998) [Phys. Usp. **41**, 469 (1998)].

Translated by V. Sakun

JETP Letters, Vol. 76, No. 1, 2002, pp. 53–55. From Pis'ma v Zhurnal Éksperimental'noĭ i Teoreticheskoĭ Fiziki, Vol. 76, No. 1, 2002, pp. 60–62.

Energy Bounds of Linked Vortex States[1]

A. P. Protogenov and V. A. Verbus

Institute of Applied Physics, Russian Academy of Sciences, ul. Ul'yanova 46, Nizhni Novgorod, 603950 Russia
Institute for Physics of Microstructures, Russian Academy of Sciences, Nizhni Novgorod, 603950 Russia
e-mail: alprot@appl.sci-nnov.ru

Received April 30, 2002; in final form, May 30, 2002

Abstract—Energy bounds of knotted and linked vortex states in a charged two-component system are considered. It is shown that a set of local minima of free energy contains new classes of universality. When the mutual linking number of vector order parameter of vortex lines is less than the Hopf invariant, these states have lower lying energies. © *2002 MAIK "Nauka/Interperiodica".*

PACS numbers: 74.20.De; 11.15.Tk; 11.10.Lm

A tangle of vortex filaments is a system which attracts attention for several reasons. Along with the coherent state, which is the background of this vortex-field distribution, the filament system also contains a disorder combination due to free motion of its fragments and a topological order because of the effects of knotting and linking [1, 2] of its separate parts.

The study of a soft condensed matter, whose universal behavior is determined by topological characteristics, is recognized as one of the most challenging problems of modern condensed matter physics [3]. The aim of this paper is to find the energy bounds for vortex states with a set of numbers determining the knotting and linking degree of the fields that take part in the description of the coherent state. We will use the Ginzburg–Landau model

$$F = \int d^3x \left[\sum_\alpha \frac{1}{2m} \left| \left(\hbar \partial_k + i \frac{2e}{c} A_k \right) \Psi_\alpha \right|^2 + \sum_\alpha \left(-b_\alpha |\Psi_\alpha|^2 + \frac{c_\alpha}{2} |\Psi_\alpha|^4 \right) + \frac{\mathbf{B}^2}{8\pi} \right] \quad (1)$$

with a two-component order parameter

$$\Psi_\alpha = \sqrt{2m}\rho\chi_\alpha, \quad \chi_\alpha = |\chi_\alpha| e^{i\varphi_\alpha}, \quad (2)$$

satisfying the CP^1 condition $|\chi_1|^2 + |\chi_2|^2 = 1$. This model is used in the context of two-gap superconductivity [4, 5] and in the non-Abelian field theory [6, 7] (see also [8]).

It was shown in paper [4] that there exists an exact mapping of the model (1), (2) into the following version of *n*-field model:

$$F = \int d^3x \left[\frac{1}{4}\rho^2 (\partial_k \mathbf{n})^2 + (\partial_k \rho)^2 + \frac{1}{16}\rho^2 \mathbf{c}^2 + (F_{ik} - H_{ik})^2 + V(\rho, n_3) \right]. \quad (3)$$

To write Eq. (3), the dimensionless units and gauge-invariant order-parameter fields of the unit vector $\mathbf{n} = \bar{\chi}\boldsymbol{\sigma}\chi$ [$\bar{\chi} = (\chi_1^*, \chi_2^*)$ and $\boldsymbol{\sigma}$ are the Pauli matrices] and the velocity $\mathbf{c} = \mathbf{J}/\rho^2$ are used. The total current $\mathbf{J} = 2\rho^2(\mathbf{j} - 4\mathbf{A})$ has a paramagnetic ($\mathbf{j} = i[\chi_1 \nabla \chi_1^* - \text{c.c.} + (1 \longrightarrow 2)]$) and a diamagnetic ($-4\mathbf{A}$) part. Besides, in Eq. (3) $F_{ik} = \partial_i c_k - \partial_k c_i$ and $H_{ik} = \mathbf{n} \cdot [\partial_i \mathbf{n} \times \partial_i \mathbf{n}] \equiv \partial_i a_k - \partial_k a_i$.

Setting in Eq. (3) $\mathbf{c} = 0$ we get the Faddeev–Niemi model [9]. The numerical study of the knotted configurations of the **n** field in this model was done in [10–12]. The lower energy bound in this case,

$$F \geq 32\pi^2 |Q|^{3/4}, \quad (4)$$

is determined [13–15] by the Hopf invariant

$$Q = \frac{1}{16\pi^2} \int d^3x \varepsilon_{ikl} a_i \partial_k a_l. \quad (5)$$

At compactification $\mathbb{R}^3 \longrightarrow S^3$ and $\mathbf{n} \in S^2$, the integer $Q \in \pi_3(S^2) = \mathbb{Z}$ shows the degree of linking or knotting of filamentary manifolds, where the vector field $\mathbf{n}(x, y, z)$ is defined. In particular, for two linked rings (Hopf linking) $Q = 1$, the trefoil knot $Q = 6$, etc. The significant point is the following: $\pi_3(CP^M) = 0$ at $M > 1$ and $\pi_3(CP^1) = \pi_3(S^2) = \mathbb{Z}$ [16]. In the latter case, the order parameter (2) is two-component [4], and the linked or knotted soliton configurations are labeled by the Hopf invariant (5). In the $(3 + 0)D$ case of free energy (3), Hopf invariant (5) is analogous to the

[1] This article was submitted by the authors in English.

Chern–Simons action $(k/4\pi)\int dt\, d^2x \varepsilon_{\mu\nu\lambda} a_\mu \partial_\nu a_\lambda$ that determines strong correlations of $(2+1)D$ modes [17, 18] at semion value $k \simeq 2$.

Let us assume that ρ can be found from the minimal value of the potential $V(\rho)$ and that the velocity $\mathbf{c}$ does not equal zero. Equation (3) in this case has the following form:

$$F = F_n + F_c - F_{\text{int}}$$
$$= \int d^3x \left[((\partial_k \mathbf{n})^2 + H_{ik}^2) + \left(\frac{1}{4}\mathbf{c}^2 + F_{ik}^2\right) - 2F_{ik}H_{ik} \right]. \quad (6)$$

It can be seen from Eq. (6) that a superconducting state with $\mathbf{c} \neq 0$ has energy which is less than the minimum in Eq. (4) due to the renormalization of the coefficient (= 1) in the second term of the functional F_n. To find the lower free-energy bound in the superconducting state with $\mathbf{c} \neq 0$, we will use the following inequality:

$$F_n^{5/6} F_c^{1/2} \geq (32\pi^2)^{4/3} |L|, \quad (7)$$

where

$$L = \frac{1}{16\pi^2} \int d^3x \varepsilon_{ikl} c_i \partial_k a_l \quad (8)$$

is the degree of mutual linking [19, 20] of the velocity $\mathbf{c}$ lines and of the magnetic-field lines $\mathbf{H} = [\nabla \times \mathbf{a}]$. It is also an integral of motion [20, 21].

The proof of inequality (7) employs the following set of inequalities:

$$|L| \leq \|\mathbf{c}\|_6 \cdot \|\mathbf{H}\|_{6/5} \leq 6^{1/6} \|[\nabla \times \mathbf{c}]\|_2 \cdot \|\mathbf{H}\|_{6/5}$$
$$\leq 6^{1/6} \|[\nabla \times \mathbf{c}]\|_2 \cdot \|\mathbf{H}\|_1^{2/3} \cdot \|\mathbf{H}\|_2^{1/3} \quad (9)$$
$$\leq (32\pi^2)^{-4/3} F_c^{1/2} F_n^{2/3} F_n^{1/6} = (32\pi^2)^{-4/3} F_n^{5/6} F_c^{1/2}.$$

Here, $\|\mathbf{H}\|_p \equiv \left(\int d^3x |\mathbf{H}|^p\right)^{1/p}$. At the first and third steps, we used the Hölder inequality $\|\mathbf{fg}\| \leq \|\mathbf{f}\|_p \cdot \|\mathbf{g}\|_q$, where $1/p + 1/q = 1$. Under the condition $\nabla \cdot \mathbf{c} = 0$, the second step corresponds to the use of the Ladyzhenskaya inequality [22] $\|\mathbf{c}\|_6 \leq 6^{1/6} \|[\nabla \times \mathbf{c}]\|_2$. The fourth step in Eq. (9) arises after comparison of the terms $\|\nabla \times \mathbf{c}\|$ and $\|\mathbf{H}\|$ with the terms F_c and F_n in Eq. (6). The coefficient in Eq. (9) in our case turns out to be the same as in Eq. (4) [15]. The last line in Eq. (9) also shows the contributions from the $\mathbf{n}$ and $\mathbf{c}$ parts of free energy (6) to the final result (7).

Applying the Schwartz–Cauchy–Bunyakovsky inequality to F_{int} in Eq. (6) yields

$$F_{\text{int}} \leq 2\|F_{ik}\|_2 \cdot \|H_{ik}\|_2 \leq 2F_c^{1/2} F_n^{1/2}. \quad (10)$$

The equality in the r.h.s. of Eq. (10) is achieved in the limit of a small size of linked vortex configurations. Substituting the boundary value of F_{int} into Eq. (6), we get

$$F \geq F_{\min} = F_n \left(1 - \sqrt{F_c/F_n}\right)^2. \quad (11)$$

The Hopf configuration with $Q = 1$, for which the equality in Eq. (4) is reached, is two linked rings of radius R and $(F_n)_{\min} = 2\pi^2 R^3 (8/R^2 + 8/R^4)|_{R=1} = 32\pi^2$. Accordingly, in our case, $\mathbf{c} \neq 0$, we will assume the existence of configurations satisfying the equality in Eq. (7). It is important to emphasize that, for small ρ in Eq. (3) and therefore for large $\mathbf{c}$ [because all terms in Eq. (3) are of the same order], we encounter the instability of linked vortex with respect to dilatation transformations [15]. This results in the restriction of F_c from above. Taking into account this remark, we will use for F_c in Eq. (11) the lower bound $F_c^{1/2} = (32\pi)^{4/3} F_n^{-5/6} |L|$ in Eq. (7) and $F_n = 32\pi^2 |Q|^{3/4}$ to have finally

$$F \geq 32\pi^2 |Q|^{3/4} \left(1 - |L|/|Q|\right)^2. \quad (12)$$

The inequality (12) is the main result of this paper. The trivial case $Q = 0$ should be considered after the limit $L = 0$. Let us also pay attention to the self-dual relation $F_n = \alpha F_c$ with $\alpha \sim 1$, which follows from $F_{\min}$.

It follows from Eq. (12) that for all numbers $L < Q$ the ground-state energy is less than in the model described in [9], for which inequality (4) is valid. The origin of the energy decrease can easily be understood. Even under the conditions of the existence of the paramagnetic part $\mathbf{j}$ of the current $\mathbf{J}$, the diamagnetic interaction in the superconducting state consumes its own current energy and a part of the energy relating to the $\mathbf{n}$-field dynamics for all state classes with $L < Q$.

The case where ρ is not a constant for both $\mathbf{c} = 0$ [23] and $\mathbf{c} \neq 0$ is of a certain interest. It is more complicated owing to certain reasons and will be considered in a separate paper (see also [24]). We only mention that in a soft case $\rho \neq$ const we must prove the compatibility of the specific value of the coefficient in the r.h.s. of Eq. (7) with the stability condition [15]. The equality in Eq. (12) under this remark should be understood as an ideal limit depending on the topological characteristics of knots and links only.

In conclusion, we have found the energy bounds of the superconducting states using the CP^1 version of Ginzburg–Landau model under conditions of the existence of linking and knotting phenomena of the $\mathbf{n}$ and $\mathbf{c}$ fields being the gauge-invariant order parameters of the considered system. We have shown that the energy space of the local minima contains new state classes with $L < Q$.

We thank A.G. Abanov, L.D. Faddeev, E.A. Kuznetsov, and G.E. Volovik for their advice, V.F. Gantmakher for crucial remarks, and G.M. Fraiman, A.G. Litvak, and V.A. Mironov for useful discussions. This

work was supported in part by the Russian Foundation for Basic Research, project no. 01-02-17225.

REFERENCES

1. V. M. H. Ruutu, U. Parts, J. H. Koivuniemi, *et al.*, Pis'ma Zh. Éksp. Teor. Fiz. **60**, 659 (1994) [JETP Lett. **60**, 671 (1994)].
2. Yu. G. Makhlin and T. Sh. Misirpashaev, Pis'ma Zh. Éksp. Teor. Fiz. **61**, 48 (1995) [JETP Lett. **61**, 49 (1995)].
3. V. Katritch, J. Bednar, D. Michoud, *et al.*, Nature **384**, 142 (1996).
4. E. Babaev, L. D. Faddeev, and A. J. Niemi, Phys. Rev. B **65**, 100512 (2002); cond-mat/0009438.
5. E. Babaev, Phys. Rev. Lett. **88**, 177 002 (2002).
6. L. D. Faddeev and A. J. Niemi, Phys. Lett. B **525**, 195 (2002).
7. Y. M. Cho, Phys. Rev. Lett. **87**, 252 001 (2001); hep-th/0110076.
8. P. van Baal and A. Wipf, hep-th/0105141.
9. L. D. Faddeev and A. J. Niemi, Nature **387**, 58 (1997).
10. J. Gladikowski and M. Hellmund, Phys. Rev. D **56**, 5194 (1997).
11. R. A. Battye and P. M. Sutcliffe, Phys. Rev. Lett. **81**, 4798 (1998).
12. J. Hietarinta and P. Salo, Phys. Lett. B **451**, 60 (1999).
13. A. F. Vakulenko and L. V. Kapitansky, Dokl. Akad. Nauk SSSR **246**, 840 (1979) [Sov. Phys. Dokl. **24**, 433 (1979)].
14. A. Kundu and Yu. P. Rubakov, J. Phys. A **15**, 269 (1982).
15. R. S. Ward, Nonlinearity **12**, 1 (1999); hep-th/9811176.
16. A. G. Abanov and P. W. Wiegmann, hep-th/0105213.
17. L. A. Abramyan, A. P. Protogenov, and V. A. Verbus, Pis'ma Zh. Éksp. Teor. Fiz. **69**, 839 (1999) [JETP Lett. **69**, 887 (1999)].
18. A. P. Protogenov, Pis'ma Zh. Éksp. Teor. Fiz. **73**, 292 (2001) [JETP Lett. **73**, 255 (2001)].
19. V. I. Arnold and B. A. Khesin, *Topological Methods in Hydrodynamics* (Springer-Verlag, New York, 1998), Appl. Math. Sci., Vol. 125, Chap. 3.
20. V. E. Zakharov and E. A. Kuznetsov, Usp. Fiz. Nauk **167**, 1137 (1997) [Phys. Usp. **40**, 1087 (1997)].
21. H. K. Moffatt, J. Fluid Mech. **106**, 117 (1969).
22. O. A. Ladyzhenskaya, *The Mathematical Theory of Viscous Incompressible Flow* (Gordon and Breach, New York, 1969).
23. M. Lübcke, S. M. Nasir, A. Niemi, and K. Torokoff, hep-th/0106102.
24. A. P. Protogenov, cond-mat/0205133.

JETP Letters, Vol. 76, No. 1, 2002, pp. 56–60. From Pis'ma v Zhurnal Éksperimental'noĭ i Teoreticheskoĭ Fiziki, Vol. 76, No. 1, 2002, pp. 63–67.

Timelapse¶

S. De Leo[1] and P. Rotelli[2]

[1]*Department of Applied Mathematics, University of Campinas PO Box 6065, SP 13083-970 Campinas, Brazil*
e-mail: deleo@ime.unicamp.br

[2]*Department of Physics and INFN, University of Lecce PO Box 193, I 73100, Lecce, Italy*
e-mail: rotelli@le.infn.it

Received 22 April, 2002

Abstract—We discuss the existence, in an arbitrary frame, of a finite time for the transformation of an initial quantum state into another, e.g., in a decay. This leads to the introduction of a timelapse $\tilde{\tau}$, by analogy with the lifetime of a particle. An argument based upon the Heisenberg uncertainty principle suggests the value of $\tilde{\tau} = 1/M_0$. Consequences for the exponential decay formula and the modifications which $\tilde{\tau}$ introduces into the Breit–Wigner mass formula are described. © *2002 MAIK "Nauka/Interperiodica".*

PACS numbers: 03.65.Ta; 14.70.Hp; 13.90.+i

The subject of this paper concerns the exponential decay law and the Breit–Wigner (BW) mass-distribution formula. These formulas are a standard part of particle physics and can indeed be connected by a simple transform, as is taught in many undergraduate physics courses [1]. In recent years, the validity of the BW has been demonstrated to an unprecedented degree by the LEP data and analysis of the Z gauge particle [2]. After substantial theoretical corrections for radiative effects, the predicted theoretical width (assuming three light neutrinos) and the experimental value, based upon a BW fit, agree to better than one percent. We will be interested later in a small discrepancy, but our first observation is that the agreement is quite impressive. These facts are somewhat surprising because neither the exponential decay law nor the BW mass curve is predicted rigorously within Quantum Mechanics (QM). On the contrary, we have precise QM objections to the former [3, 4] and only approximate derivations of the latter [5, 6]. Nor does a field theoretical treatment change the situation. To some, these QM results relegate our two formulas to little more than phenomenological games. We, on the other hand, start with these two formulas and argue for a modification which will in part reconcile the decay law with QM and provide an explanation for the discrepancy in the Z width described above.

One of the implicit assumptions in particle physics is that decays occur instantaneously. However, as Einstein has taught us, istantaneity, for anything other than a point, can at best be valid in a single Lorentz frame. Thus, even if, say, in its rest frame, a particle decayed instantaneously, a general observer would find different times for decays at different points within the wave packet. Of course, this could only be determined in a statistical sense since the wave function is not an observable. Thus, in general, there will exist times during which the quantum state is neither the initial nor the final state but a linear combination of both that tends towards the latter with increasing time. We shall call a measure of this time interval the "timelapse."

There is only one exception to the above observations; a measurement process may involve (ideally) the localization in space and time of a particle. This wave function collapse is instantaneous for all observers (it defines the corresponding event in each frame) and is fundamentally irreversible, since the creation of a particle at a given space-time point cannot instantaneously inflate to finite space regions without violating the limiting velocity of light. The wave function collapse is a subject of great interest in itself but will not concern us further in this paper.

Why cannot we avoid the discussion of timelapse by considering particle or state creation to be a delta function in space and time? First, because in many practical problems we know that this is not the case, e.g., as for a particle trapped in a potential well, e.g., a muon within a muonic atomic state. Second, because we often know or desire to study particles which approximate energy–momentum eigenstates, and this implies large spatial dimensions.

An earlier introduction of a type of timelapse is contained in the book by Jackson [7]. In one of the classical derivations of essentially quantum effects, Jackson introduces the "formation time" of an electron in the nuclear beta decay. Arguing that the outgoing energetic electron could be considered as accelerated from rest to its final velocity over a finite formation time, he calculates the induced spectrum of radiation by the electron

¶This article was submitted by the authors in English.

(inner bremsstrahlung). Jackson also notes that the same effect would occur if a charge was created during the same time interval. Invoking the uncertainty principle, he evaluates this time interval Δt as

$$\Delta t \sim 1/E, \tag{1}$$

where E is the electron energy. Now, while acknowledging the precedence of Jackson's idea of a formation time, his approach is significantly different from ours. The use of the particle energy in Eq. (1) implies that different particles take different times for acceleration. Of course, the antineutrino does not contribute to the inner bremsstrahlung and the heavy nucleon contributions are negligible, so this may appear to be an academic question. However, to us, it is obvious that the same timelapse must occur for each of the particles in the final state, independent of their final energy or momentum. It is not conceivable that the outgoing electron is created with a certainty close to unity, while the antineutrino is, perhaps, to all extents still to be created. We will take care to define for each decay a common timelapse that depends, at most, upon the kinematics of the initial system in a preferential Lorentz frame. Of course, one must also guarantee that the timelapse of the outgoing state coincides with that of the vanishing incoming state.

Is the timelapse a function of the spatial localization of the quantum state? We believe not. There is a Δt directly connected to Δx, but this is what we might call "passage time." Consider a single particle with a sufficiently large Δx in the approximate $(E, p, 0, 0)$ eigenstate (for simplicity we take its momentum along the x axis). Using the uncertainty principle $\Delta x \Delta p \sim 1$ and the Einstein relation $E^2 = p^2 + M^2$, we find

$$\Delta x \longrightarrow \Delta p \longrightarrow \Delta E = p\Delta p/E \sim v/\Delta x;$$

hence,

$$\Delta t \sim \Delta x/v, \tag{2}$$

where v is the velocity of the particle. Thus, Δt is for our wave packet a measure of the time it takes to pass a given y–z plane, hence, the name passage time. This Δt obviously has nothing to do with a timelapse, and indeed becomes infinite in the particle rest frame. On the other hand, we expect from the approximate validity of the exponential decay law that a timelapse must be small compared to the lifetime of a particle in any frame (see below).

We believe that timelapse must be a close relative of lifetime. As for lifetime, we will define it in the rest frame of an initial single-particle state, or, more precisely, the frame in which the average velocity is null. By analogy with the lifetime τ, we will denote the timelapse for a process by $\tilde{\tau}$. What does the Heisenberg uncertainty principle tell us? We have excluded a connection to ΔE and can also exclude the halfwidth ΔM for a decay particle, since this is reserved for τ,

$$\tau = 1/\Delta M. \tag{3}$$

This leaves us with essentially only one choice,

$$\tilde{\tau} = 1/M_0, \tag{4}$$

for a decaying particle with central mass M_0.

Now, a decay of a composite particle such as a J/ψ may be considered an annihilation and/or interaction at the quark level. Thus, a timelapse for interactions should also be defined. The natural choice for $\tilde{\tau}$ in these cases is

$$\tilde{\tau} = 1/E_{CM}, \tag{5}$$

where E_{CM} is the center-of-mass energy. Equation (5) would automatically include Eq. (4) if it was not for the fact that a given decay may occur at a mass diverse from M_0 due to the existence of mass curves. To reconcile the two, we should modify Eq. (4) as

$$\tilde{\tau} = 1/M, \tag{6}$$

but in the subsequent applications in this paper we will employ Eq. (4) for simplicity.

How does the existence of a $\tilde{\tau}$ modify the exponential decay law? This can easily be derived after assuming a given analytic form for a state during timelapse. For simplicity and by analogy with the original decay law, we will assume this to be an exponential form. Exponential decrease $\exp[-t/\tilde{\tau}]$ is assumed for the incoming state and its complement, $1 - \exp[-t/\tilde{\tau}]$, for the corresponding outgoing state. Thus, when we consider an ensemble of $N(t)$ particles with a given lifetime τ and timelapse $\tilde{\tau}$, we must divide them into two classes: N_u, the number of undecayed particles, and N_d, those that have begun the decay process but have still a residual probability of being found in a measurement of $N(t)$. N_d would be zero if the instantaneous decay ($\tilde{\tau} = 0$) was valid.

The differential equation that governs $N_u(t)$ is the standard one

$$dN_u(t) = -\frac{1}{\tau}N_u(t)dt, \tag{7}$$

while that for $N_d(t)$ must allow for a source term proportional to $dN_u(t)$,

$$dN_d(t) = -\frac{1}{\tilde{\tau}}N_d(t)dt - dN_u(t); \tag{8}$$

the negative sign of the last term is correct since $dN_u(t) < 0$ for $dt > 0$.

Now, solving these coupled equations and using initial condition $N_d(0) = 0$, we find

$$N(t) = \frac{N(0)}{\tau - \tilde{\tau}}\left[\tau\exp\left(-\frac{t}{\tau}\right) - \tilde{\tau}\exp\left(-\frac{t}{\tilde{\tau}}\right)\right]. \tag{9}$$

This is the modification of the standard exponential decay law that our timelapse $\tilde{\tau}$ introduces. Note that for

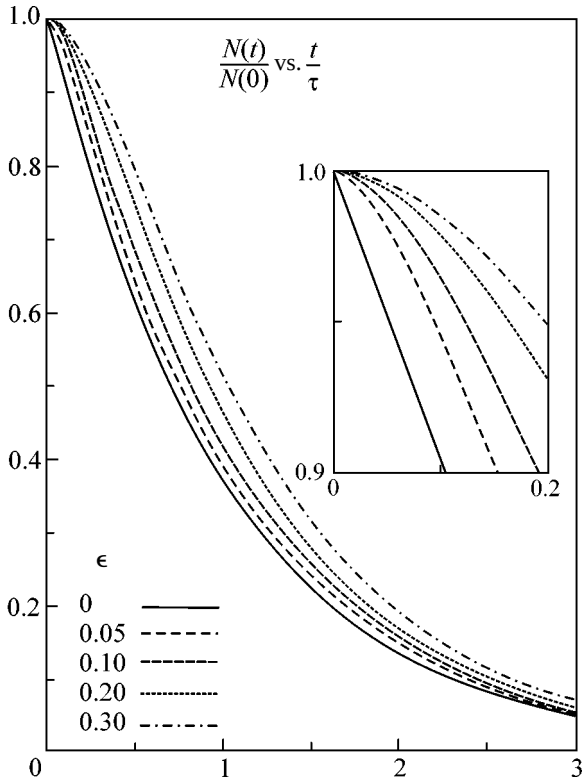

Fig. 1. The decay law $N(t)/N(0)$ versus t/τ for various values of ϵ.

$\tilde{\tau} = 0$ we obtain the single exponential form, and the limit $\tau = 0$ yields an exponential decay with lifetime $\tilde{\tau}$. Whence $\tilde{\tau} = 1/M_0$ sets a lower limit to the effective lifetime and, hence, an upper limit to the halfwidth.

A simple calculation yields, for the effective lifetime τ_{eff},

$$\tau_{\text{eff}} = (\tau^3 - \tilde{\tau}^3)/(\tau^2 - \tilde{\tau}^2). \tag{10}$$

For $\tilde{\tau} \ll \tau$, we can write

$$\tau_{\text{eff}} = \tau[1 + \epsilon^2 + O(\epsilon^3)], \tag{11}$$

where $\epsilon = \tilde{\tau}/\tau$. However, we note that the decay rate Γ remains connected to τ, $\Gamma = 1/\tau$. This follows from our assumption that $\tilde{\tau} \sim 1/M_0$, and, hence, it is independent of any interaction coupling constants, in contrast to Γ and τ, which obviously are directly dependent.

Another very interesting observation is that, for very small t, Eq. (9) has no linear term in t. Indeed for $t \ll \tilde{\tau}, \tau$

$$N(t) = N(0)\left[1 - \frac{t^2}{2\tau\tilde{\tau}} + O(t^3)\right]. \tag{12}$$

This reconciles, for short times, our modified decay law (no longer a single exponential) with basic quantum-mechanical arguments [8–10], which have led, amongst other things, to the so-called quantum Zeno effect [11, 12]. This, at least, in principle allows $\tilde{\tau}$ to be calculated from Eq. (12) and the quantum-mechanical result $P(t) = 1 - t^2(\Delta H)^2 + \ldots$ [13]; specifically $\tilde{\tau} = 1/[2\tau(\Delta H)^2] = \Gamma/[2(\Delta H)^2]$.

In Fig. 1, we show the modification of $|\psi(t)|^2 \equiv P(t)$ for various ϵ values. In this plot, the increase of the effective lifetime is evident, as is the annulment of $dP(t)/dt$ (insert) for $t \longrightarrow 0$ (source of the quantum Zeno effect). The direct measurement of $|\psi(t)|^2$ is often possible (e.g., in muon decay). However, for muons $\epsilon \sim 3 \times 10^{-16}$, so that no effect due to $\tilde{\tau}$ could ever be detected.

Let us now calculate the modification in the standard BW mass formula produced by Eq. (9). We have

$$|\psi(t)| \propto \exp\left(-\frac{t}{2\tau}\right)\left\{1 - \epsilon\exp\left[\frac{t(\epsilon-1)}{\epsilon\tau}\right]\right\}^{1/2}.$$

Hence,

$$\chi(x) = \int_0^\infty dt \exp\left(i\frac{x}{2\tau}t\right)|\psi(t)|$$

$$\propto \frac{1}{x+i} - \sum_{n=1}^{\infty}\frac{n!!}{2^n n!}\frac{\epsilon^n}{x + ia_n},$$

where $x = 2\tau(M - M_0)$ and $a_n = 1 + 2n(1-\epsilon)/\epsilon$. Treating ϵ as a small quantity, we may perform an analytic calculation of $|\chi(x)|^2$ to the lowest order in ϵ. We find our modified Breit–Wigner (MBW) as follows:

$$\text{MBW} \equiv |\chi(x)|^2 = BW\left\{1 - \epsilon\frac{x^2 + a_1}{x^2 + a_1^2} + \frac{\epsilon^2}{4}\left[\frac{7}{2} + \frac{x^2+1}{x^2+a_1^2} - \frac{x^2+a_2}{x^2+a_2^2}\right] + O(\epsilon^3)\right\}, \tag{13}$$

where $BW = 2\tau M_0/\{[\pi/2 + \arctan(2\tau M_0)](x^2 + 1)\}$ is the standard BW.

Now, ϵ is so small for almost all weak or electromagnetic decays that one might think of passing directly to the strong decays in search of the evidence of a MBW. However, of all weak processes, a special role is played by the decays of heavy intermediate vector bosons W and Z. These have widths of several GeV and, thus, correspond to ϵ of a few %. Furthermore, the data on Z are particularly precise with errors in M_z and Γ_z on the order of 10^{-5}. The LEP data yield such precise results that there are even two standard deviations from the theory in Γ_z. This is expressed by two equivalent numbers [2]

$$\Gamma_{\text{inv}} = -2.7^{+1.7}_{-1.5}\ \text{MeV}$$

and/or

$$N_\nu = 2.9841 \pm 0.0083.$$

Now, for Z we can apply the formula given above, since $\epsilon_Z = 2.7\%$. From this formula (see also Fig. 2) we readily see that

(1) the maximum modification to the underlying BW ($\tilde{\tau} = 0$) occurs at $M = M_0$, i.e., at the peak. This effect is an increase of the peak value by $1 + 3\epsilon^2/8$. Note, however, that this underlying BW must not be confused with the best fit BW need to the data in the presence of a non-negligible $\tilde{\tau}$;

(2) the halfwidth of the underlying BW and the MBW are almost the same for small ϵ. That of the MBW is reduced by a factor of order ϵ^3 and not ϵ^2, as might have been expected from Eq. (11) for the lifetime modification.

The smallest errors of the curve are around the peak value $M = M_0$. In a fit with a BW to data, in accord with our modified curve, one would be inclined to raise the peak value with consequently the same decrease in percentage of the halfwidth. Hence, we expect the fitted BW to yield a width lower than ours by, at most, the factor $1 - 3\epsilon^2/8$. Hence our estimate of Γ_{inv} is

$$-0.7 \text{ MeV} \le \Gamma_{\text{inv}} < 0$$

less than 1/4 of the measured central value. It is amusing to note that, using the result $\Gamma_{\text{eff}} = (1 + \epsilon^2)\Gamma$, one might have expected an effect on Γ_{inv} in good agreement with the experimental value.

The modified BW can also be calculated numerically for any ϵ, and in Fig. 2 we show the ratio of this with the underlying BW for various ϵ values. The width is indeed reduced. From Fig. 2, we see that, for $\epsilon \le 0.3$ and such that $1.4 > M/M_0 > 0.6$, the main modification indeed occurs at $M = M_0$ and is an increase on the order of a few % or less. This means that no significant evidence for the existence of $\tilde{\tau}$ from mass curves is possible until the individual errors of the data points are of this order or better.

Obviously, in looking for evidence for our modified BW, we are led to consider the largest ϵ values available. This means particles with strong interaction decays. For example, the $\rho(770)$, where $\epsilon \sim 20\%$. However, the best data points for ρ [14] are somewhat dated and are not yet precise enough to yield evidence for a $\tilde{\tau}$.

It is natural to extend the concept of timelapse from the realm of decays to interactions in general. We have already anticipated that in these cases $\tilde{\tau} = 1/E_{CM}$. However, what is $\tilde{\tau}$ to be compared with? What plays the role of τ, here? The only thing available is $\sqrt{\sigma}$ the square root of the cross section. For numerical comparisons, we recall that $\sqrt{60 \text{ mb}} \sim 10^{-23}$ s, while 1 GeV $\sim 6.6 \times 10^{-25}$ s.

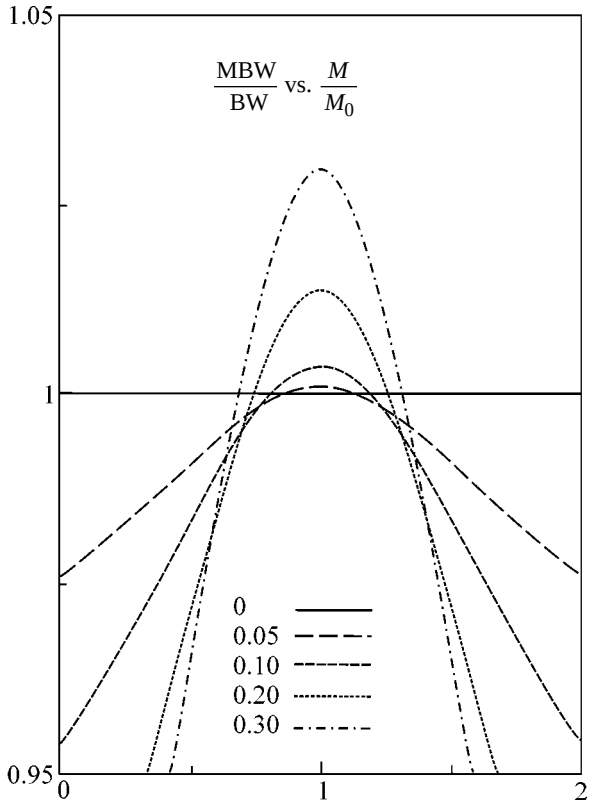

Fig. 2. Numerical calculation of the ratio of the modified and standard BW mass formulas MBW/BW versus M/M_0 for different values of ϵ.

Finally, we wish to discuss briefly our motive for this investigation, which seems at first sight far removed from the content of this paper. In oscillation studies, some authors insist that a single time interval is involved. The argument is essentially that both the creation of, say, a flavor neutrino and its detection, possibly as a different flavor, occur at fixed times. Now, as we explained in our introduction, such a situation, instantaneous creation, could at most be valid in a unique Lorentz frame, which improbably coincides with the laboratory. However, the existence of an intrinsic timelapse $\tilde{\tau}$ would imply that instantaneous creation is a myth in any frame. In practice, this means that in interference studies we must deal with multiple times in a similar way that the slippage of interfering wave packets obliges us to consider multiple distance intervals between creation and observation.

In conclusion, we have argued that, in an arbitrary frame, a wave packet will take a finite time to "grow" to or decay from its full normalized value. This encouraged us to postulate the existence, in the preferential center of a mass frame, of an intrinsic timelapse $\tilde{\tau}$ by analogy with τ. Such an assumption leads to a modifi-

cation of the decay formula and, consequently, of the BW mass formula. We have also suggested that $\tilde{\tau} = 1/E_{CM}$ on the basis of the Heisenberg uncertainty principle. In practice, the modification of the decay formula is not experimentally detectable. However, it has, as an aside, reconciled for small times the decay law with basic quantum-mechanical arguments (at least within the hypothesis of an exponential dependence upon $\tilde{\tau}$). The BW mass formula is a more practical tool for detecting a $\tilde{\tau}$. Comparing the fits to the data upon ρ decay suggest that, with improved experiments (precision on the order of 10^{-3}), we could distinguish between the standard and modified BW. Note that with $\epsilon = \Delta M/M_0$ the modified version has no extra free parameters. We may simply compare the best χ^2 fits of both to the data. At the moment, the most promising source for evidence of a $\tilde{\tau}$ appears to be in the Z decay. Timelapse provides a justification for the existence of a negative Γ_{inv}. But we must remember that this is experimentally only a two sigma effect.

We thank R. Anni and G. Co' for interesting discussions. One of the authors (SdL) is grateful for the hospitality of the Physics Department of Lecce University, where the paper was written. This work was supported in part by the FAEP (UniCAMP).

REFERENCES

1. F. Halzen and A. D. Martin, *Quarks and Leptons: An Introductory Course in Modern Particle Physics* (Wiley, New York, 1984; Mir, Moscow, 1987).
2. J. Drees, hep-ex/0110077.
3. L. A. Khalfin, Phys. Lett. B **112B**, 223 (1982).
4. Y. N. Srivastava and A. Widom, Lett. Nuovo Cimento **37**, 267 (1983).
5. V. F. Weisskopf and E. Wigner, Z. Phys. **63**, 54 (1930).
6. S. Cohen-Tannoudji, V. Diu, and F. Lalo'e, *Quantum Mechanics* (Wiley, New York, 1977), Chap. 13.
7. J. D. Jackson, *Classical Electrodynamics* (Wiley, New York, 1975), Chap. 15.
8. M. Namiki and N. Mugibayashi, Prog. Theor. Phys. **10**, 474 (1953).
9. E. Arnous and S. Zienau, Helv. Phys. Acta **34**, 279 (1951).
10. H. Nakazato, M. Namiki, and S. Pascazio, Int. J. Mod. Phys. B **10**, 247 (1996).
11. V. Misra and E. S. G. Sudarshan, J. Math. Phys. **18**, 756 (1977).
12. P. Facchi, H. Nakazato, and S. Pascazio, Phys. Rev. Lett. **86**, 2699 (2001).
13. P. Facchi and S. Pascazio, Physica A (Amsterdam) **271**, 133 (1999).
14. L. Capraro *et al.*, Nucl. Phys. B **288**, 659 (1987).

JETP Letters, Vol. 76, No. 1, 2002, pp. 61–65. Translated from Pis'ma v Zhurnal Éksperimental'noĭ i Teoreticheskoĭ Fiziki, Vol. 76, No. 1, 2002, pp. 68–73.

On the Reactions $A + A + \ldots + A \longrightarrow 0$ at a One-Dimensional Periodic Lattice of Catalytic Centers: Exact Solution

A. A. Naidenov[1] and S. K. Nechaev[1, 2]

[1] *Landau Institute for Theoretical Physics, Russian Academy of Sciences, ul. Kosygina 2, Moscow, 117940 Russia*
[2] *UMR 8626, CNRS-Université Paris XI, LPTMS, Université Paris Sud, 91405 Orsay Cedex, France*
e-mail: nechaev@ipno.in2p3.fr

Received February 27, 2002; in final form, May 7, 2002

Abstract—The kinetics of the diffusion-controlled chemical reactions $A + A + \ldots + A \longrightarrow 0$ that occur at catalytic centers periodically arranged along a straight line is considered. Modes of the behavior of reaction probability $W(t)$ were studied at different times and different densities of the catalyst. Within the Smoluchowski approximation, it was rigorously proved that at large times the function $W(t)$ is independent of the lattice period. This means that, in the given asymptotic mode, the probability of the reaction on a lattice with a catalyst placed in each lattice site is the same as on a lattice with a catalyst placed in sparse sites. © *2002 MAIK "Nauka/Interperiodica".*

PACS numbers: 82.20.-w

In this work, we discuss the kinetics of the polymolecular irreversible diffusion-controlled chemical reactions $A + A + \ldots + A \longrightarrow 0$ that occur at catalytic centers arranged in a periodic lattice in space. To our knowledge, the problem of the decrease in the amount of the reactant with time in catalytic diffusion-controlled chemical reactions $A + A \longrightarrow 0$ was first studied within the random phase approximation in [1].

The problem considered in this article "rests on two whales": on the one hand, it has characteristic features of the dynamics of diffusion-controlled chemical reactions, and, on the other hand, it is typical for the adsorption kinetics of particles diffusing in the medium of stationary "traps" (absorbers). Before going into the description of the model under study, let us briefly formulate the main features of its fundamental problems: diffusion-controlled chemical reactions and kinetics of the adsorption of particles on traps.

For several decades, bimolecular diffusion-controlled reactions $A + A \longrightarrow B$ served as the basic model for studying the kinetics of chemical reactions on the microscopic scale. The main ideas of the description of chemical reactions in the medium of diffusing reactants were formulated by Smoluchowski in 1917 [2]. Mean field methods, which were proposed by Smoluchowski and further developed by his numerous disciples (see, e.g., review [3]) are widely used up to now and yield reasonable results for problems related to the determination of the rate of chemical reactions and change in the concentration of the reactant with time. However, in the case of strong stirring, i.e., when the diffusion of particles is significant, mean field methods become inappropriate because, along with pair interactions of particles, correlations that occur at triple, quadruple, etc. particle collisions should be taken into account. In works that date back to the 1980s, fluctuation effects in the kinetics of chemical reactions were included [4]. Later the range of problems under study was significantly expanded by the inclusion of problems of chemical kinetics involving macromolecules, so-called transport-controlled chemical reactions [3]. However, the comparison of the results that were obtained within the Smoluchowski approximation with exact solutions for some model systems, e.g., for a one-dimensional bimolecular reaction $A + A \longrightarrow 0$ (without catalyst) demonstrates that the mean field method provides correct scaling for the probability of particle decay at large times [5, 6], which differs from the exact solution only by a numerical coefficient.

The problems of determining the evolution of survival or decay probability for particles diffusing in d-dimensional space in the presence of stationary randomly arranged absorber traps is the subject of many studies in both the physicochemical and mathematical literature that have appeared over the last two decades or more. The great interest in this topic is obviously caused by its significance in studying such physical chemistry problems as photoconductivity and photosynthesis, the kinetics of binding biopolymers with ligands, and the adsorption of polymer molecules on surfaces with chemically active regions and on colloidal particles in solutions and gels. Works dating back to the 1970s [7] demonstrated that the probability of the survival of independent diffusing particles in a medium

with absorbing traps at large times cannot be described within the Smoluchowski mean field approximation and is controlled by the diffusion time of a particle in a cavity of typical size free from traps. The method that provides correct asymptotic relationships is identical to the optimal fluctuation method by I.M. Lifshitz for estimating the density of states of a disordered system in the vicinity of the band edge (so-called Lifshitz singularities). Thus, works [7, 3, 4] stimulated the interest of mathematicians in the problem of particle decay in a medium of randomly arranged absorbers. Subsequent studies of model systems demonstrated the relation of this problem to percolation, the statistics of polymers in a medium of random obstacles, and some aspects of supersymmetric quantum mechanics [4, 8–10].

Now, with the general notion as to what type of problem of statistical physics our problem belongs, we can turn to the discussion of the model, which, as noted above, was formulated in [1]. Let us consider a region ("reservoir") in d-dimensional space containing an ensemble of identical particles A of finite size involved in Brownian motion and some quantity of stationary catalytic centers (traps). In the course of a random walk, there is the probability of encountering of m particles. If this encounter takes place at a trap, the elementary event of the chemical reaction

$$\overbrace{A + A + \ldots + A}^{m} \longrightarrow 0$$

occurs and all the particles decay, i.e., are removed from the reservoir; if particles encounter outside the trap, the reaction does not occur. The task consists in calculating the probability $W(t|m)$ of particle decay within the given time interval t depending on the spatial arrangement of the traps.

The probability of particle decay $W(t|m = 2)$ for a bimolecular chemical reaction was estimated in [1] within the Smoluchowski mean field theory for the periodic and random arrangements of traps, and the effect of catalytic centers was included in [1] within the random phase approximation. In our work, we restrict our consideration to the case of $d = 1$ and the periodic lattice of traps. For this model, the distribution function $W(t|m)$ can be determined exactly without any additional assumptions. We emphasize that by the exact solution we mean only the possibility of the rigorous inclusion of the effect of the spatially distributed catalyst on the probability of particle decay $W(t|m = 2)$. Note that, from the standpoint of real physical problem when a finite concentration c of a reacting particles occurs in the system, we still remain within the Smoluchowski approximation. At the end of the article, we discuss the range of applicability of the given mean field approach.

Although one-dimensional, the problem in hand has a particular physicochemical application. Chemical reactions that occur at cathodes in the presence of a catalyst (platinum particles) can be readily described within the model under consideration [11, 12]. This is related to the fact that on the microscopic scale the cathode is a porous structure with one-dimensional channels in which the catalyst is deposited and the diffusion-controlled chemical reaction occurs. A problem of fundamental importance consists in the optimization of the adsorption process: increasing the rate of the chemical reaction and decreasing the concentration of the expensive catalyst.

Let L be the distance between the adjacent traps in a straight line. We denote the time dependence of the coordinates of the particles under consideration by $x_1(t)$, $x_2(t)$, …, $x_m(t)$. The condition that all particles at the instant of time t occur at an arbitrary trap with the coordinate nL is as follows: $x_1(t) = x_2(t) = \ldots = x_m(t) = nL$. It is easy to realize that the random walk of m independent particles is equivalent to the effective one-particle random walk in the m-dimensional Euclidean space $\mathcal{E}_m = (x_1, x_2, \ldots, x_m)$. Thus, the probability $W(t|m)$ of the decay of m identical independent particles randomly wandering along a straight line at their simultaneous encounter at any of the traps is equivalent to the probability of the first occurrence of the random walk in the $\mathcal{E}_m$ space at the instance of time t in an arbitrary trap located in the straight line defined by the equation $x_1 = x_2 = \ldots = x_m$. In our case, this statement of the problem is a starting point. The recurrence equation for the probability $W_t(\mathbf{x}) \equiv W(t|m, \mathbf{x})$ to find the random walk over lattice edges in the m-dimensional space $\mathcal{E}_m$ in the point $\mathbf{x}$ at the instance of time t has the form

$$W_{t+1}(\mathbf{x}) = D\sum_{\mathbf{u}} W_t(\mathbf{x} + \mathbf{u})\eta(\mathbf{x} + \mathbf{u}), \qquad (1)$$

where $D = 1/2m$ is the diffusion coefficient in m-dimensional space, summation is performed over the nearest neighbors, and $\eta(\ldots)$ is the discrete δ-function, which is defined as follows:

$$\eta(\mathbf{x}) = \begin{cases} 0 \text{ if } \mathbf{x} \text{ coincides with the trap;} \\ 1 \text{ in all the other cases.} \end{cases} \qquad (2)$$

As usual in translation-invariant problems, it is convenient to transform to the momentum Fourier representation:

$$W_t(\mathbf{k}) = \frac{1}{N^m}\sum_{\mathbf{x}} W_t(x)e^{i\mathbf{kx}}, \qquad (3)$$

where

$$W_t(\mathbf{x}) = \sum_{|k_1, \ldots, k_m| < \pi} W_t(\mathbf{k})e^{-i\mathbf{kx}}, \quad k_j = \pm\frac{2\pi s_j}{N}. \qquad (4)$$

As a result of the Fourier transform, Eq. (1) yields

$$W_{t+1}(\mathbf{k}) = \frac{1}{2m}\sum_{\mathbf{u}} e^{-i\mathbf{ku}}\sum_{\mathbf{q}} W_t(\mathbf{q})\eta(\mathbf{k} - \mathbf{q}), \qquad (5)$$

where

$$\eta(\mathbf{k}) = \delta(\mathbf{k}) - \frac{1}{N^m}\sum_{|nL|<N/2} e^{ik_1 nL}. \quad (6)$$

In Eq. (6), we assumed that the straight line in which the traps are located coincides with the $[0, x_1)$ axis in the $\mathscr{E}_m$ space.

Let us use the equation

$$\sum_{n=-\frac{N}{2L}}^{\frac{N}{2L}} e^{ik_1 nL} = \frac{N}{L}\sum_{|n|<\frac{L}{2}} \delta\left(k_1 - \frac{2\pi n}{L}\right),$$

in which, for the sake of definiteness, we assume $[N/2L] = N/2L$. Using the latter expression, Eq. (5) can be written in the form

$$W_{t+1}(k) = \frac{1}{m}(\cos k_1 + \ldots + \cos k_m) \times \left\{ W_t(k) - \frac{1}{N^{m-1}L}\sum_{\substack{q_2,\ldots,q_m \\ |n|<L/2}} W_t\left(k_1 - \frac{2\pi n}{L}, q_2, \ldots, q_m\right)\right\}, \quad (7)$$

where

$$-\pi \le \{k_1, \ldots, k_m\} < \pi, \quad -\pi \le \{q_2, \ldots, q_m\} < \pi.$$

Equations of this type are conveniently solved by the generating function method:

$$W(\mathbf{k}, s) = \sum_{t=0}^{\infty} W_t(\mathbf{k}) s^t, \quad W(t) = \frac{1}{2\pi i}\int_C \frac{W(s)ds}{s^{t+1}}. \quad (8)$$

Multiplying both parts of expression (7) by s^t, after simple algebraic transformations we obtain

$$W(\mathbf{k}, s) = \frac{W_0(\mathbf{k})}{1 - A(\mathbf{k}, s)} - \frac{A(\mathbf{k}, s)}{1 - A(\mathbf{k}, s)} \frac{S\left(\frac{W_0(\mathbf{k})}{1 - A(\mathbf{k}, s)}\right)}{S\left(\frac{1}{1 - A(\mathbf{k}, s)}\right)}, \quad (9)$$

where the following designations are introduced:

$$A(\mathbf{k}, s) = \frac{s}{m}(\cos k_1 + \ldots + \cos k_m),$$

$$S(W(\mathbf{q})) = \frac{1}{N^{m-1}L}\sum_{\substack{q_2,\ldots,q_m \\ |n|<L/2}} W\left(q_1 - \frac{2\pi n}{L}, q_2, \ldots, q_m\right). \quad (10)$$

Let us select uniform starting conditions, i.e., $W_0(\mathbf{k}) = \delta(k_1)\ldots\delta(k_m)$ and proceed to limit $N \longrightarrow \infty$:

$$W(\mathbf{k}, s) = \frac{\delta(\mathbf{k})}{1 - A(\mathbf{k}, s)} - \frac{A(\mathbf{k}, s)}{1 - A(\mathbf{k}, s)}\frac{1}{(1-s)} \times \left(\sum_{q_1}\int\ldots\int \frac{dq_2\ldots dq_m}{1 - \frac{s}{m}(\cos q_1 + \ldots + \cos q_m)}\right)^{-1}, \quad (11)$$

where q_1 takes on the values $q_1 = k_1 - 2\pi n/L$, $|n| < L/2$. The second term, which enters into the expression with the minus sign, describes particle decay at traps. We are interested in the zeroth harmonic of this term, which determines the probability of the reaction

$$W(s) = \frac{s}{(1-s)^2} \times \left(\sum_{q_1}\int\ldots\int \frac{dq_2\ldots dq_m}{1 - \frac{s}{m}(\cos q_1 + \ldots + \cos q_m)}\right)^{-1}. \quad (12)$$

For further consideration of the problem, we must evaluate the integral

$$I(\alpha) = \int\ldots\int \frac{dq_2\ldots dq_m}{\alpha - (\cos q_2 + \ldots + \cos q_m)}, \quad (13)$$

where $\alpha = m/s - \cos q_1$. This function can have poles only on two points $\alpha = \pm(m-1)$, i.e., $s_{1,2} = \frac{m}{\cos q_1 \pm (m-1)}$, $s_{1,2} \ge 1$. Integral (13) in these regions is determined by the values of q_i, which are nearly zero; therefore, cos(…) in the integrand can be expanded. The change $\cos q_i \approx 1 - \frac{1}{2}q_i^2$ corresponds to the changing from the lattice to the continuous limit with respect to the ith coordinate. In the vicinity of the point $\alpha = m - 1$, $\epsilon = \alpha - m + 1$, we have

$$I_m(\epsilon) = 2\int\ldots\int \frac{dq_2\ldots dq_m}{2\epsilon + q_2^2 + \ldots + q_m^2}. \quad (14)$$

Changing to spherical coordinates (S_{m-1} is the area of the sphere in the $(m-1)$-dimensional space, A is some constant, $A \sim \pi$), we obtain

$$I_m(\epsilon) \approx 2S_{m-1}\int_0^A \frac{q^{m-2}dq}{2\epsilon + q^2}. \quad (15)$$

The values of $I_m(\epsilon)$ at different values of m are

$$I_m(\epsilon) = \begin{cases} \frac{2\pi^2}{\sqrt{2\epsilon}}, \text{ at } m = 2; \\ 8\pi\log\left(1 + \frac{A^2}{2\epsilon}\right), \text{ at } m = 3; \\ \sim A^{m-3}, \text{ at } m \geq 4. \end{cases} \quad (16)$$

The probability of decay at traps within these designations is

$$W(s) = m\left(L(1-s)^2\frac{1}{L}\sum_{p=-L/2}^{L/2} I\left(\frac{m}{s} - \cos\frac{2\pi p}{L}\right)\right)^{-1}. \quad (17)$$

The integrand in the function $W(t)$ has singularities s^t and $(1 - s)^2$. We are interested in the behavior of $W(t)$ governed by the vicinity of the point $s = 1$, which corresponds to $\alpha = m - \cos q_1$. Hence, the expression for the generating function $W(s)$ within a numerical multiplier can be rewritten as follows:

$$W(s) \sim \left((1-s)^2\sum_{p=-L/2}^{L/2} I_m\left(\frac{m}{s} - \cos\frac{2\pi p}{L} - m + 1\right)\right)^{-1}. \quad (18)$$

The time dependence $W(t)$ is restored from the generating function $W(s)$ by inverse Laplace transformation (8). The contour integral depends on singular points of the integrand, and the pole at the point $s = 1$ makes the largest contribution. Recall that the probability $W(t)$ of particle decay unambiguously characterizes the decrease in the reactant concentration with time and, thus, determines the effective rate constant of the chemical reaction.

Further calculations will be based on the Tauberian theorem, which readily provides asymptotic estimations in the cases of interest without explicit use of the inverse Laplace transformation.

Reactions with $m = 1$ and $m \geq 4$. Retaining only the divergent part in expression (12), we obtain the asymptotics

$$W_{m=1}(t \longrightarrow \infty) \sim \sqrt{t}. \quad (19)$$

In the case of $m \geq 4$, the result is also readily obtained because $I_m \sim$ const in the region of $s = 1$. Therefore, the behavior of the function at large times is governed by the pole $1/(1 - s)^2$, which corresponds to

$$W_{m\geq 4}(t \longrightarrow \infty) \sim t. \quad (20)$$

Reactions with $m = 2$. The behavior of $W(t)$ at $m = 2$ is more interesting. In this case, the generating function $W(s)$ of the absorption probability is as follows:

$$W(s) \sim \left((1-s)^2\sum_{p=-L/2}^{L/2}\left(2 - s\cos\frac{2\pi p}{L} - s\right)^{-1/2}\right)^{-1}. \quad (21)$$

Applying the Tauberian theorem and replacing the sum with the integral, we obtain

$$W_{m=2}(t) \sim t \times\left(\sqrt{t} + \sigma^{-1} + \frac{2L}{\pi}\left[\log 4 - \log\left(\frac{\pi}{L} + \sigma\right)\right]\right)^{-1}, \quad (22)$$

where $\sigma = \sqrt{\pi^2/L^2 + 1/t}$. In the two limiting cases,

$$W_{m=2}(t) \sim \begin{cases} \frac{t}{t^{1/2} + \text{const}} \sim \sqrt{t}, \quad t \gg \frac{L^2}{\pi^2} \\ \frac{t}{L\log 8t}, \quad 1 \ll t \ll \frac{L^2}{\pi^2}. \end{cases} \quad (23)$$

Reactions with $m = 3$. Expression (16) for $I_{m=3}$ gives the correct relationship; however, it contains an undefined constant, which complicates estimations. By the integration of Eq. (13) without expanding cosines in series, we can obtain the more accurate formula

$$I(\alpha) \approx \pi\log\left(\frac{16}{3 - 2s - s\cos q}\right). \quad (24)$$

The asymptotics for $t \longrightarrow \infty$ can be obtained directly by applying the Tauberian theorem to generating function (17), which leads to the following expression:

$$W_{m=3}(t) \approx \frac{t}{C + \log t - \log(3/t + 2\pi^2/L^2)}, \quad (25)$$

where

$$C = 5L\log 2 + 4\log\left(\frac{2\pi}{L}\right) - 4 - \log\frac{4}{3}.$$

Absorption probabilities that were obtained above are insufficient for the exact calculation of the reaction rate but are directly related to the Smoluchowski constant $K_{\text{Smol}}(t) = dW(t)/dt$. Indeed, this constant by definition is the probability of the decay of a solitary particle (i.e., without inclusion of cooperative effects) at the catalyst trap. Within the Smoluchowski approximation, the concentration of particles in the polymolecular reaction of m particles is determined from the kinetic equation

$$dc(t)/dt = -K_{\text{Smol}}(t)c_{\text{tr}}c^m(t). \quad (26)$$

After simple calculations, we obtain ($c_0 = c(t = 0)$, $m > 1$)

$$c(t) = (c_0^{1-m} + (m-1)c_{\text{tr}}W(t))^{-1/(m-1)}. \quad (27)$$

The Smoluchowski approximation is valid in cases when stirring in the system due to the diffusion of particles is a slower process than the chemical reaction event. That is, if the motion of particles is nearly absent, the chemical reaction event involves only the particles that are occasionally the closest to each other. This is the reason why the Smoluchowski approximation is

adequate at a low density of particles in the system, when the free diffusion path of particles is sufficiently large compared to the time of the chemical reaction event.

To demonstrate the validity of the mean field approximation in the problem under consideration for any distance L between the catalytic centers, it is sufficient to show that the Smoluchowski theory works in the two limiting cases: (a) at $L = 1$, i.e., when the reaction occurs each time on the encounter of a pair of particles and, consequently, is independent on the position of the catalytic center; and (b) at $L \longrightarrow \infty$, i.e., when the system contains a solitary catalytic center. The exact solution of the many-particle problem in case (a) for bimolecular reactions was reported in [5, 6]. As noted in the introduction, the exact and mean-field solutions have the same asymptotics and differ only by a numerical coefficient. For the case (b), the decrease in concentration $c(t)$ because of the chemical reaction can be easily estimated ($m \geq 2$):

$$\frac{dc_{\text{chem}}(t)}{dt} = -K_{\text{chem}}c^m_{\text{chem}}(t)$$
$$\longrightarrow c_{\text{chem}}(t) \sim \frac{c_0}{K_{\text{chem}}}t^{-1/(m-1)}. \quad (28)$$

In order to find the decrease in concentration $c_{\text{diff}}(t)$ because of diffusion in the case of the reaction of m particles at a center, we must solve the diffusion equation in m-dimensional space, where each coordinate corresponds to the concentration of one of the particles involved in the reaction. As can be easily seen,

$$c_{\text{diff}}(t) \sim c_0\frac{\log t}{t} \quad (m = 2),$$
$$c_{\text{diff}}(t) \sim c_0\text{const} \quad (m = 3, 4, \ldots). \quad (29)$$

For all $m \geq 2$, the following condition is fulfilled: after some instant of time $t = t(c_0, K_{\text{chem}})$, the concentration because of diffusion is larger than the concentration because of the chemical reaction, and, consequently, the rate of diffusion is lower than the rate of the chemical reaction, which means that the Smoluchowski approximation is valid.

Of particular interest are the relationships $W_m(t)$ at large times (for $t \longrightarrow \infty$), namely, expressions (20), (23), and (25). As can be seen from the corresponding formulas, the probability of reaction $W_m(t)$ is independent of the period of the lattice of catalytic centers. This means that in the given asymptotic mode the probability of the reaction on the lattice with the catalyst placed in each lattice site is the same as on the lattice with the catalyst placed in sparse sites. Recall that this result was first formulated in [1] within the random phase approximation. Thus, our work can be considered as rigorous proof of the effect, which has promising technical applications.

We are grateful to G. Oshanin for helpful discussions of the work. The work was supported by the Russian Foundation for Basic Research, project no. 00-15-99302.

REFERENCES

1. G. Oshanin and A. Blumen, J. Chem. Phys. **108**, 1140 (1998).
2. M. V. Smoluchowski, Z. Phys. Chem. B **35**, 113 (1924).
3. G. Oshanin, M. Moreau, and S. Burlatsky, Adv. Colloid Interface Sci. **49**, 1 (1994).
4. S. F. Burlatskiĭ and A. A. Ovchinnikov, Zh. Éksp. Teor. Fiz. **92**, 1618 (1987) [Sov. Phys. JETP **65**, 908 (1987)].
5. D. C. Torney and H. M. McConnel, J. Phys. Chem. **87**, 1941 (1983).
6. A. A. Lushnikov, Phys. Lett. A **120**, 135 (1987).
7. B. Ya. Balagurov and V. G. Vaks, Zh. Éksp. Teor. Fiz. **65**, 1939 (1973) [Sov. Phys. JETP **38**, 968 (1973)].
8. T. C. Lubensky, Phys. Rev. A **30**, 2657 (1984).
9. S. R. Renn, Nucl. Phys. B **275**, 273 (1986).
10. C. Monthus, G. Oshanin, A. Comtet, and S. F. Burlatsky, Phys. Rev. E **54**, 231 (1996).
11. G. C. Bond, *Heterogeneous Catalysis: Principles and Applications* (Clarendon, Oxford, 1987).
12. D. Avnir, R. Gutfraind, and D. Farin, in *Fractals in Science*, Ed. by A. Bunde and S. Havlin (Springer-Verlag, Berlin, 1994).

Translated by A. Safonov

JETP Letters, Vol. 76, No. 1, 2002, pp. 66–70. Translated from Pis'ma v Zhurnal Éksperimental'noĭ i Teoreticheskoĭ Fiziki, Vol. 76, No. 1, 2002, pp. 74–78.

Electromagnetically Induced Transparency; Writing, Storing, and Reading Short Optical Pulses

V. G. Arkhipkin* and I. V. Timofeev

Kirenskiĭ Institute of Physics, Siberian Division, Russian Academy of Sciences, Akademgorodok, Krasnoyarsk, 660036 Russia

** e-mail: avg@iph.krasn.ru*

Krasnoyarsk State University, Krasnoyarsk, 660041 Russia

Received May 8, 2002

Abstract—The spatiotemporal propagation dynamics of a weak probe pulse in an optically dense medium of three-level atoms is studied in the adiabatic approximation under conditions of electromagnetically induced transparency. The atomic coherence induced at the dipole-forbidden transitions is found to be spatially localized. This effect is used for the analysis of the reversible writing (reading) of short optical pulses. The method of pulse time reversal is suggested. © *2002 MAIK "Nauka/Interperiodica".*

PACS numbers: 42.50.Gy; 42.65.Tg

1. The phenomenon of electromagnetically induced transparency (EIT) is caused by quantum interference. It renders an absorbing medium transparent to the probe resonance radiation in the presence of a control coherent field interacting with the adjacent transition. This effect was predicted and experimentally implemented back in the late 1960s and early 1970s (nonlinear interference effect; see, e.g., [1, 2]). At present, the EIT effect is being extensively studied and widely developed, e.g., in the context of lasing without inversion [3], nonlinear optics, including the interacting radiations with energy corresponding to several photons ("one photon for one atom") [4, 5], subfemtosecond pulse generation [6], atomic coherence control [3, 7], etc.

EIT gives rise to unusual propagation laws for resonant pulses in a medium: matched pulses [8, 9], field-dressed pulses [10], and adiabatons [11] propagating without absorption and changing their shape at a distance exceeding linear absorption length by several orders of magnitude (see also [12–15]). EIT also leads to a giant (by 10^7 times or more) decrease in the group velocity of an optical pulse ("slow light"). In recent experiments, ultraslow propagation was observed in the Bose–Einstein condensate of sodium atoms (~17 m/s [16] and ~1 m/s [17]), in ruby vapor (~90 m/s [18] and ~8 m/s [19]), and in a $Pr:Y_2SiO_5$ crystal (~45 m/s [20]).

Moreover, the optical pulse can be "stopped" [21] (dynamic EIT); the possibility of obtaining negative group velocity has also been the subject of discussion [22]. At low velocities (tens of m/s and lower), the probe pulse is spatially compressed and localized in a medium. Based on this fact, the authors of [23] suggested and experimentally demonstrated a method of writing, storing, and reconstructing (reading) optical pulses in ruby vapor in the situation where the pulse switching-on and switching-off times are much longer than the lifetime of the intermediate state. In [24], this idea was implemented in the Bose–Einstein condensate of sodium atoms.

In this work, the possibility of writing, storing, and reading light is considered for the case where the pulse duration is shorter than all relaxation times in a medium (short pulses). It is not assumed from the outset that the signal pulse is spatially localized. We consider the case where the propagation of a weak probe (signal) pulse with frequency ω_p in a three-level optically dense medium occurs in the presence of a strong control (write) pulse with frequency ω_c resonant with the frequency of an adjacent $|2\rangle$–$|1\rangle$ transition (Fig. 1). The lower state $|0\rangle$ is the atomic ground state and state $|2\rangle$ is metastable. The pulses are assumed to be plane waves $E_{p,c} = 1/2E_{p,c}\exp[-i(\omega_{p,c}t - k_{p,c}z)]$ + c.c. propagating in one direction along the z axis ($k_{p,c}$ are the moduli of wavevectors of the probe and control pulse, respectively). The intensity of the probe pulse is much lower than the intensity of the control pulse and has virtually no effect on the population of levels with which the pulse interacts. At the medium input, the pulses may have various shapes, but their duration satisfies the condition $T_c > T_p$, where T_c and T_p are the durations of the control and probe pulse, respectively.

In this work, the spatiotemporal evolution of the probe pulse and atomic (Raman) coherence induced at the $|0\rangle$–$|2\rangle$ transition in an optically dense medium under EIT conditions is analyzed. The spatial localization of atomic coherence is demonstrated and, on this basis, the possibility of writing, storing, and reading optical pulses through their transformation into atomic coherence and vice versa is considered.

0021-3640/02/7601-0066$22.00

2. We first consider the spatiotemporal evolution of atomic coherence under EIT conditions. The interaction of optical fields with a three-level quantum system is described by the standard system of Maxwell–Bloch equations, which is solved self-consistently. To the first order in probe field G_p, it has the following form in the coordinate system with local time $\tau = t - z/c$:

$$\frac{\partial \rho_{10}}{\partial \tau} = i(G_p \rho_0 + G_c \rho_{20}),$$
$$\frac{\partial \rho_{20}}{\partial \tau} = iG_c^* \rho_{10}, \quad \frac{\partial G_p}{\partial z} = iK_p \rho_{10}. \tag{1}$$

Here, ρ_{ij} and d_{ij} are nondiagonal elements of the density matrix and the dipole transition moment, respectively; $2G_p = d_{10}E_p(t)\hbar$ and $2G_c = d_{12}E_c(t)\hbar$ are the Rabi frequencies; $K_p = (\pi\omega_p N|d_{10}|^2/c\hbar)$ is the propagation constant; and N is the atomic concentration.

The system of Eqs. (1) is written on the assumption that the pulse carrier frequencies are resonant with the corresponding atomic transitions. At the instant the fields are switched on, all atoms are in the ground state $|0\rangle$ ($\rho_0 = 1$ and $\rho_{1,2} = 0$, where $\rho_{0,1,2}$ are the populations of corresponding levels), and the pulse durations satisfy the following conditions: $T_p \ll \Gamma_{10}^{-1}$, $T_c \ll \Gamma_{20}^{-1}$, $\Gamma_{10} \gg \Gamma_{20}$ (Γ_{10} and Γ_{20} are, respectively, the halfwidths of the $|1\rangle$–$|0\rangle$ and $|2\rangle$–$|0\rangle$ transitions), $T_c > T_p$, and the adiabaticity condition $G_c^0 T_p \gg 1$ (see, e.g., [25]).

We will assume hereafter that the Rabi frequency G_c of the control pulse is a given time-dependent function and that it does not depend explicitly on the coordinate z. Numerical calculations will be carried out with the Gaussian input ($z = 0$) pulses $G_p(t) = G_p^0 \exp(-\ln 2t^2/2T_p^2)$ and $G_c(t) = G_c^0 \exp(-\ln 2t^2/2T_c^2)$ ($G_p^0 \ll G_c^0$).

In the adiabatic approximation (with allowance for the leading nonadiabatic correction to ρ_{10}), the solutions for ρ_{10} and ρ_{20} in Eqs. (1) can be represented in the form

$$\rho_{20} = -\frac{G_p(\tau, z)}{G_c(\tau)}, \quad \rho_{10} = -\frac{i}{G_c^*(\tau)}\frac{\partial \rho_{20}}{\partial \tau}. \tag{2}$$

By differentiating ρ_{20} with respect to z and using the third equation in (1), one can obtain the equation for the spatial evolution of the nondiagonal density matrix elements ρ_{20}:

$$\frac{\partial \rho_{20}}{\partial \tau} + \frac{G_c^2(\tau)}{K_p}\frac{\partial \rho_{20}}{\partial z} = 0. \tag{3}$$

When deriving Eq. (3), it was assumed that G_c is a real quantity and that it does not depend explicitly on z. The parameter G_c^2/K_p has the meaning of the coherence (ρ_{20}) propagation velocity in a medium. The boundary condition is written as $\rho_{20}^0 = \rho_{20}(\tau, z = 0) = -G_p(\tau, z = 0)/G_c(\tau)$.

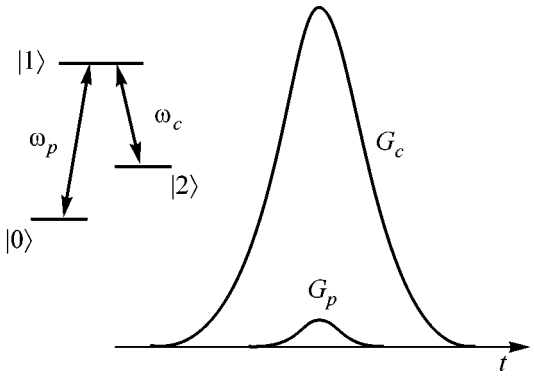

Fig. 1. Scheme of atomic levels and the configuration of interacting optical pulses at the medium input $z = 0$.

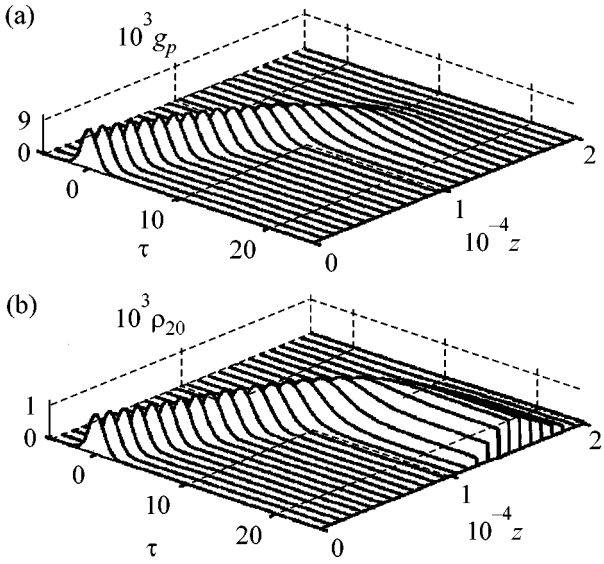

Fig. 2. Time dependences of (a) atomic coherence ρ_{20} and (b) normalized Rabi frequency $g_p = G_p T_p$ of the probe field at different points of the medium. $G_c^0 T_p = 10$ and $T_c/T_p = 10$. Time is measured in units of probe pulse duration and length is in units of linear absorption length.

Equation (3) can be solved, e.g., by the method of characteristics. The solution has the form

$$\rho_{20}(\tau, z) = \rho_{20}^0(Z^{-1}(Z(\tau) - z)), \tag{4}$$

where $Z(\tau) = K_p^{-1}\int_{-\infty}^{\tau} G_c^2(\tau')d\tau'$ and Z^{-1} is the inverse of the function $Z(\tau)$.

The spatiotemporal evolution of atomic coherence ρ_{20} and probe pulse $g_p = G_p T_p$ is illustrated in Fig. 2. One can see that, as the pulse propagates through the medium, it decelerates and its energy gradually decreases because of the energy transfer to the control

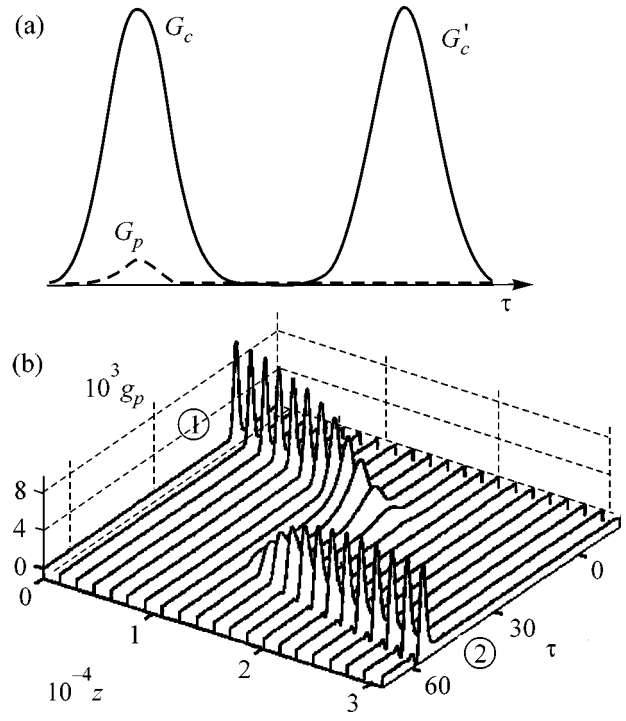

Fig. 3. (a) Signal (G_p), write (G_c), and read (G_c') pulses at the medium input $z = 0$. (b) Writing (circled figure 1) of the signal pulse G_p and (circled figure 2) its reading by the pulse G_c'. Conditions as in Fig. 2.

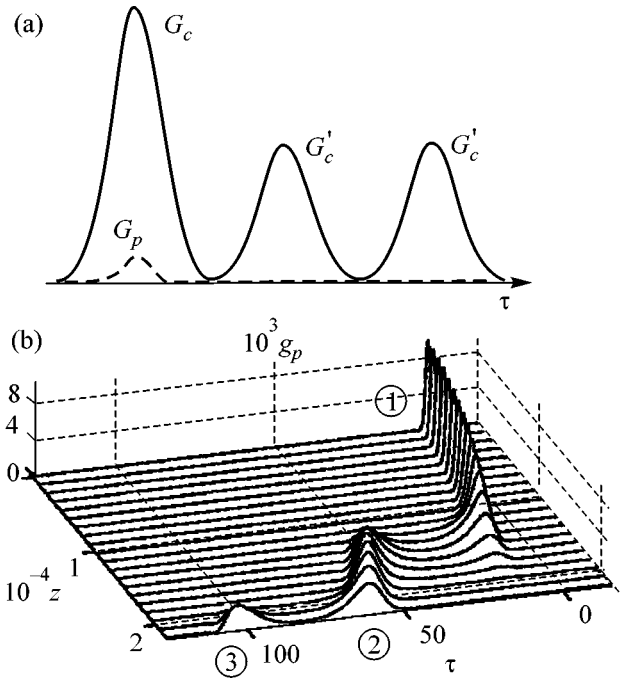

Fig. 4. Double readout of a written pulse. (a) Signal (G_p), write (G_c), and read (G_c') pulses at the medium input $z = 0$. (b) Time dependences of the signal pulse G_p in the course of (circled figure 1) writing and (circled figures 2 and 3) reading at different points of the medium. Condition are as in Fig. 2.

pulse. The coherence described by the nondiagonal element ρ_{20} of the density matrix is spatially localized and its spatial profile is similar to the shape of the input signal pulse. This can also be considered as a pulse-induced phase grating in the medium. A comparison of the numerical results for ρ_{20} with the data obtained using Eq. (4) shows that the agreement is good.

The results obtained have a certain relevance to the predictions of [21] but present the problem in a different aspect. The difference is that, first, we consider short pulses with duration shorter than the medium relaxation time. Second, what is more important, the boundary conditions are specified. With such an approach, it is not assumed from the outset that the probe pulse is spatially localized in the medium, as was done in [21], where the spatial distribution of the probe pulse in a medium was specified at zero time. By contrast, we specify the pulse time distribution at the boundary $z = 0$, i.e., solve the boundary-value problem. In our opinion, this formulation of the problem is more natural and allows one to trace the pulse deceleration and the spatial localization of atomic coherence.

3. The spatial distribution of atomic coherence in a medium contains information on the probe pulse. This can be used for writing and storing the probe optical pulse in a medium followed by its reading. The term "writing" implies the conversion of a probe (signal) pulse into the atomic coherence ρ_{20}, whose lifetime is determined by its relaxation time and can be as long as several milliseconds or longer. If a "read" optical pulse is fed into the medium with a time delay relative to the control pulse, the output pulse will arise as a result of read pulse scattering by the atomic coherence; i.e., the atomic coherence converts back into light (reading process).

The properties of the reconstructed pulse depend on the read pulse. In the case when the read pulse is identical with the control (write) pulse and propagates in the same direction, the reconstructed (red) pulse will be the exact copy of the signal pulse, as illustrated in Fig. 3. During the atomic coherence lifetime, reading can be performed repeatedly (see Fig. 4). The curves in Fig. 4 were calculated numerically using Eqs. (1), where G_p and G_c imply the red (reconstructed) and read pulses, respectively. The initial and boundary conditions were taken in the form $G_p = 0$, $G_p = G_p = G_p(\tau)$ at the boundary $z = 0$, and $\rho_{20} = \rho_{20}(z)$ at the instant of time τ_0 corresponding to the onset of reading.

For the close transition frequencies ω_{10} and ω_{12}, the written pulse can be reconstructed by sending the read pulse in the direction opposite to the initial writing direction. The reading process is described by the equations of type (1), in which G_p and G_c should be regarded as the reconstructed and read pulses, respectively, and τ

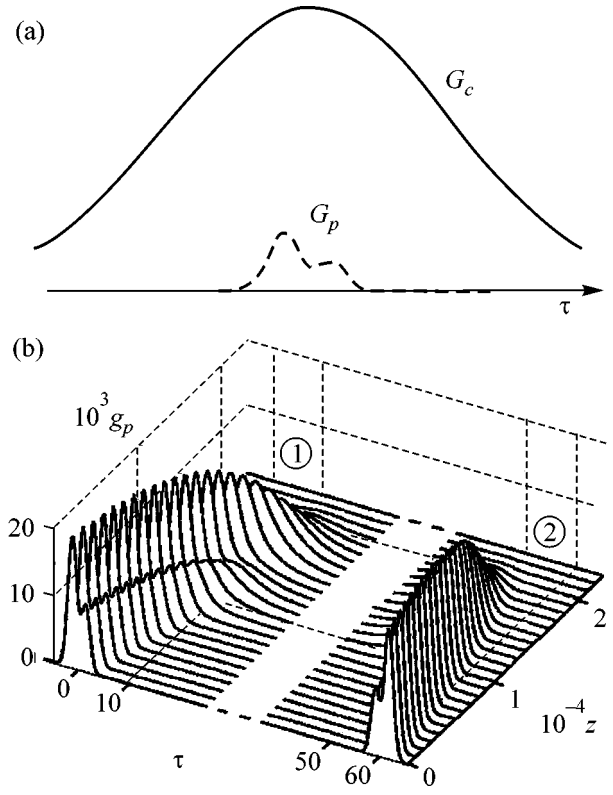

Fig. 5. Time-reversal reading. The read and write pulses propagate in opposite directions. (a) Signal (G_p) and write (G_c) pulses at the medium input $z = 0$. (b) Time dependence of the signal pulse at different points of the medium in the course of writing (circled figure 1), and the same for the pulse reconstruction (circled figure 2).

and z should be replaced by $\tau' = t - z'/c$ and $z' = L - z$, respectively, where L is the medium length. The boundary conditions for fields are specified at the output plane $z = L$ of the medium: the red field is zero, and the write field reflected from a mirror can be taken as a read field. The initial condition for ρ_{20} is specified by the spatial distribution $\rho_{20}(\tau, z)$ induced in the course of reading. It should be written in the τ' and z' coordinates. The result of reading is demonstrated in Fig. 5. It is worth noting that the reconstructed pulse is time-inverted; i.e., its leading and trailing edges are reversed, as is seen in the figure. The time reversal is caused by the fact that the information about the pulse leading edge is carried by the leading (spatial) front of atomic coherence, which penetrates into the medium deeper than the trailing front that carries information on the trailing (temporal) edge of the probe pulse (see Fig. 2b). Evidently, the pulse portion scattered at the tail of atomic coherence will escape the medium earlier than the portion scattered at the leading part, because the propagation velocity of the reconstructed pulse is lower than that of the read pulse. Similar results are obtained for the case $T_c/T_p < 10$, with the only difference that the coherence ρ_{20} is localized in a larger part of the medium.

Since the read pulse scattering by atomic coherence is independent of the pulse frequency, one can use read pulses with the carrier frequency ω_1 differing from the frequency of the control (write) field. In this case, the frequency of the reconstructed pulse will be shifted to $\omega_s = \omega_p - \omega_c + \omega_1$.

4. In this work, the spatiotemporal evolution of a weak probe pulse with a duration shorter than all the relaxation times in a medium has been studied under conditions of electromagnetically induced transparency. The atomic (Raman) coherence was shown to be spatially localized in a medium. Its spatial profile contains information on the signal pulse. These facts were used to demonstrate the possibility of writing and reading short optical pulses. The results obtained are complementary to the results in [21] and extend the range of their applicability. Various variants of read signal pulse were considered. It was shown that the pulses can be time-reversed. Interestingly, the pulses with steep edges, including rectangular ones, can be used as write and read pulses. Similar effects also arise in the case when the signal Rabi frequency is comparable with the control Rabi frequency, as well as if the counterintuitive pulse sequence is used (the control pulse is switched on and off before the signal pulse, and the pulses partially overlap). These results will be reported in a separate publication.

The results obtained may be of interest for the quantum processing of optical signals and images.

This work was supported by the Russian Foundation for Basic Research (project no. 02-02-16325) and the program "Fundamental Research of Institutions of Higher Education in the Natural Sciences and Humanities. Russian Universities" (no. UR.01.01.003).

REFERENCES

1. S. G. Rautian, G. I. Smirnov, and A. M. Shalagin, *Nonlinear Resonances in Atomic and Molecular Spectra* (Nauka, Novosibirsk, 1979).
2. A. K. Popov, *Introduction to the Nonlinear Spectroscopy* (Nauka, Novosibirsk, 1983); Izv. Akad. Nauk, Ser. Fiz. **60**, 99 (1996).
3. S. E. Harris, Phys. Today **50** (7), 36 (1997).
4. S. E. Harris and Y. Yamamoto, Phys. Rev. Lett. **81**, 3611 (1998).
5. S. E. Harris and V. H. Lene, Phys. Rev. Lett. **82**, 4611 (1999).
6. F. L. Kien, N. H. Shon, and K. Hakuta, Phys. Rev. A **64**, 051803(R) (2001).
7. E. Arimondo, in *Progress in Optics*, Ed. by E. Wolf (Elsevier, Amsterdam, 1996), Vol. 35, p. 257.
8. S. E. Harris, Phys. Rev. Lett. **72**, 52 (1994).
9. G. Vemuri, K. V. Vasavada, G. S. Agarwal, *et al.*, Phys. Rev. A **54**, 3394 (1996).
10. J. H. Eberly, M. L. Pons, and H. R. Hag, Phys. Rev. Lett. **72**, 56 (1994).

11. R. Grobe, F. T. Hioe, and J. H. Eberly, Phys. Rev. Lett. **73**, 3183 (1994); Phys. Rev. A **54**, 794 (1996).
12. V. G. Arkhipkin, D. V. Manushkin, and V. P. Timofeev, Kvantovaya Élektron. (Moscow) **25**, 1084 (1998).
13. V. G. Arkhipkin and I. V. Timofeev, Kvantovaya Élektron. (Moscow) **30**, 180 (2000); V. G. Arkhipkin, I. V. Timofeev, and E. A. Sizykh, in *Proceedings of the International Conference "Mathematical Models and Methods for Their Study," Krasnoyarsk, 2001*, Vol. 1, p. 36.
14. G. G. Grigoryan and Y. T. Pashayan, Phys. Rev. A **64**, 013816 (2001).
15. V. G. Arkhipkin and I. V. Timofeev, Phys. Rev. A **64**, 053811 (2001).
16. L. V. Hau, S. E. Harris, Z. Dutton, *et al.*, Nature (London) **397**, 594 (1999).
17. S. Inouye, R. F. Low, T. Gupta, *et al.*, cond-mat/0006455.
18. M. M. Kash, V. A. Sautenkov, A. S. Sibrov, *et al.*, Phys. Rev. Lett. **82**, 5229 (1999).
19. D. Budker, D. F. Kimball, S. M. Rochester, *et al.*, Phys. Rev. Lett. **83**, 1767 (1999).
20. A. V. Turukhin, M. S. Sudarshanam, M. S. Shariar, *et al.*, Phys. Rev. Lett. **88**, 023602 (2002).
21. M. Fleischhauer and M. D. Lukin, Phys. Rev. Lett. **84**, 5094 (2000).
22. O. Kocharovskaya, Yu. Rostovtsev, and M. Scully, Phys. Rev. Lett. **86**, 628 (2001).
23. D. F. Phillips, A. Fleischhauer, A. Mair, *et al.*, Phys. Rev. Lett. **86**, 783 (2001).
24. Ch. Liu, Z. Dutton, C. H. Behroozi, *et al.*, Nature (London) **409**, 490 (2001).
25. R. N. Shakhmuratov, J. Odeurs, R. Coussement, *et al.*, Phys. Rev. Lett. **87**, 153 601 (2001).

Translated by V. Sakun

JETP Letters, Vol. 76, No. 1, 2002, pp. 71–76. Translated from Pis'ma v Zhurnal Éksperimental'noĭ i Teoreticheskoĭ Fiziki, Vol. 76, No. 1, 2002, pp. 79–85.

Relativistic Quantum Cryptography on "Arrested" Photons

S. N. Molotkov

Institute of Solid State Physics, Russian Academy of Sciences, Chernogolovka, Moscow region, 142432 Russia
e-mail: molotkov@issp.ac.ru

Received May 28, 2002

Abstract—A new relativistic quantum cryptosystem is proposed in which the information is carried by the extended single-photon states with orthogonal polarizations and effective length exceeding the communication channel length. The light "arrest" effect is used as a procedure for the detection and preparation of extended states. The cryptosystem is secure against any eavesdropping attempts, because its states are quantized and the propagation velocity is limited. In this scheme, the preparation and detection procedures are local in space but require a finite time, depending on the extension of the states. The preparation for detecting at the receiver end begins before the state left the source at the input end. © *2002 MAIK "Nauka/Interperiodica".*

PACS numbers: 03.67.Dd, 03.67.Hk

The absolute security of key propagation in quantum cryptosystems is based not on the eavesdropper's technical restrictions but on the fundamental exclusions that are dictated by quantum mechanics and quantum field theory and allow the detection of any eavesdropping attempt. The detection of eavesdropping attempts in quantum cryptosystems is ensured by the exclusion of cloning quantum states and the impossibility of gaining information about the nonorthogonal states without perturbing them (the no-cloning theorem) [1, 2]. As a rule, the properties of state vectors as elements of an abstract Hilbert space $\mathcal{H}$ are only taken into account in quantum cryptosystems, while the particular realization of $\mathcal{H}$ (its relation to the coordinate space or to Minkowski spacetime in the nonrelativistic and relativistic cases, respectively) is usually not specified. The information transmission is a physical process which is realized in Minkowski spacetime by particular physical classical or quantum objects. The quantum states (vectors in $\mathcal{H}$) should be associated with the particular particles (photons, electrons, etc.). In quantum field theory, different particle types are described by the basis vectors belonging to the different unitary representations of the Poincaré group and inevitably having carriers (amplitudes, smoothing functions) in Minkowski spacetime. This correspondence between the unitary representations of the Poincaré group is the fundamental principle in the interpretation of quantum field theory [3].

In relativistic quantum cryptosystems, in which the spacetime structure of quantum states, their propagation in spacetime, and the existence of a limited propagation speed are explicitly taken into account, the nonorthogonality requirement, necessary for cryptosystems where only the properties of state vectors as elements of $\mathcal{H}$ are used, is not necessary [4, 5].

The orthogonal states can be distinguished with certainty and cloned only when they are entirely accessible (the spacetime domain where the state amplitude is nonzero is entirely accessible). If the orthogonal states are inaccessible as entire objects, they are indistinguishable with certainty and cannot be cloned.

This situation is not in conflict with the no-cloning theorem but, rather, reveals the validity range of this theorem. Its proof is based only on the properties of state vectors as elements of Hilbert space [2]. The theorem *does not forbid* one to gain information about the states without perturbing them. In this respect, the orthogonal states are similar to the classical states. For this reason, they are considered as being of little interest for the quantum information theory. However, once the existence of Minkowski spacetime is taken into account,[1] the variety of situations involving the orthogonal states becomes richer. The cryptosystem considered below is an example of this kind.

Relativistic quantum protocols on the orthogonal states are organized so that the state propagating through a communication channel is never present in this channel entirely at the same time (in the domain accessible to an eavesdropper). This circumstance, together with the finiteness of the speed of light, allows the detection of any eavesdropping attempt. One should distinguish between two cases. In the first case, the states, being subject to the spacetime restriction in the channel region, become effectively nonorthogonal, and in the second case they remain orthogonal (locally orthogonal) in the domain accessible to the eavesdropper. In essence, the indistinguishability of the locally orthogonal states under conditions of incomplete access to them follows from the normalization condi-

[1] Otherwise, the observers, being classical objects, could not gain information about the results of measurements on quantum objects.

0021-3640/02/7601-0071$22.00 © 2002 MAIK "Nauka/Interperiodica"

tion for the states. Even if the states are locally orthogonal in the accessible spacetime domain, the probability of their detection is always less than unity and cannot exceed the contribution from this domain to the normalization integral. Attempts at extending the accessible domain (in space or time) inevitably result in a delay at the receiver end, which can be detected.

Since the spatiotemporal structure of states is essential for relativistic cryptographic protocols, the preparation, propagation through a communication channel, and measurement procedures should be described explicitly. The measurement of the *whole* extended single-photon state of a length of several tens of kilometers is a nontrivial problem.[2] Formally, a measurement reliably distinguishing between a pair of extended orthogonal states $|\varphi_{0,1}\rangle$ is described by the orthogonal projectors $E_{0,1} = |\varphi_{0,1}\rangle\langle\varphi_{0,1}|$, which realize the decomposition of unity in the $\mathcal{H}$ subspace spanned by the given vectors. The decomposition of unity formally describes a physical device that must be extended in the coordinate space because of the nonlocality of the projectors. The nonlocality of a measurement described by the projectors onto the given states arises because the device must project onto the states in a certain space domain at a certain instant of time, but such a spatially nonlocal detector can technically hardly be realized.

A further idea of measuring by a spatially localized device that reliably distinguishes between a pair of orthogonal states extending over tens of kilometers is based on the use of an ancillary localized system. Such a measurement is nonlocal in time in the following sense. Because of the interaction (joint unitary evolution) between an extended single-photon state and the ancilla during the time $\Delta t \approx L/c$ (L is the effective length of the single-photon state and c is the speed of light), the single-photon state transforms to the vacuum state and the ancilla undergoes transition to a certain new state depending on the input photon state. After the time Δt, one measures the new state of the ancilla. The preparation procedure is analogous. A state can be prepared by a spatially distributed device at a certain instant of time or by a spatially localized device during time Δt. Since the amplitude (smoothing function; see below) of a photon field propagating in one direction depends only on the difference $\tau = x - ct$, the requirement for "much space" L can be replaced by the requirement for "much time" L/c.

We briefly describe a cryptography scheme that uses much space. The orthogonal states $|\varphi_{0,1}\rangle$ are prepared at a preset time t_A in the space domain controlled by participant A. The extended single-photon states with orthogonal polarizations can be written in the form

$$\varphi_\mu^+(\hat{x}) = \frac{1}{\sqrt{2\pi}}\int d\hat{k}\,\delta(\hat{k}^2)\theta(k_0)e^{i\hat{k}(\hat{x}-\hat{x}_A)}a_\mu^+(k), \qquad (1)$$

where

$$\hat{k} = (k, k_0), \quad \hat{x} = (x, t), \quad d\hat{k} = dk\,dk_0,$$
$$\hat{k}\hat{x} = kx - k_0 t, \quad [a_\nu^-(k), a_\mu^+(k)] = k_0\delta(k-k')\delta_{\nu,\mu},$$

and $\hat{x}_A = (x_A, t_A)$ specifies the time origin and the origin on the coordinate axis. The subscripts μ, $\nu = 0$ and 1 correspond to two basis polarization states. The physical states $|\varphi_\mu\rangle \in \mathcal{H}$ of a quantized field are obtained by smoothing the generalized operator functions with the basic functions $\varphi(\hat{x}) \in \Omega(\hat{x})$ ($\Omega(\hat{x})$, which is the space of basic functions [3]), $\varphi_\mu^+(\hat{x})|0\rangle \in \Omega(\hat{x})^*$, which are the generalized eigenvectors (linear continuous functionals in $\mathcal{H}$), and $\Omega(\hat{x}) \subset \mathcal{H} \subset \Omega^*(\hat{x})$, which is the equipped Hilbert space (Gel'fand triad) [6]:

$$|\varphi_\mu\rangle = \int d\hat{x}\varphi(\hat{x}-\hat{x}_A)\varphi_\mu^+(\hat{x})|0\rangle$$
$$= \int d\hat{k}\tilde{\varphi}(\hat{k})\delta(\hat{k}^2)\theta(k_0)e^{-i(kx_A-k_0t_A)}a_\mu^+(k)|0\rangle$$
$$= \int_{-\infty}^{\infty}\frac{dk}{k_0}e^{-i(kx_A-k_0t_A)}\tilde{\varphi}(k, k_0 = |k|)|k, \mu\rangle \qquad (2)$$
$$= \int_{-\infty}^{\infty}dx\varphi(x - x_A - (t - t_A))|x - t\rangle,$$

$$\varphi(\tau) = \int_0^\infty dk e^{-k\tau}\varphi(k), \quad \tau = x - t,$$

$$|k, \mu\rangle = a_\mu^+(k)|0\rangle, \quad \langle k', \nu|k, \mu\rangle = k_0\delta_{\mu,\nu}\delta(k-k').$$

The normalization condition is

$$\langle\varphi_\mu|\varphi_\mu\rangle = \int_{-\infty}^{\infty}\frac{dk}{k_0}|\tilde{\varphi}(k, k_0 = |k|)|^2 = \int_{-\infty}^{\infty}dk|\varphi(k)|^2 = 1, \qquad (3)$$
$$\varphi(k) = \frac{\tilde{\varphi}(k, k_0 = |k|)}{\sqrt{k_0}}.$$

The states $|\varphi_\mu\rangle$ are specified by the amplitude $\tilde{\varphi}(\hat{k})$ at the mass shell $k_0 = |k|$. When the information is transmitted between two participants, it is natural to consider the states propagating in one direction ($k > 0$). In this case, all quantities depend on the difference $\tau = x - t$ representing the variable in one of the light-cone branches.

The state given by Eqs. (1) and (3) can be treated as a state with amplitude $\varphi(x - x_A - (t - t_A))$ prepared at time t_A in the domain controlled by participant A. There are no constraints on the preparation of the state in a

[2] Modern solid-state rare-earth-doped distributed-feedback lasers compatible with optical fiber systems can produce output states with a frequency spectrum of width $\Delta\omega \sim 1$ kHz. The recalculation to the effective state length gives $L \sim c/\Delta\Omega \sim 300$ km.

certain domain at time t_A. The size of the spatial domain where the state amplitude shown in Fig. 1a is nonzero is ~size$\varphi(x - x_A) \neq 0$.

Strictly speaking, the amplitude is nonzero outside any compact spacetime domain, because the smoothing function $\varphi(\tau)$ belongs to the space $\Omega(\tau)$ of rapidly decreasing basic functions (for detail, see [3]). Any function belonging to $\Omega(\tau)$ can be approximated with an arbitrary accuracy by the functions with compact carriers from $\tilde{\varphi} \in \mathcal{D}(\tau)$ so that $\|\|\varphi\rangle - |\tilde{\varphi}\rangle\| < \delta$ for any δ (the norm is generated by the scalar product in $\mathcal{H}$) [3, 6].[3]

The propagation through a communication channel of length L_{ch} is described by the operator of unitary spacetime translation:

$$U_{\text{ch}} = \bigoplus_{\mu = 0, 1} \int_0^\infty \frac{dk}{k} e^{-ik(L_{\text{ch}} - t_{\text{ch}})} |k, \mu\rangle\langle k, \mu|, \tag{4}$$

$$|\varphi_\mu\rangle_{\text{ch}} = U_{\text{ch}}|\varphi_\mu\rangle$$

$$= \int_0^\infty dk e^{-ik(x - L_{\text{ch}} - x_A - (t - t_{\text{ch}} - t_A))} \varphi(k)|k, \mu\rangle. \tag{5}$$

At time $t_B = t_A + \text{size}\{\varphi(x - t_A)\} + x_A + L_{\text{ch}}$, when the state reaches the domain controlled by participant B, the latter carries out a measurement that is described by the orthogonal decomposition of unity in terms of the projectors onto the states transmitted in the spacetime:

$$I = \bigoplus_{\mu = 0, 1} |\varphi_\mu\rangle_{\text{ch}}\langle\varphi_\mu| = U_{\text{ch}} \left\{ \bigoplus_{\mu = 0, 1} |\varphi_\mu\rangle\langle\varphi_\mu| \right\} U_{\text{ch}}^{-1}. \tag{6}$$

This decomposition formally describes a spatially distributed device interacting with the state simultaneously over the whole domain of its localization at the time t_B.

To ensure security and detect any eavesdropping attempt, the state must be longer than the communication channel. More formally, this requirement means that the probability of detecting the state in the spatial domain of size L_{ch} must be less than unity at any time instant. The corresponding probability is given by

$$\Pr(t, L_{\text{ch}}) = \text{Tr}\{\mathcal{M}(t, L_{\text{ch}}, \mu)|\varphi_\mu\rangle\langle\varphi_\mu|\} < 1, \tag{7}$$

where the projector-valued measure is

$$\mathcal{M}(t, L_{\text{ch}}, \mu) = \int_{L_{\text{ch}}} dx \left(\int_0^\infty dk e^{ik(x - t)} |k, \mu\rangle \right) \times \left(\int_0^\infty dk' \langle k', \mu| e^{-ik'(x - t)} \right) \tag{8}$$

[3] A decrease in the amplitude at infinity can be directly estimated [5] using the Wiener–Palley theorem [7].

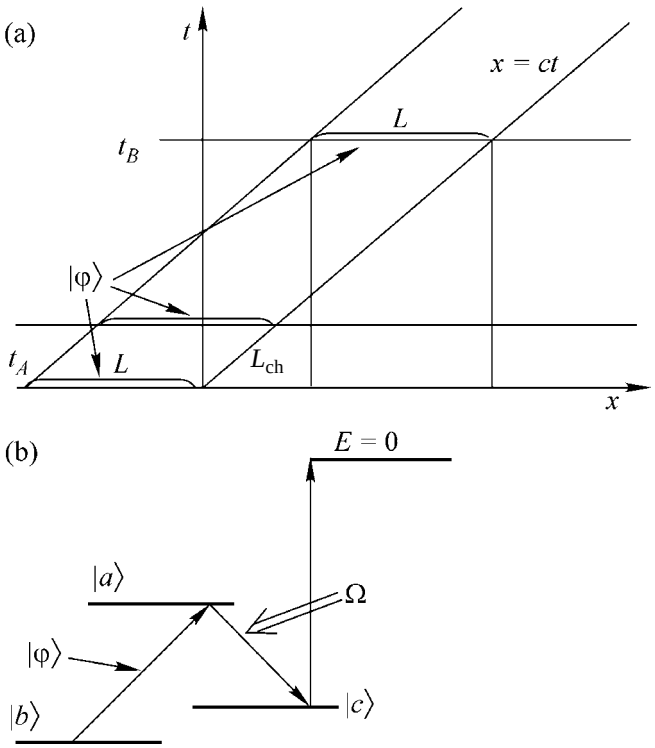

Fig. 1.

$$I = \bigoplus_{\mu = 0, 1} \mathcal{M}(t, \infty, \mu) = \bigoplus_{\mu = 0, 1} \int_0^\infty \frac{dk}{k} |k, \mu\rangle\langle k, \mu|;$$

in these expressions, time is a parameter. A formal proof of security is beyond the scope of this paper; it is given in [5]. Although the type of measurement is immaterial to the formal proof, technically, the procedure of detection at a fixed time in the "much space" regime seems to be practically unrealizable.

We now turn to the case for which the states are prepared and detected by a localized device during a certain time. Such a measurement is realized by photon "arrest" [8]. The idea is to use an ancillary spatially localized (with size $\ll L_{\text{ch}}, L$) quantum system (a cell with atomic gas or a solid matrix doped with rare-earth elements [9, 10]). When the single-photon state reaches the ancilla in its initial state $|\mathbf{b}\rangle$, an external classical driving field is turned on for the time $\Delta t \approx L/c$ to superpose the photon field and the atomic system. As soon as the photon field enters into the cell entirely, the external field is turned off, the atomic system occurs in a new state $|\mathbf{c}_\mu\rangle$, and the photon component of the quantum state occurs in the vacuum state $|0\rangle$. Here, $|\mathbf{b}\rangle$ and $|\mathbf{c}_\mu\rangle$ are a shorthand for the collective variables of the atomic

subsystem (for detail, see [8]). This process is described by the joint unitary evolution

$$|\varphi_\mu\rangle \otimes |\mathbf{b}_\mu\rangle \longrightarrow \bigoplus_{\mu=0,1} U_\mu(\Delta t)(|\varphi_\mu\rangle \otimes |\mathbf{b}_\mu\rangle) \longrightarrow |0\rangle \otimes |\mathbf{c}_\mu\rangle. \quad (9)$$

Thereupon, the projection measurement $\mathcal{P}_\mu = |\mathbf{c}_\mu\rangle\langle\mathbf{c}_\mu|$ is carried out on the spatially localized atomic system.

The extended single-photon state can be prepared by inverting the joint unitary evolution (9):

$$|0\rangle \otimes |\mathbf{c}_\mu\rangle \longrightarrow U_\mu(\Delta t)(|0\rangle \otimes |\mathbf{c}_\mu\rangle) \longrightarrow |\varphi_\mu\rangle \otimes |\mathbf{b}_\mu\rangle. \quad (10)$$

For this reason, we will consider only the detection procedure. The unitary transformation is accomplished using the interaction of a single-photon state with the gas atoms in a magnetic field. The magnetic field splits the near-degenerate level $\{|\mathbf{b}\rangle, |\mathbf{c}\rangle\}$. The level spacing and ordering are controlled by varying the magnitude and direction of the magnetic field. The $|\mathbf{b}\rangle \longleftrightarrow |\mathbf{a}\rangle$ and $|\mathbf{c}\rangle \longleftrightarrow |\mathbf{a}\rangle$ transitions occur between the orthogonal circularly polarized (with a certain helicity) states σ_+ and σ_-. Originally, the lowest energy level $|\mathbf{b}\rangle$ (or $|\mathbf{c}\rangle$, depending on the direction of magnetic field) is singly occupied. The extended single-photon state (with narrow frequency spectrum) induces $|\mathbf{b}\rangle \longrightarrow |\mathbf{a}\rangle$ transitions due to the interaction with gas atoms, while the classical driving radiation, which can be turned on for the desired time, induces $|\mathbf{a}\rangle \longrightarrow |\mathbf{c}\rangle$ transitions from the upper excited level to the lower level. Since the transitions between $|\mathbf{c}\rangle$ and $|\mathbf{b}\rangle$ are forbidden, an electron can occupy level $|\mathbf{c}\rangle$ for an infinitely long time. The entangled state consisting of atomic levels with this configuration and a single-photon state is called dark polariton. The degree of entanglement of the atomic levels and the quantized photon field depends on the intensity of the classical driving radiation. *In a cell with atom*s, the entangled state, e.g., with helicity $\mu = 0$ (indices $\mu = 0$ and 1 correspond to the states with circular polarizations $\sigma_\pm$), can be represented as

$$|\Psi\rangle = \cos\theta(t)|\mathbf{b}_0\rangle \otimes |\varphi_0(\theta(t))\rangle - \sin\theta(t)|\mathbf{c}_0\rangle \otimes |0\rangle, \quad \tan\theta(t) = \frac{g\sqrt{N}}{\Omega(t)}, \quad (11)$$

where N is the number of atoms in the cell, g is the coupling constant of the quantized photon field to the atomic system, and $\Omega(t)$ is the so-called classical driving field frequency. The state-vector component corresponding to the quantized single-photon field in a medium with atoms has the form (medium is assumed to be in $x > 0$)

$$|\varphi_0(\theta(t))\rangle = \int_0^\infty dx\varphi\left(x - \int_0^t dt'\cos^2\theta(t'), 0\right)|\tau(\theta(t))\rangle, \quad \tau(\theta(t)) = x - \int_0^t dt'\cos^2\theta(t'). \quad (12)$$

Upon changing the field such that $\theta = 0 \longrightarrow \theta = \pi/2$, the single-photon state transforms into the atomic degrees of freedom (light arrest). For $\theta \longrightarrow \pi/2$, the propagation velocity and the amplitude of photon state tend to zero, $v = \cos^2(\theta)$ (accordingly, the squared modulus of the amplitude of single-photon state $\propto\cos^2\theta \longrightarrow 0$, and the vacuum component of photon field $\propto\sin^2\theta \longrightarrow 1$). Note that, in this case, the intensity of the classical driving field $\Omega \propto \cos\theta \longrightarrow 0$ corresponds, in effect, to its absence. At first sight, this contradicts our intuition. As long as the field is turned on (its intensity is high) and the quantized photon field enters the cell with atoms (during the characteristic time $\Delta t \approx L/c$, where L is the effective length of the state), the field induces $|\mathbf{b}\rangle \longrightarrow |\mathbf{a}\rangle$ transitions, and the classical field induces fast $|\mathbf{a}\rangle \longrightarrow |\mathbf{c}\rangle$ transitions ($\Omega \gg g\sqrt{N}$). After the single-photon state entered into the cell entirely, the classical field should be turned off. Otherwise, it will induce inverse electron transitions from $|\mathbf{c}\rangle$ to $|\mathbf{a}\rangle$. The light arrest is not a stop in the ordinary sense, as in the case of massive particles. As the velocity tends to zero, the amplitude of the single-photon state also tends to zero, because the photon field is massless.

The joint unitary evolution (transformation of the photon state into the atomic degrees of freedom) is not yet a measurement. The problem reduces to measuring the state of the atomic subsystem (realization of the projection measurement $\mathcal{P}_c = |\mathbf{c}\rangle\langle\mathbf{c}|$). After the time Δt of joint unitary evolution elapses, an additional classical radiation with frequency corresponding to the transition from the bound state $|\mathbf{c}\rangle$ to the continuum is turned on. Thereafter, the current carried directly by the excited electrons or preliminary amplified to a workable level is detected. This photon-arresting scheme is a special kind of detector that allows one to distinguish between the extended single-photon states (roughly speaking, to realize the projection measurements for photons). For almost all types of photodetectors, the final stage consists in knocking out an electron from a bound state and the current detection (Fig. 1b).

Thus, the cryptographic protocol consists of state preparation, state propagation through a communication channel, and its detection.

(i) The preparation of either of the orthogonal states $\rho_A(\mathbf{c}_\nu) = |\mathbf{c}_\nu(A)\rangle\langle\mathbf{c}_\nu(A)|$ with polarization $\nu = 0$ or 1 starts by participant A at t_A and takes the time $\Delta t \approx L/c$. Simultaneously, participant B prepares an ancilla consisting

of two atomic systems in the mutually orthogonal states $\mu = 0$ and 1: $\rho_B(\mathbf{b}_\nu) = |\mathbf{b}_\nu(B)\rangle\langle\mathbf{b}_\nu(B)|$. The photon field is in the vacuum state. This stage is described as

$$U_\nu^{-1}(t_A, t_A + \Delta t)\left(\rho_A(\mathbf{c}_\nu) \otimes |0\rangle\langle 0| \otimes \bigoplus_{\mu = 0, 1} \rho_B(\mathbf{b}_\mu)\right) \times U_\nu(t_A, t_A + \Delta t). \quad (13)$$

(ii) The state propagates through the communication channel and entirely reaches the receiver end in the time $\approx (L + L_{ch})/c$,

$$U_{ch}U_\nu^{-1}(t_A, t_A + \Delta t) \times\left(\rho_A(\mathbf{c}_\nu) \otimes |0\rangle\langle 0| \otimes \bigoplus_{\mu = 0, 1} \rho_B(\mathbf{b}_\mu)\right)U_\nu(t_A, t_A + \Delta t)U_{ch}^{-1}. \quad (14)$$

(iii) The arrest of the single-photon state starts at $t_B = t_A + L_{ch}/c$ and lasts for the time $\Delta t \approx L/c$,

$$\begin{aligned}\bigoplus_{\mu = 0, 1} U_\mu(t_B, T_B + \Delta t)U_{ch}U^{-1}(t_A, t_A + \Delta t) &\times (\rho_A(\mathbf{c}_\nu) \otimes |0\rangle\langle 0| \otimes \rho_B(\mathbf{b}_\mu)) \\ \times U_\mu(t_B, t_B + \Delta t)^{-1}U_{ch}^{-1}U_\nu(t_A, t_A + \Delta t) &= \delta_{|\nu - \mu|, 0}\rho_A(\mathbf{b}_\nu) \otimes |0\rangle\langle 0| \otimes \rho_B(\mathbf{c}_\mu) \bigoplus \delta_{|\nu - \mu|, 1} \\ &\times \rho_A(\mathbf{c}_\nu) \otimes |0\rangle\langle 0| \otimes \rho_B(\mathbf{b}_\mu).\end{aligned} \quad (15)$$

(iv) Using the spatially local projection measurement

$$I_\mathbf{c}(\mathrm{B}) = \bigoplus_{\mu = 0, 1} |\mathbf{c}_\mu(B)\rangle\langle\mathbf{c}_\mu(B)|, \quad (16)$$

participant B measures the atomic degrees of freedom $|\mathbf{c}_\mu(B)\rangle$.

We use in Eqs. (13)–(16) the subspace sum symbol instead of the tensor product, because our interest is only with the outcomes in one of the cells ($\mu = 0$ or 1) and not in both ($\mu = 0$ and 1).

This procedure can be implemented by preparing two cells with atoms situated, e.g., sequentially one after another so that the magnetic field differ for them in magnitude and direction. In this case, the quantized single-photon field, together with the classical driving field, induce Raman transitions in that subsystem B (with that μ value) for which these transitions are possible. Then, another classical field is turned on to induce electron transitions from the state $|\mathbf{c}_\mu\rangle$ to the continuum followed by the detection with an ordinary photomultiplier. Each cell is exposed to classical radiation with its own frequency that is necessary for inducing transitions to the continuum. The current signal will arise only in the cell where the Raman transitions occur (the state $|\mathbf{c}_\mu\rangle$ is occupied by electrons). In principle, the dead light arrest is not necessary; it suffices only to decelerate the propagation in the cell. It is desirable that the duration of a signal exciting electrons to the continuum be shorter than the propagation time of the decelerated single-photon field in the cell. As compared to the dead arrest, the signal ratio in this case will be equal to $\sin^2\theta$, i.e., to the filling of the state $|\mathbf{c}_\mu\rangle$ [see Eq. (11)].

The preparation, propagation, and detection (arrest of a single-photon state) is a unified process. Equations (13)–(15) demonstrate that the leading front starts stopping before the trailing front leaves the source. Strictly speaking, Eqs. (11) and (12) were derived in the adiabatic approximation (for detail, see [8]). However, this circumstance is not restrictive, because the classical driving field can be smoothly turned on and off at the tails of the leading and trailing fronts of a single-photon state, respectively.

An extended state can be prepared by filtering a narrow spectral band from a short-duration (broadband) state. In the above examples, the length L is determined by the spectral width of atomic levels $|\mathbf{a}\rangle$ (in experiments [9], L was several kilometers long). The spacetime extension of the state amplitude is determined by the spectral width $\Delta\omega$, and the probability of detection during the time Δt [time of action of the classical driving field in Eq. (9)] is equal, with a high accuracy, to $\approx 1 - \mathcal{O}(e^{-\Delta\omega\Delta t})$ (for exact relations, see [11]).

The well-known simple and elegant proof of the no-cloning theorem [2] *does not forbid* the existence of a unitary operator that acts in the space $\mathcal{H}_A \otimes \mathcal{H}_B$ and transforms the ancilla to different states, depending on one of the input orthogonal states, without disturbing the latter. The fact that the unitary operator acts in $\mathcal{H}_A \otimes \mathcal{H}_B$ implies that the quantum states are accessible as entire objects. The theorem says nothing about the structure of this unitary operator. Allowing for the spacetime structure of quantum states, which inevitably exists, extends the variety of different applications for the orthogonal states. The above simple example of using orthogonal states for quantum cryptography does not exhaust all their possible applications.

I am grateful to S.S. Nazin for stimulating discussions and critical remarks. This work was supported by the Russian Foundation for Basic Research, project nos. 02-02-16289, 40.020.1.1.1170, and 37.029.1.1.0031.

REFERENCES

1. W. K. Wootters and W. H. Zurek, Nature **299**, 802 (1982).
2. C. H. Bennett, Phys. Rev. Lett. **68**, 3121 (1992); C. H. Bennett, G. Brassard, and N. D. Mermin, Phys. Rev. Lett. **68**, 557 (1992).
3. N. N. Bogolyubov, A. A. Logunov, A. I. Oksak, I. T. Todorov, *General Principles of Quantum Field Theory* (Nauka, Moscow, 1987).
4. L. Goldenberg and L. Vaidman, Phys. Rev. Lett. **75**, 1239 (1995); quant-ph/9506030.

5. S. N. Molotkov and S. S. Nazin, Pis'ma Zh. Éksp. Teor. Fiz. **73**, 767 (2001) [JETP Lett. **73**, 682 (2001)]; quant-ph/106046.
6. I. M. Gel'fand and N. Ya. Vilenkin, *Generalized Functions*, Vol. 4: *Applications of Harmonic Analysis* (Fizmatgiz, Moscow, 1961; Academic, New York, 1964).
7. N. Wiener and R. Palley, *Fourier Transform in the Complex Domain* (American Mathematical Society, New York, 1934; Nauka, Moscow, 1964).
8. M. Fleischhauer and M. D. Lukin, Phys. Rev. Lett. **84**, 5094 (2000).
9. C. Liu, Z. Dutton, C. H. Behroozi, and L. V. Hau, Nature **409**, 490 (2001); D. F. Phillips, A. Fleischhauer, A. Mair, *et al.*, Phys. Rev. Lett. **86**, 783 (2001).
10. A. V. Turukhin, V. S. Sudarshanam, M. S. Shahriar, *et al.*, Phys. Rev. Lett. **88**, 023602 (2002).
11. S. N. Molotkov, Pis'ma Zh. Éksp. Teor. Fiz. **75** (10), 617 (2002) [JETP Lett. **75**, 521 (2002)].

Translated by R. Tyapaev

JETP Letters, Vol. 76, No. 1, 2002, pp. 8–10. Translated from Pis'ma v Zhurnal Éksperimental'noĭ i Teoreticheskoĭ Fiziki, Vol. 76, No. 1, 2002, pp. 11–13.

The Interference Sensitivity of Bistable Systems to Subthreshold Signals

G. M. Drabkin

Hahn–Meitner Institute, 14109 Berlin, Germany

St. Petersburg Institute of Nuclear Physics, Russian Academy of Sciences, Gatchina, Leningrad region, 188300 Russia

Received April 25, 2002; in final form, June 3, 2002

Abstract—A new approach to studying the influence of intense noise on the sensitivity of bistable systems detecting subthreshold signals is proposed. It is shown that the interference interaction between two identical bistable systems coherently excited by the same above-threshold noise may increase the sensitivity with respect to a subthresold signal by more than two orders of magnitude. © *2002 MAIK "Nauka/Interperiodica".*

PACS numbers: 75.60.Jk; 75.60.Ej

If two metastable states of a nonlinear system are separated by an energy barrier, such bistable systems are usually insensitive to the signals with amplitudes below the barrier. A different situation can take place in excited bistable systems, that is, under conditions when above-threshold excitation induces continuous transitions between the metastable states. In the case of a stochastic resonance [1, 2], joint action of the above-threshold excitation noise of a certain intensity and a periodic subthreshold signal results in the fact that the average frequency of transitions becomes dependent on the amplitude and frequency of the subthreshold signal. As the amplitude of exciting noise grows further, the effect vanishes, after which the frequency of barrier crossing is determined only by the spectrum of above-threshold excitation signal and is independent of the presence of subthreshold signals.

If the duration of such above-threshold excitation signals is greater than the time constant of transitions between the metastable states, the duration of the output signal due to the transition will be much shorter as compared to the period of excitation signals, and the time separation of the neighboring response signals will be much greater than the signal duration. This phenomenon opens up new possibilities for studying the dynamics of excited systems. In this paper, it is suggested that dynamic features of the barrier crossing events (barrier crossing time and duration) be studied, rather than the average frequency of transitions.

In the experiment, the transitions between metastable states were modeled by the process of magnetization reversal in a ferromagnet with a quasi-rectangular hysteresis loop. In this case, a barrier between the magnetization states $+B_s$ and $-B_s$ is represented by a coercive force H_c. The experiments were performed with a 20-μm-thick $Co_{66}Si_{16}B_{12}Fe_4Mo_2$ foil. The hysteresis loop was characterized by the parameters: $B_s = 0.55$ T, $H_c \approx 1$ A/m, and $\Delta H_c \approx 0.3H_c$. The foil was bent so as to form a closed ring and placed inside a toroidal solenoid. The input signals were determined by a magnetic field of the solenoid. The transitions between metastable states $+B_s$ and $-B_s$, that is, crossings of the barrier H_c, were detected by measuring the emf induced in a probing coil wound around the foil cross section.

The amplitude of the above-threshold excitation signal was $H_b^0 \approx 6H_c$, while that of the subthreshold signal was $H_p^0 \leq 0.4H_c$. Both signals fall within the frequency interval from 30 to 140 Hz. One period of the excitation signal $H_b = H_b^0 \sin\omega_0 t$ features two barrier crossings ($+H_c$ and $-H_c$), the responses of which differ only in sign. Therefore, we may consider only one branch of the transitions (e.g., through $+H_c$). Since $\Delta H_c < H_c \ll H_b^0$, we may assume to the first approximation that, under the action of above-threshold signal $H_b = H_b^0 \sin\omega_0 t$, the H_c barrier is crossed at the time instants

$$t_c^0 \approx H_c/\omega_0 H_b^0, \tag{1}$$

and the duration of transition is

$$\Delta t_c^0 \approx \Delta H_c/H_0\omega_0. \tag{2}$$

When subthreshold signals $H_p = H_p^0 \sin(\omega t + \varphi_n)$ $(\omega \leq \omega_0)$ are added to the above-threshold H_b excitation, the time instant t_c^n of crossing the H_c barrier is determined by the formula

$$t_c^n \approx \frac{H_c - H_p^0 \sin\varphi_n}{H_0\omega_0}\left(1 - \frac{H_p\omega}{H_b^0\omega_0}\cos\varphi_n\right), \tag{3}$$

and the duration of transition is

$$\Delta t_c^n \approx \Delta t_c^0\left[1 - \frac{H_p\omega}{H_0\omega_0}\left(\cos\varphi_n - \frac{\omega H_c}{\omega_0 H_0}\sin\varphi_n\right)\right], \quad (4)$$

where φ_n is the subthreshold signal phase at the time instant when the phase of the above-threshold excitation signal is zero. The time of barrier crossing is counted from this point of zero phase.

Since the phases of subthreshold signals φ_n are not correlated with the above-threshold excitation signals, formulas (1) and (4) indicate that averaging over time greater than $1/(\omega_0 - \omega)$ yields $\langle\Delta t_c^0\rangle = \langle\Delta t_c^n\rangle$. Thus, under the conditions of strong excitation, both the average frequency of barrier crossing and the average time of crossings are independent of the presence of subthreshold signals.

The influence of the subthreshold signals on the time of barrier crossing is more conveniently characterized by the quantity $St = (t_0^n - t_c^0)/\Delta t_c^0$ having a physical meaning of the relative displacement. Using formulas (1)–(4), we obtain

$$St = \frac{t_c^n - t_c^0}{\Delta t_c^0} = \frac{H_p^0}{\Delta H_c} \times\left\{\sin\varphi_n + \cos\varphi_n\left[\frac{\omega}{\omega_0 H_0}(H_c - H_p\sin\sigma)\right]\right\}. \quad (5)$$

For determining the *St* value, we used an interferometric setup comprising a signal generator, two identical foil remagnetization devices (A and B), a subtractor, and a mean-square voltmeter. When identical above-threshold signals are coherently applied to the inputs of devices A and B, the output signals of A and B simultaneously enter the subtractor and exhibit mutual compensation. If an additional subthreshold signal is applied to the input of one device (for example, A) simultaneously with the coherent identical excitation signals entering both channels, the output signals from A will enter the subtractor with a shift of $t_c^n - t_c^0$ relative to the output signal from B. As a result, a differential response will appear at the subtractor output. The magnitude and sign of this signal depend on the subthreshold signal phase and on the branch of the barrier crossing ($+H_c$ versus $-H_c$). Measured with a mean-square voltmeter possessing an averaging time greater than $1/(\omega_0 - \omega)$, this differential signal will be proportional (except at the resonance points, where sub- and above-threshold signals are coherent) to

$$\frac{H_p^0}{\Delta H_c} f\left(\frac{\omega}{\omega_0}, \frac{H_p}{H_0}, \frac{H_c}{H_0}\right),$$

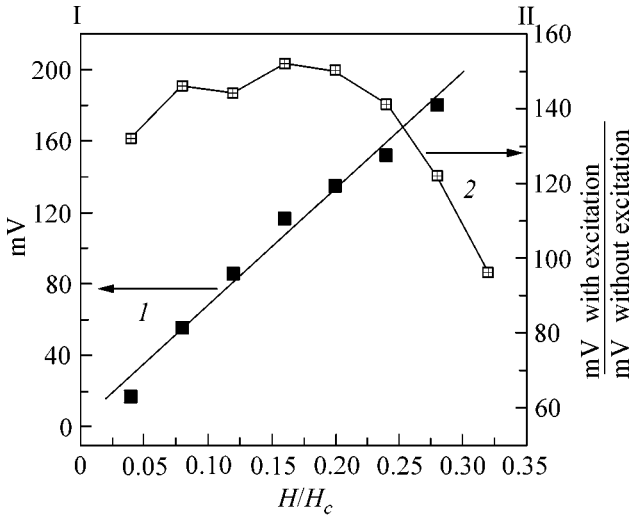

Figure.

where $f(\omega/\omega_0, H_p/H_0, H_c/H_0)$ is a quantity on the order of unity, which is virtually independent of ω/ω_0, H_p/H_0, and H_c/H_0.

The advantages of the proposed method of detecting subthreshold signals can be most clearly demonstrated for noise signals. The main process characteristics remain virtually unchanged when the sinusoidal excitation is replaced by a noise excitation and a subthreshold noise is detected.

The results of measurements using a coherent excitation of A and B by the same color noise (30–130 Hz) at an effective intensity of $6H_c$ are presented in the figure. In addition to the noise excitation, a subthreshold color noise (30–130 Hz) was applied at the input of A and B with the effective noise intensity (in H_c units) indicated on the ordinate axis. The subthreshold noises entering A and B are mutually uncorrelated. Nor are these subthreshold signals correlated to the above-threshold excitation noise (three different noise generators were employed). Ordinate I (curve *1*) shows the readings of a mean-square voltmeter measuring the signal at the subtractor output when A and B are coherently excited and receive uncorrelated subthreshold color noise signals. Ordinate II (curve *2*) plots the same voltmeter readings related to the case when only subthreshold color noise signals are present, while the coherent excitation is switched off.

In order to compare the proposed approach to traditional stochastic resonance, let us consider the results of measurements using only one remagnetization device, for example, A. In this case, adding the noise excitation does not lead to any significant increase in the response to the subthreshold signal. The amplification effect is only observed with sinusoidal subthreshold signals, provided that the component of the signal spectrum with a frequency equal to that of the subthreshold signal is measured rather than the mean-

square output signal. In this experiment, the mean-square voltmeter was replaced with a spectrum analyzer of the HP3632A type. The optimum amplitude of the excitation noise was (0.6–0.8)H_c. The subthreshold signal frequency was 73 Hz. The gain factor was 5 for subthreshold signals with an amplitude of up to $0.2H_c$.

A comparison of these results to the data presented in the figure (curve *2*) shows that the sensitivity of the interference scheme is 10 times higher than that of the traditional one. However, the most important advantage of the interference scheme is that, in the presence of intense external noise, the combination of two identical bistable systems allows weak uncorrelated noise signals to be detected with a sensitivity increased by one to two orders of magnitude. Another important advantage is the possibility of restricting measurements to the mean-square output signal intensity. These factors are very important for the analysis of neuron operation under noise conditions.

I am grateful to Prof. F. Mezei for his interest in this study and fruitful discussions and to B. Nemashok, N. Boil, I. Lazebnik, and V. Khavronin for their help in conducting experiments.

REFERENCES

1. V. S. Anishchenko, A. B. Neĭman, F. Moss, and L. Schimansky-Geier, Usp. Fiz. Nauk **169**, 7 (1999).
2. Yu. L. Klimontovich, Usp. Fiz. Nauk **169**, 39 (1999).

Translated by P. Pozdeev